PhD Thesis

Characterization of hepatocyte-specific lysosomal acid lipase-deficient mice

submitted by

Christina LEOPOLD, BSc. MSc.

for the Academic Degree of

Doctor of Philosophy

(PhD)

at the

Medical University of Graz

Gottfried Schatz Research Center for Cell Signaling, Metabolism and Aging

Molecular Biology and Biochemistry

under the supervision of

Univ. Prof.in Mag.a Dr.in rer. nat.

Dagmar KRATKY

2019

Declaration

I hereby declare that this thesis is my own original work and that I have fully acknowledged by name all of those individuals and organizations that have contributed to the research for this thesis. Due acknowledgement has been made in the text to all other material used. Throughout this thesis and in all related publications I followed the "Standards of Good Scientific Practice and Ombudsmen Committee" at the Medical University of Graz.

Graz, March 2019 .....

Christina Leopold

Disclosures

Please note that parts of this thesis have been published in a peer-reviewed journal and permission for re-print of the figures has been given with the Open-Access-Publication agreements of the publishing group (Appendix).

The thesis is based on the following publication:

Hepatocyte-specific lysosomal acid lipase deficiency protects mice from diet-induced obesity but promotes hepatic inflammation

Leopold C, Duta-Mare M, Sachdev V, Goeritzer M, Maresch LK, Kolb D, Reicher H, Wagner B, Stojakovic T, Ruelicke T, Haemmerle G, Hoefler G, Sattler W, Kratky D.

Biochim Biophys Acta Mol Cell Biol Lipids. 2019 Jan 9;1864(4):500-511.

All co-authors gave their consent to re-use data from the publication within this thesis. The following co-authors contributed to the data shown in the thesis:

- Thomas Rülicke and Bettina Wagner (Institute of Laboratory Animal Science, University of Veterinary Medicine Vienna) generated the mice.
- Tatjana Stojakovic (Clinical Institute of Medical and Chemical Laboratory Diagnostics, Medical University of Graz) performed ALT and AST measurements shown in Figures 11 and 28.
- Silvia Schauer (Diagnostic and Research Institute of Pathology, Medical University of Graz) performed sectioning and staining of tissues in Figures 12, 13, 17, 23, 25, and 29.
- Lisa Katharina Maresch (Institute of Molecular Biosciences, University of Graz) helped with the bomb calorimeter analysis shown in Figure 15.
- Dagmar Kolb (Center for Medical Research, Medical University of Graz) visualized and quantified LD size shown in Figure 24.
- Helga Reicher (Gottfried Schatz Research Center, Medical University of Graz) performed GC analysis shown in Figure 26.
- Madalina Duta-Mare, Vinay Sachdev, Madleine Göritzer, Günther Hämmerle, Gerald Höfler and Wolfgang Sattler contributed to data collection and analyses.

This thesis was performed with full financial support from the Austrian Science Fund (FWF) within the PhD program Metabolic and Cardiovascular Disease (DK-MCD).

„Success is not final,

failure is not fatal;

it is the courage to continue

that counts.”

Winston Churchill

Acknowledgments

First I would like to thank my supervisor Dagmar Kratky for the opportunity to do my PhD in her lab. Thank you for your support, motivation and for the opportunity to independently develop ideas and reach my scientific goals. I really appreciate that you always care for your students and have an open door, no matter how stressful times are.

I owe my gratitude to my thesis committee members Peter Fickert and Achim Lass, as well as my mentor Robert Zimmermann, for their critical advice and helpful comments. Furthermore, I want to thank our collaborators Wolfgang Sattler, Helga Reicher, Thomas Rülicke, Günter Hämmerle, Tatjana Stojakovic, Gerald Höfler, and Silvia Schauer for their help and support. I also would like to thank Douglas G. Mashek for giving me the chance to work in his lab for my research stay abroad.

In addition, I want to thank all current and former members of the Kratky lab for their help and support, especially Madalina-Cristina Duta-Mare for having serendipitous ideas and never giving up on me. Thank you Vinay, for being a mentor not only during my master thesis, but also in PhD and for always seeing the positive in everything. The friday night “Skybar meetings” were very welcome not only in times of frustration but also in times of joy. Cheers to you two! Many thanks to Madeleine and my current lab collegues for your help and support, as well as great laughs during the lunch-breaks.

I want to thank my friends in science and outside, for always being there for me. Special thanks go to my “E-Heim girls” Natascha and Karin for always having a legal advice, to the “BioTechMed girls” Lisa Katharina Maresch and Kathi Huber for our fun meetings, and to Christiane Klec for being such a great friend and sports buddy.

I would like to thank the funding institutions FWF, Medical University of Graz and DK-Program “Metabolic and Cardiovascular Disease”. Special thanks go to Karin Osibow for her great help and outstanding administration skills.

Last, but definitely most important, I want to thank my family, especially my mum and grandma for being my greatest fans and always believeing in me and my dreams. Thank you Stephan for this amazing years, for your patience, your moral support, and for always encouraging me. Having you by my side makes all the difference and I could not wish for a better partner in crime.

Table of Contents

Abbreviations and Definitions

ABC	ATP-binding cassette
ACC	acetyl-CoA carboxylase
ACAT	acetyl-Coenzyme A acetyltransferase
ALT	alanine aminotransferase
AMPK	AMP-activated protein kinase
APO	apolipoprotein
AST	aspartate aminotransferase
ATP	adenosisne triphosphate
BAT	brown adipose tissue
BW	body weight
CAB	chromotrope aniline blue
CCL	chemokine (C-C motif) ligand
CCR	C-C chemokine receptor
CE	cholesteryl ester
CESD	cholesteryl ester storage disease
CKT19	cytokeratine 19
CHREBP	carbohydrate responsive element binding protein
CREBP	cAMP response element-binding protein
COL3A	collagen type III alpha
CPT1	carnitine palmitoyl acyl-CoA transferase 1
CS	citrate synthase
CT	computed tomography
DBS	dried blood spot
DG	diacylglycerol
DGAT	acyl-CoA: diacylglycerol acyltransferase
DNL	*de novo* lipogenesis

ER	endoplasmic reticulum
ERT	enzyme replacement therapy
FA	fatty acid
FABP	fatty acid binding protein
FAME	FA methyl esters
FAT/CD36	caveolins fatty acid translocase
FATP	fatty acid transporters
FAS	fatty acid synthase
FH	fumarate hydratase
FPLC	fast protein liquid chromatography
G6P	glucose 6-phosphate
G6Pase	glucose-6-phosphatase
GK	glucokinase
GLUT2	glucose transporter type 2
GPAT4	glycerol-3-phosphate O-acyltransferase
GS	glycogen synthase
GSK3	glycogen synthase kinase 3
HDL	high-density lipoprotein
HDL-C	high-density lipoprotein cholesterol
HF/HCD	high fat/high cholesterol diet
H&E	hematoxylin and eosin staining
HSC	hepatic stellate cell
HSCT	hematopoietic stem cell transplantation
HMG-CoA	3-hydroxy-3-methyl-glutaryl-coenzyme A
HMGCR	HMG-CoA reductase
HNF4α	hepatocyte nuclear factor 4 alpha
HOMA	homeostasis model assessment
IL-6	interleukin-6

LAL	lysosomal acid lipase
LAL-D	lysosomal acid lipase deficiency
LIV-LIPA$^{-/-}$	hepatocyte-specific lysosomal acid lipase-deficient mice
LD	lipid droplet
LDL	low-density lipoprotein
LDL-C	low-density lipoprotein cholesterol
LDLR	low desinsity lipoprotein receptor
LCAT	lecithin-cholesterol acyltransferase
LCFA	very long-chain FA
L-PK	liver-type pyruvate kinase
LSD	lysosomal storage diseases
LXR	liver-specific X receptor
µCT	micro-computed tomography
MCP1	monocyte chemoattractant protein 1
MCSF	macrophage colony stimulating factor
MDH	malate dehydrogenase
MRI	magnetic resonance imaging
MTP	microsomal triglyceride transfer protein
NADH	nicotine amide dinucleotide
NADPH	nicotine amide dinucleotide phosphate
NAFLD	non-alcoholic fatty liver disease
NASH	non-alcoholic steatohepatitis
NMR	nuclear magnetic resonance
NPC	non-parenchymal cell
NPC1L1	Niemann-Pick C1-like 1
O-PLS-DA	Orthogonal Partial Least Squares Discriminant Analysis
ORO	Oil Red O
PAS	periodic acid Schiff

PCA	principle component analysis
PCX	pyruvate carboxylase
PDGF	platelet-derived growth factor
PDHB	pyruvate dehydrogenase
PEP	phosphoenolpyruvate
PEPCK	phosphoenolpyruvate carboxykinase
PGC1α	peroxisome proliferator-activated receptor gamma coactivator 1-alpha
PFK-1	phosphofructokinase-1
PI3K	phosphoinositide-3-kinase
PKA	protein kinase A
PL	phospholipid
PPARα	peroxisome proliferator-activated receptor alpha
PYGL	glycogen phosphorylase
RCT	reverse cholesterol transport
RE	retinyl ester
RER	respiratory exchange ratio
ROS	reactive oxygen species
SUCLG2	succinate-Coenzyme A ligase
SR-BI	scavenger receptor BI
SRE	sterol response element
SREBP-1c	sterol-regulatory element binding protein 1c
TCA	tricarboxylic acid cycle
TG	triglyceride
TGFB	transforming growth factor beta
TNFα	tumor necrosis factor alpha
WAT	white adipose tissue
WD	Wolman disease
VLDL	very low-density lipoprotein

VLDL-C very low-density lipoprotein cholesterol

Zusammenfassung

Lysosomale saure Lipase (LAL) hydrolisiert Cholesterinester (CE) und Triglyzeride (TG) zu Fettsäuren und Cholesterin. LAL-defiziente (Lipa$^{-/-}$) Mäuse sind lebensfähig, zeigen aber auf Grund eines veränderten Fettstoffwechsels ein vermindertes Größenwachstum sowie fehlendes Fettgewebe. Charakteristisch sind CE und TG Akkumulationen in verschiedenen Zellen und Organen, speziell in der Leber, was zu schwerer Hepatomegalie und Steatose führt. Während einige Studien bereits die Defizienz von LAL untersucht haben, war es bis zum jetzigen Zeitpunkt unklar, ob Kupfferzellen oder Hepatozyten für den in Mäusen und Menschen beobachteten Phenotyp verantwortlich sind. Wir generierten daher Mäuse mit einer gezielten Mutation von LAL in Hepatozyten (Liv-Lipa$^{-/-}$) um die Auswirkungen auf den hepatischen und systemischen Fett- und Glukosestoffwechsel zu untersuchen.

Liv-Lipa$^{-/-}$ Mäuse, die mit einer normalen Diät gefüttert wurden, zeigen im Vergleich zu den Kontrollmäusen nur eine erhöhte hepatische Akkumulation von Cholesterin und CE. Nach der Fütterung einer HF/HC Diät jedoch nahmen die Mäuse weniger an Gewicht zu und zeigten eine 70% Reduktion des weißen Fettgewebes. Futteraufnahme, Aktivität und Energieumsatz waren vergleichbar mit den Kontrollmäusen. Lipoproteinanalysen zeigten deutlich erhöhte Cholesterinwerte, vor allem in der LDL-Fraktion von Liv-Lipa$^{-/-}$ Mäusen. Obwohl sie ein deutlich verringertes Fettgewebe hatten, zeigten Liv-Lipa$^{-/-}$ Mäuse eine verbesserte Glukoseverwertung, sowohl bei Glukose- als auch Insulin Toleranztests. mRNA Expression von Glukoneogenesegenen unterstützten diese Erkenntnis. Biochemische Untersuchungen des Fettgehaltes in der Leber, zeigten weiters eine deutliche Reduktion an TG, während die Cholesterinkonzentration erhöht war. Darüber hinaus belegten elektronenmikroskopische Aufnahmen die reduzierte Anzahl und Größe an Lipidtropfen sowie Cholesterinkristallbildung in der Leber von Liv-Lipa$^{-/-}$ Mäusen. Dies führte zu entzündlichen Lebererkrankungen und in der Folge zu Leberfibrose.

Zusammenfassend liefert diese Arbeit den Nachweis, dass Liv-Lipa$^{-/-}$ Mäuse auf HF/HC Diät den gleichen Phenotyp wie Lipa$^{-/-}$ Mäusen zeigen. Unsere Beobachtungen führen weiter zu neuen Erkenntnissen über LAL und zeigen, dass das Fehlen von LAL in

Hepatozyten verantwortlich für die Lipidakkumulationen in der Leber ist und in der Folge zur Bildung eines Leberschadens und Entzündungen führt.

Abstract

Lysosomal acid lipase (LAL) hydrolyzes cholesteryl esters (CE) and triglycerides (TG) to generate fatty acids (FA) and cholesterol. LAL-deficient (Lipa$^{-/-}$) mice are viable but due to an abnormal lipid metabolism they exhibit growth retardation and lack white adipose tissue. Characteristically, these mice accumulate CE and TG in multiple cells and organs, especially in the liver, resulting in severe hepatomegaly and steatosis. While numerous studies have already investigated LAL deficiency in detail, it still remained elusive whether Kupffer cells or hepatocytes are primarily responsible for the observed phenotype in humans and mice. We therefore generated mice with a specific targeted deletion of LAL in hepatocytes (Liv-Lipa$^{-/-}$) and studied the consequences on hepatic and systemic lipid and glucose metabolism.

Liv-Lipa$^{-/-}$ mice fed a chow diet remained metabolically comparable to their littermate controls and only showed hepatic cholesterol crystal accumulations. When challenged with a high fat/high cholesterol diet (HF/HCD), Liv-Lipa$^{-/-}$ mice gained less body weight and showed a 70% reduction in white adipose tissue mass. Food intake, locomotor activity, and energy expenditure, however, remained comparable between the genotypes. Plasma lipoprotein profile analyses after FPLC separation revealed markedly increased total cholesterol concentrations in the low-density lipoprotein fraction of Liv-Lipa$^{-/-}$ mice. Despite a reduction in adipose tissue mass, Liv-Lipa$^{-/-}$ mice exhibited improved glucose clearance during both glucose and insulin tolerance tests. mRNA expression of genes involved in gluconeogenesis support the theory of improved glucose metabolism. Biochemical estimation of hepatic lipid content revealed a reduction of TG, whereas cholesterol concentrations were increased. In agreement, electron micrographs showed reduced number and size of cytosolic lipid droplets as well as cholesterol crystals in livers of Liv-Lipa$^{-/-}$ mice. This consequently drives liver inflammation and fibrosis.

In summary, the present work provides profound evidence that Liv-Lipa$^{-/-}$ mice on HF/HCD mimic the phenotype observed in global Lipa$^{-/-}$ mice. Our observations expand the knowledge about hepatic LAL deficiency (LAL-D) and that loss of LAL in hepatocytes is responsible for increased hepatic lipid stores in LAL-D, ultimately leading to liver damage and inflammation.

1. Introduction

1.1 Physiology of the liver

The liver is a key metabolic organ that plays a major role in synthesis, storage, and redistribution of carbohydrates, proteins, and lipids (Figure 1). Imbalance in this complex regulation system is often associated with pathologies such as obesity, non-alcoholic fatty liver disease (NAFLD), insulin resistance and type 2 diabetes as well as atherosclerosis and cardiovascular disease.

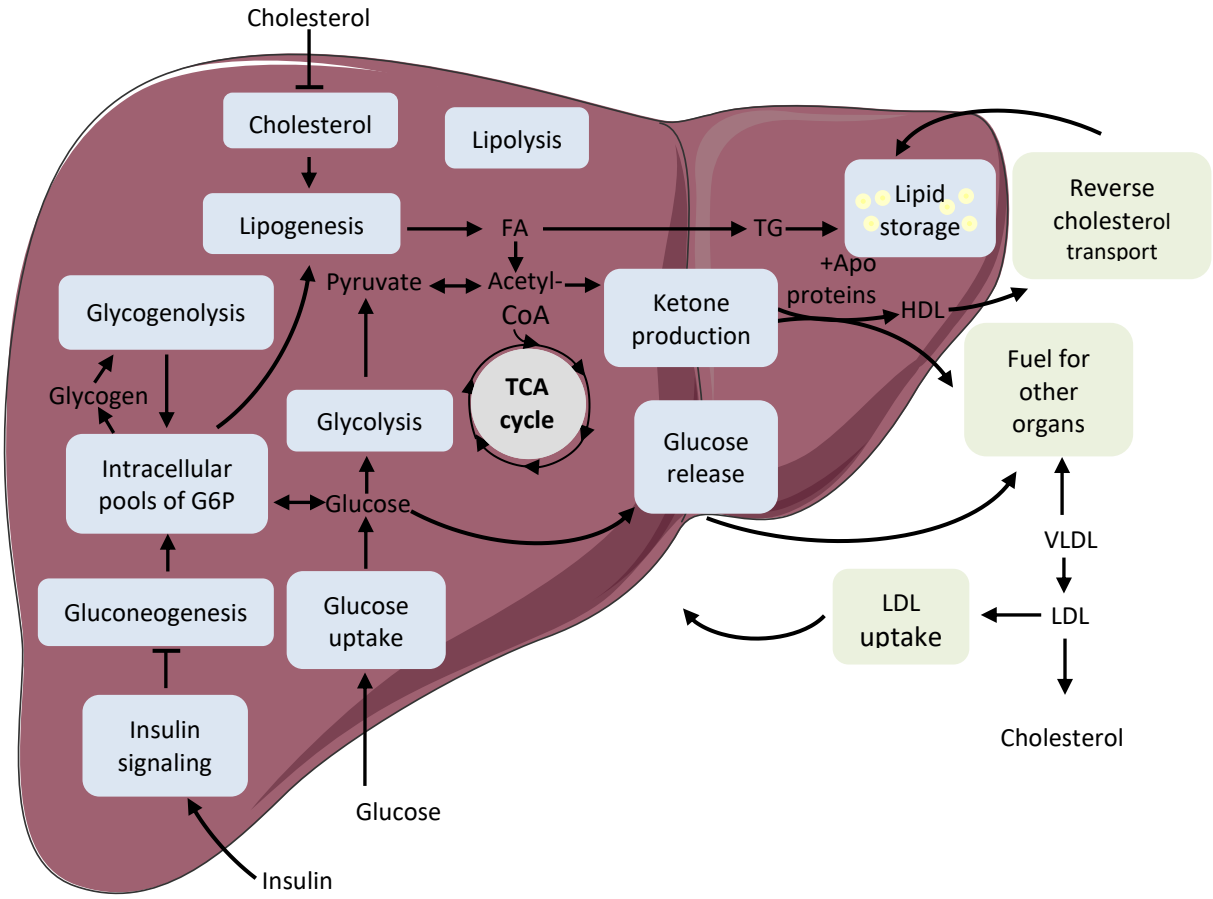

Figure 1: Major metabolic pathways in the liver.

The scheme describes the major metabolic routes of glucose in the liver and how glucose and lipid metabolism are tightly connected.

1.1.1 Hepatic glucose metabolism

1.1.1.1 Glucose uptake

Hepatocytes are the main cell type in the liver and take up blood glucose via the glucose transporter type 2 (GLUT2), which is a membrane-bound glucose transporter with high capacity for glucose uptake. Inside hepatocytes, glucose is phosphorylated to glucose 6-phosphate (G6P) by glucokinase (GK), the rate-limiting enzyme for hepatic glucose utilization (1). Consequently, a reduction in intracellular glucose concentrations further increases glucose uptake. In contrast to other hexokinases, GK is not inhibited by its own product, and therefore, postprandial glycogen can be stored in hepatocytes.

1.1.1.2 Glycolysis and glycogen synthesis

Depending on the metabolic state, G6P is either used as an energy source (glycolysis) or stored for later usage as glycogen. Glycolysis is a ten-step process, which metabolizes glucose to pyruvate with a net gain of two adenosine triphosphate (ATP) and two nicotine amide dinucleotide (NADH) molecules per molecule glucose (2). Glycolytic intermediates and products are further decarboxylized to acetyl-CoA and processed in the tricarboxylic acid cycle (TCA) to generate ATP or utilized for *de novo* lipogenesis (DNL). Alternatively, G6P can be degraded via the pentose phosphate pathway to generate nicotine amide dinucleotide phosphate (NADPH), which is an important antioxidant and co-substrate for DNL and cholesterol synthesis. The key rate-limiting enzymes of glycolysis are GK, phosphofructokinase-1 (PFK-1), which converts fructose 6-bisphosphate into fructose 1,6-bisphosphate, and liver-type pyruvate kinase (L-PK), which converts phosphoenolpyruvate (PEP) into pyruvate. These enzymes are tightly controlled by allosteric mediators that generally promote the catabolism of glucose in the cell (3-6). L-PK is activated by its substrate and inhibited by the abundance of ATP (2). Furthermore, insulin, epinephrine, and glucagon regulate PK via the phosphoinositide-3-kinase (PI3K) pathway and carbohydrate responsive element-binding protein (ChREBP) induces transcription of PK in the presence of glucose (7).

Glycogen synthesis is catalyzed by glycogen synthase (GS) after conversion of G6P to UDP-glucose (8). GS is inactive in the phosphorylated state and regulated by the allosteric activator G6P. GS gets phosphorylated by glycogen synthase kinase 3 (GSK3),

which is a down-stream target of Akt/PI3K and therefore insulin signaling. GSK3 is a multifunctional kinase, involved in cell senescence, apoptosis, and lipid metabolism via phosphorylation of sterol-regulatory element-binding protein 1c (SREBP-1c) (9). Other protein kinases that phosphorylate GS are AMP-activated protein kinase (AMPK) and protein kinase A (PKA). Insulin activates glycogen synthesis via repression of PKA. GS synthesizes the glycogen polymer, which is then further branched by a branching enzyme.

1.1.1.3 Glycogenolysis and gluconeogenesis

In the fasted state, the liver supplies the body with energy by breaking down glycogen. When hepatic glycogen stores are empty, the liver switches to gluconeogenesis (1, 10). Glycogen breakdown is catalyzed by glycogen phosphorylase (PYGL), which cleaves glucose from the glycogen polymer to produce G1P. G1P is further converted to G6P by phosphoglucomutase before a debranching enzyme cleaves the last four glucose monomers. PYGL is regulated through allosteric activation via AMP and phosphorylation by PKA, which is inhibited by insulin.

During prolonged fasting periods, when acetyl-CoA levels are high or abundantly available, gluconeogenesis takes place intra-mitochondrially via the induction of pyruvate carboxylase. Interestingly, inhibition of hepatic carnitine palmitoyl acyl-CoA transferase 1 (CPT-1) and therefore mitochondrial fatty acid oxidation significantly represses hepatic gluconeogenesis in mice (11). In addition, gluconeogenesis is regulated via allosteric and transcriptional activation of phosphoenolpyruvate carboxykinase (PEPCK), fructose-1,6-bisphosphatase, and glucose-6-phosphatase (G6Pase). Insulin inhibits PEPCK expression via AKT-mediated FOXO1 phosphorylation. FOXO1, a transcriptional activator of PEPCK and G6Pase, is both directly and indirectly activated by peroxisome proliferator-activated receptor gamma coactivator 1-alpha (PGC1α), hepatocyte nuclear factor 4 alpha (HNF4α), cAMP response element-binding protein (CREBP), and peroxisome proliferator-activated receptor alpha (PPARα) (12). Nuclear receptors, glucagon, and glucocorticoids also mediate expression of PEPCK and G6Pase (10, 13). PEPCK knock-out mice not only show decreased gluconeogenesis, but more importantly a decreased removal of TCA anions, which causes hepatic TG accumulation and steatosis (14). These processes further

demonstrate the close inter-relation between gluconeogenesis and hepatic lipid metabolism. [reviewed in (2)]

1.1.2 Hepatic lipid metabolism

1.1.2.1 *De novo* lipogenesis

Hepatic DNL takes place in a quantitatively more efficient way than in adipose tissue. It consists of synthesis of FAs from acetyl-CoA or malonyl-CoA leading to the synthesis of phospholipids (PL), mono-, di- and triglycerides (TG), and cholesterol. In mammals, FA synthesis is catalyzed by acetyl-CoA carboxylase (ACC) and fatty acid synthase (FAS) and is tightly regulated by various nuclear receptors like PPARα, PPARγ, and farnesoid receptor (FXR) (15-17).

Since nuclear receptors are also important mediators of insulin signaling and DNL occurs under anabolic conditions, this indicates a close link between glucose and lipid metabolism. On the transcriptional level, ChREBP, a glucose-dependent transcription factor, and SREBP-1c regulate DNL (7).

While a diet rich in carbohydrates mainly leads to transcription of lipogenic enzymes with an increase in high-density lipoproteins (HDLs) and hypertriglyceridemia (18, 19), polyunsaturated FAs decrease lipogenesis by suppressing gene expression in murine liver (20).

1.1.2.2 Lipid distribution & storage

FAs and their metabolites are known to be the major cause for lipotoxicity and promote the formation of reactive oxygen species (ROS). Therefore, excess lipids are stored in form of TGs, which are relatively inert and consist of three FAs esterified to a glycerol backbone. Lipids produced by the liver are processed to very low-density lipoprotein (VLDL) particles and supplied to other tissues either as energy source or structural component. Furthermore, they can be stored in cytosolic lipid droplets (LD), which are the main form of hepatic fat accumulation (21).

Enzymes involved in neutral lipid synthesis are acetyl-Coenzyme A acetyltransferases (ACATs) and acyl-CoA: diacylglycerol acyltransferases (DGATs), which are primarily located in the endoplasmic reticulum (ER). Other enzymes such as glycerol-

3-phosphate O-acyltransferase (GPAT4) and DGAT2, however, localize to both, the ER and LD (22, 23). LD are considered as dynamic, tightly controlled, metabolically active cellular organelles rather than simple storage depots. They consist of a TG core with a PL monolayer containing amphiphilic structural proteins. Important members of these LD-associated proteins are perilipin 1,2 and 3, which are crucial for the formation, maintenance, and modification of LDs. Perilipin 2 is thought to be a general marker for the lipid load in non-adipose tissue, and transcription of the perilipin 2 gene is upregulated by all three PPARs (α, γ, and δ) (24). LD formation, however, is still not fully understood. It is thought that LD are synthesized between the leaflets of the ER bilayer. As soon as they reach a critical concentration, the nascent LDs bud of into the cytoplasm, where they can interact with mitochondria in times of metabolic demand. Whether LD remain associated with the ER or separate immediately after their formation and whether LD biogenesis occurs at specific ER regions remains to be defined. (22, 25, 26)

1.1.2.3 Hepatic FA metabolism

The liver plays a major role in lipid metabolism as hepatocytes take up FAs mainly from two sources: Either via hydrolysis of TG, which are transported by gut-driven chylomicrons during the postprandial period or via adipose tissue-derived lipolysis in the fasted state. Furthermore, hepatocytes possess the ability to generate FAs from excess glucose via DNL or lipolysis of hepatic TGs.

1.1.2.4 FA uptake

Beside DNL, hepatic FAs can also be recruited from the plasma pool. The rate of FA uptake from the plasma, however, depends on plasma FA concentrations as well as hepatocellular capacity. During the fasted state, adipocyte-derived lipolysis is stimulated by catecholamines, natriuretic peptides, and glucagon, while it is repressed by insulin in the fed state (27). In insulin-resistant individuals, enhanced lipolysis leads to increased plasma FA concentraions independent of the nutritional state (28, 29). FAs are taken up by hepatocytes in a facilitated fashion rather than by passive processes (30). The number and activity of transporter proteins also determines successful FA uptake. Specific fatty acid transporters (FATPs), caveolins, fatty acid translocase (FAT)/CD36, and fatty acid-

binding proteins (FABPs) are expressed on the sinusoidal plasma membrane of hepatocytes. FATP2 and FATP5 are highly expressed in the liver and most likely facilitate the majority of hepatic FA uptake (31). FAT/DC36 is a membrane glycoprotein present on platelets, mononuclear phagocytes, adipocytes, and hepatocytes, contributing to FA uptake (32).

1.1.2.5 FA oxidation

Oxidation of FAs takes place within mitochondria, peroxisomes or the ER and facilitates degradation of activated FAs to acetyl-CoA as a rapid and effective way to generate energy. Recycled cellular components as well as catabolized lipoproteins and TG, normally stored in adipose tissue, are transported to the liver via specific FATPs (33). The process of FAs being activated by acyl-CoA synthetase to acyl-CoA is indispensable for enabling FAs to cross membranes and enter organelles. In general, short-, medium-, and long-chain FAs are oxidized within mitochondria, while toxic and very long-chain FAs (LCFAs) are oxidized within peroxisomes (34, 35). CPT1, which mediates the transfer of activated LCFAs, is a rate-limiting enzyme in mitochondrial FA oxidation. Malonyl-CoA, an early intermediate of DNL that accumulates upon insulin receptor activation, is an allosteric inhibitor of CPT1 (36). Hence, in the fed state, FA oxidation is inhibited and DNL promoted, allowing storage and distribution of lipids (37). During FA oxdiation, electrons are indirectly donated to the electron transport chain to drive ATP synthesis. The resulting acetyl-CoA can be further used in the TCA cycle, or if FAs are abundant, converted into ketone bodies (38). In the liver, PPARα is involved in the regulation of FA oxidation and the formation of ketone bodies via transcriptional regulation of mitochondrial 3-hydroxy-3-methyl-glutaryl-coenzyme A (HMG-CoA) synthase. Interestingly, succinyl-CoA, an intermediate of the TCA cycle, inactivates HMG-CoA synthase by succinylation. Furthermore, PPARα upregulates the expression of genes involved in mitochondrial and peroxisomal FA oxidation and mediates hepatic fat storage (39, 40).

1.1.3 Cholesterol metabolism and reverse cholesterol transport

In general, the majority of intracellular cholesterol is esterified with FAs by ACAT enzymes, which catalyze the formation of CE from cholesterol and fatty acyl-CoA (41). An abundance of cholesterol consequently promotes FA production for its esterification. In hepatocytes, FA as well as cholesterol metabolism are tightly regulated via liver-specific X receptor (LXR) and oxysterols. These are oxidized derivatives of cholesterol and act as endogenous agonistic ligands of LXR (42, 43). Plasma LDL-cholesterol (LDL-C) is taken up by hepatocytes via the LDL receptor-mediated pathway. Cholesterol homeostasis in the body is tightly controlled as uptake of dietary cholesterol in chylomicron remnants results in the suppression of the cholesterol-synthesizing system in the liver. Furthermore, cholesterol synthesis is regulated through the circadian rhythm, being two- to threefold higher during the dark phase, with a peak in synthesis few hours after food intake (44).

Cholesterol production is regulated by SREBPs, which bind the nuclear sterol-response element (SRE) when cells are depleted of sterols and activate the transcription of genes involved in cholesterol synthesis (45, 46). The major isoform expressed in the liver is SREBP-1c and has overlapping functions with SREBP-2. While SREBP-1c activates the transcription of genes regulating FA biosynthesis, SREBP2 is more involved in cholesterol metabolism (46, 47). SREBP2 synchronously activates the gene expression of LDL receptor (LDLR) and HMG-CoA reductase (HMGCR), a key enzyme in cholesterol synthesis. Accumulation of cholesterol in hepatocytes and activation of LXRα downregulate SREBP2 activity by reducing cholesterol synthesis and uptake (48). For secretion into serum, cholesterol together with TG and apolipoprotein B (apoB) is packed into VLDL particles via microsomal triglyceride transfer protein (MTP). Alternatively, cholesterol is secreted into bile via the ATP-binding cassette (ABC) transporters ABCG5 and ABCG8 (49). Another protein essential for the absorption/reabsorption of cholesterol from bile is Niemann-Pick C1-like 1 (NPC1L1) (49, 50).

The process of transferring cholesterol from extra-hepatic tissue back to the liver, where it is converted to bile acids and excreted via the feces, is called reverse cholesterol transport (RCT). The transport is mainly facilitated by HDL. The main component of HDL particles is apoA1, which binds lecithin-cholesterol acyltransferase (LCAT) (51), ABCA1 (52) and the scavenger receptor BI (SR-BI) (53). Nascent HDLs have a discoidal shape and

undergo a multistep process of maturation exchanging cholesterol, TG, CE with potentially atherogenic LDL and VLDL particles (52, 54).

1.1.4 Lipoprotein metabolism

Lipoprotein metabolism starts with the intestinal absorption of dietary lipids. In order to cross the intestinal lumen into the plasma, dietary lipids need to be emulsified by bile acids, which are synthesized within the hepatocyte and secreted into the bile duct. Hydrolyzed lipids are then absorbed by enterocytes, where they become re-synthesized and packed into chylomicrons. Nascent chylomicrons are secreted into the lymphatic system and enter the circulation within two hours after food intake (55). While circulating in blood, chylomicrons exchange apo E and apo C-II with circulating HDL particles, converting them into mature chylomicrons (56). Apo C-II activates adipocyte lipoprotein lipase (LPL) which further promotes hydrolysis of TG into FA and glycerol (57). FA are partly taken up and stored in adipocytes, while chylomicron remnants re-enter the blood stream. Apo E is recognized by the hepatocyte LDLR, the LDLR related protein and SR-BI to facilitate endocytotic uptake of the chylomicron remnants. Their lipid content gets further hydrolyzed and is used for the synthesis of new VLDL particles (58, 59).

VLDL particles are formed from the hepatic lipidation of apo B-100 with TG, PL, and CE (60) and follow the same route as chylomicron remnants. They acquire apo C-II and apo E from HDL particles and release FA to muscle and adipose tissue after LPL activation. Finally, VLDL particles are transformed to intermediate density lipoproteins and removed from the blood stream by the liver. Alternatively, after further lipase activity, VLDL can become LDL particles and they can be taken up via the LDLR-mediated endocytosis pathway (61-63).

1.2 Pathology of the liver

The prevalence of the metabolic syndrome has become a major health burden in the western civilization in adults as well as in children (64, 65). An imbalance between energy uptake and removal leads to energy storage in the form of fat in adipose tissue. Consequently, insulin resistance drives the pathogenic event responsible for developing the metabolic syndrome, which is characterized by obesity, increased fasting plasma glucose, type 2 diabetes, hypertriglyceridemia, low HDL cholesterol, and NAFLD (66-68). Similar to the metabolic syndrome, NAFLD is associated with both type 2 diabetes and cardiovascular disease (69-71).

In the western civilization 15-46% of adults suffer from NAFLD (72, 73) and between 1997 and 2014 the number of NAFLD has increased by 5-fold (74). Moreover, NAFLD is found in 70-80% of obese and diabetic patients with alterations in hepatic lipid metabolism (75). NAFLD represents the most prevalent liver disease ranging from simple steatosis, defined by the absence of substantial inflammation and fibrosis (76), to non-alcoholic steatohepatitis (NASH), which is characterized by varying degrees of hepatic inflammation, ballooning of hepatocytes, and fibrosis in addition to hepatic steatosis (Figure 2). Hepatic steatosis is defined as an intrahepatic accumulation of TG and was long thought to be the first step in the 'two hits' hypothesis and further progression toward fibrosis and cirrhosis due to liver inflammation and damage (77). Recently, this paradigm has been replaced by a multiple 'parallel hits' model also as emerging evidence points to FAs and their metabolites being drivers of liver damage (21). In addition, the increased amount of FAs causes lipotoxicity via the induction of ROS release, which causes inflammation and the progression to NASH and fibrogenesis (78). Simple hepatic fat accumulation alone can therefore not be used as prognostic tool and has now been separated from NASH (79). In conclusion, NAFLD and NASH follow two distinct pathways with inflammation, lipotoxicity, and fibrosis being their main differences (21, 79).

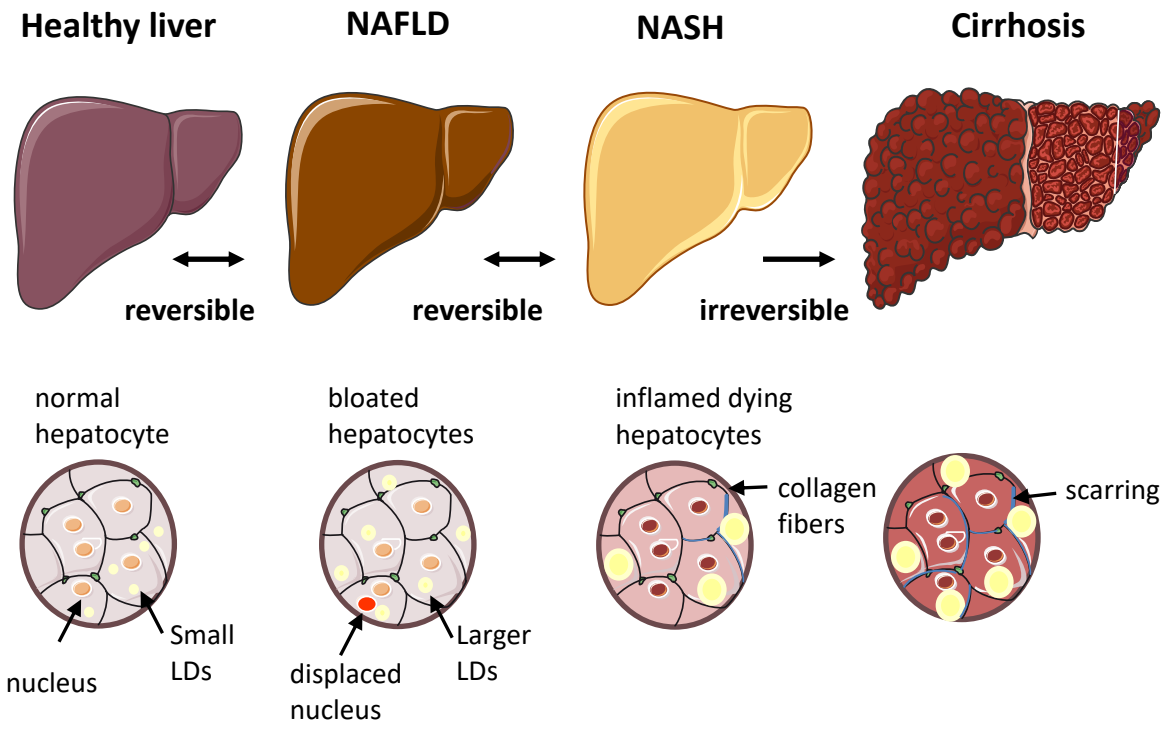

Figure 2: Different stages of liver damage.

While normal hepatocytes contain small LD the progression to NAFLD starts with an accumulation of cytosolic LDs and subsequent displacement of nuclei in hepatocytes. When further progressing to NASH, the accumulation of lipids gets even worse and as a response, the tissue starts to produce collagen fibers around dying hepatocytes. The last and irreversible step in the progression of liver damage is cirrhosis, which ultimatively leads to hepatocellular carcinoma and requires liver transplantation.

1.3 Hepatic lipid and glucose metabolism in NAFLD

Patients suffering from NAFLD typically exhibit a pro-atherogenic lipid profile, characterized by high VLDL, reduced HDL and increased LDL concentrations. This is often associated with hyperinsulinemia, which in turn increases lipolysis and FA transport to the liver, thereby enhancing hepatic lipogenesis while simultaneously suppressing VLDL secretion (80). Numerous studies in NAFLD patients have shown that an increased hepatic uptake of FAs from peripheral adipose tissue and an augmented DNL cause hepatic TG accumulation when FA oxidation and VLDL secretion are not balanced (81, 82). In the presence of NAFLD and insulin resistance, hepatic LPL is upregulated and the production of small dense LDL particles is increased (83, 84). In addition, reduced hepatic LDLR expression increases the number of circulating LDL particles, which is a typical feature of atherogenic dyslipidemia. Hyperinsulinemia decreases HDL synthesis and enhances HDL particle uptake, leading to a reduction in the overall effect of improved HDL levels in plasma (85, 86).

FAs mainly derive from the circulation or DNL. Increased adipose tissue lipolysis in obese individuals elevates plasma FAs leading to augmented FA uptake. Additionally, increased hepatic DNL further contributes to hepatic steatosis development. Interestingly, elevated dietary lipid intake also adds to hepatic lipid accumulation accounting for 15% of the lipid content within the steatotic liver (87). Obesity and intrahepatic fat accumulation lead to a reduction of mitochondrial function and formation of ROS, which are both known to induce Kupffer cell activation, hepatic inflammation, and hepatocyte apoptosis (88). Abnormal mitochondrial function and mitochondrial metabolism is enhanced in NAFLD by 50 and 30% with regard to lipolysis and gluconeogenesis (89, 90). In addition to mitochondrial dysfunction, ER stress has also been linked to hepatic inflammation and metabolic disease progression (91). Incorporation of saturated phospholipids into the ER membrane causes loss of functionality, activates the unfolded protein response stress signaling pathway, thereby further disrupting mitochondrial function (92).

Hepatic inflammation is the final result of this intracellular dysregulation inducing transcriptional upregulation of proinflammatory cytokines, such as interleukin-6 (IL-6), tumor necrosis factor α (TNFα) and its receptor (93). TNF receptor activation increases

hepatic lipogenesis and lipid accumulation via SREBP-1c induction (94). TNFα and IL-6 production are increased in adipocytes of obese patients and those with insulin resistance, contributing to the overall pool of released cytokines (95, 96). Adiponectin and leptin, two adipokines with a protective role in inflammation and lipotoxicity, however, are reduced (97, 98). In patients with NASH, the anti-inflammatory and anti-diabetic effects are impaired as serum adiponectin levels are reduced. Moreover, mRNA expression of adiponectin and its specific receptor ADIPOR2 are lower in patients with NASH compared to those with NAFLD (34, 99).

While it seems that hepatic TG accumulation is a benign symptom of hepatic steatosis, FAs and their metabolites play a major role in the progression of NAFLD. One possibility to maintain hepatic lipid homeostasis is autophagy (100). Autophagy is a highly regulated catabolic process important for balancing sources of energy at critical times in development and in response to nutrient stress. It targets cellular components, including proteins, lipids, carbohydrates, and nucleic acids to the lysosome for degradation (101). Recently, autophagy was described to be highly relevant to the pathogenesis of NAFLD, including regulation of cellular insulin sensitivity, metabolism of cellular lipid stores, mediation of hepatocyte resistance to injurious stimuli such as oxidants and cytokines, and prevention of over activation of the innate immune response (102-104). Autophagy can be either non-selective or selective in the removal of specific organelles, ribosomes and protein aggregates. However, the mechanisms regulating autophagy are still not fully understood. Autophagy is initiated by the formation of a sequestering membrane which leads to an autophagosome formation. The subsequent fusion of this autophagosome with a lysosome creates an autolysosome and leads to the degradation of the cytoplasmic cargo (105) (Figure 3). In 2009, lipid droplets (LDs) were identified in double-membrane vesicles suggesting for the first time a role of autophagy in regulation of lipid mobilization and metabolism. This process was termed lipophagy (100). To date, lysosomal acid lipase (LAL) is the sole lipase known to be involved in CE, TG, DG and retinyl ester (RE) hydrolysis at acidic pH in mammalian lysosomes and plays a key role in lipophagy and lipid metabolism (106-108).

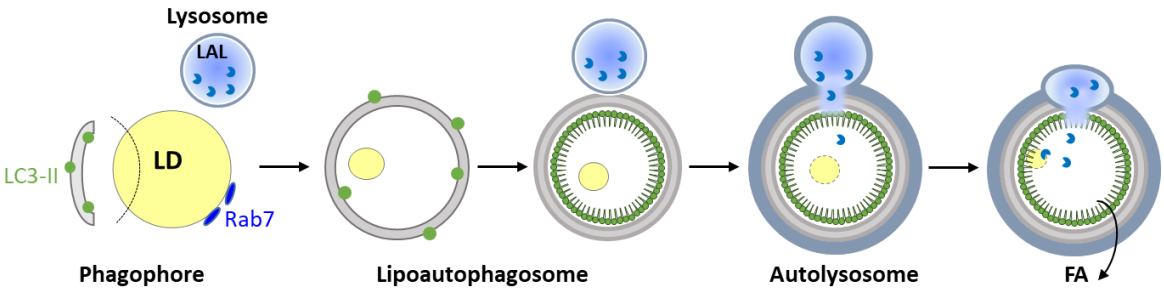

Figure 3: The process of lipophagy.

Microtubule-associated protein 1A/1B-light chain 3 (LC3)-II-positive membranes, which originate from ER membranes, engulf small lipid droplets (LDs) or sequester portions of large LDs. Lipoautophagosomes fuse with lysosomes to autolysosomes. Lysosomal acid lipase (LAL) degrades the lipid cargo. Non-esterified fatty acids (FA) are released into the cytosol. Alternatively, lysosomes directly bind to „primed“ LDs in a process that requires ras-related protein 7 (Rab7).

1.4 Lysosomal acid lipase

Lysosomes are major degradative compartments of eukaryotic cells and were first described by Christian de Duve et al. (109) as vesicular structures. They have an acidic lumen, which is surrounded by a single bilayer lipid membrane and contains proteins that are either involved in transport of substances into and out of the lumen, acidification of the lysosomal lumen, or fusion of the lysosome with other cellular structures (110). In addition to cellular clearance and secretion, the lysosome mediates a range of biological processes, such as plasma membrane repair, cell homeostasis, energy metabolism, and the immune response. In contrast to the proteasome, lysosomes degrade a wide variety of structurally diverse substances, such as proteins, glycosaminoglycans, nucleic acids, oligosaccharides, and complex lipids for balancing energy at critical times during development and in response to nutritional stress (111). The lysosomal system is the main intracellular machinery for catabolizing endogenous and exogenous macromolecules and subsequent recycling of constituent monomeric components.

The lysosomal lumen contains approximately 60 different soluble hydrolases, which are only active at acidic pH. They include members of protein families such as sulfatases, glycosidases, peptidases, phosphatases, lipases, and nucleases. Mutation in genes encoding these enzymes are responsible for a group of over 70 autosomal recessive human genetic diseases, which are referred to as lysosomal storage diseases (LSDs) (112).

The ability of specific targeting as well as uptake via the mannose-6-phosphate receptor is the basis for enzyme replacement therapy in LSDs (113, 114). One of these enzyme mutations leading to LSD are mutations in *LIPA*.

LIPA, the gene encoding LAL, has a size of approximately 36.5 kb and is located on the human chromosome locus 10q23.2-23.3 (115-117). Human LAL cDNA encodes a 372 amino acid mature protein and a 27 amino acid signaling sequence (118). Different molecular weights have been reported for purified human LAL due to its diverse glycosylation grades between cell types and localization (118, 119). Two molecular forms (46 and 41 kDa) have also been reported for human LAL expressed in insect cells (106), and three molecular forms (49.3 kDa, 50.66 kDa, and 51.24 kDa) have been reported for human LAL expressed in tobacco leaves (120). The protein is synthesized in the rough ER and is co-translationally glycosylated as it proceeds into the ER lumen (121, 122). Following the cleavage of the leader sequence (21 amino acids), oligosaccharides that are remodeled during transit through the Golgi apparatus are added to the enzyme. Post co translational glycosylation in the ER and attachment of mannose-6-phosphate residues in the Golgi apparatus, LAL is targeted to pre-lysosomal compartments (106, 122), where it is active as monomer without requiring co-factors for optimal hydrolysis (115).

Loss of function mutation of LAL results in a deficient regulation of intracellular cholesterol pools with subsequent up-regulation of the endogenous cholesterol synthesis and LDL receptor activity. Affected cells become overloaded with cholesterol, resulting in fibrosis and ultimately cell death (121). Complete deficiency of LAL in patients results in WD, which is fatal in the first year of life, while near-total and non-fatal deficiency is known as CESD. Both WD and CESD share common genetic and enzymatic abnormalities (123). While phenotypic expression of the disease depends on residual LAL activity, the genotype-to-phenotype relationship has not been fully elucidated. The amount of CE and TG in tissues appears to be directly proportional to the severity of the disease and inversely proportional to the age of onset.

1.4.1 LAL deficiency in humans

1.4.1.1 History

The first case reports of LAL-D described xanthomata in the liver, adrenal glands, spleen, bone marrow, small intestine, lymph nodes, lungs, and thymus in three siblings (124, 125). The affected children died with three months of age and showed changes in the skin, retina, and central nervous system. The adrenal glands were calcified while blood lipids were normal or moderately elevated. The term primary familial xanthomatosis was used to describe these patients (124, 125). In 1946, a similar patient had been described by Alexander having Niemann-Pick disease, but due to the calcified adrenal glands, this patient most likely was misdiagnosed and rather had Wolman disease (WD) (126). In the following years, three more cases of infants failing to thrive, with foam cell formation and high cholesterol deposits in their bone marrow and other organs, lymphocytes in peripheral blood, as well as with adrenal calcifications were reported. The authors diagnosed these patients with WD, thereby replacing the initial term of primary familial xanthomatosis (127).

In parallel, less severe variants of older patients presenting with similar features were reported. In 1968, Schiff and colleagues (128) described six siblings. While the eldest brother and sister had orange livers with septate cirrhosis and excess deposition of CE, the four younger siblings only showed milder changes. These variants ranged in age from the first to the fourth decade and were associated with hepatomegaly and increased hepatic CE levels. Later, also Partin and Schubert used the term CE storage disease (CESD) for such variants (129). In the following 20 years, further cases of CESD started emerging around the world, including Argentina (130), Czech Republic (131), France (132), Germany (133), Ireland (134), North America (135), and Thailand (136). Only later, it was recognized that both WD and the later-onset CESD share the same molecular defect that results from autosomal recessive mutations in the *LIPA* gene. Therefore, WD as well as CESD are now termed LAL deficiency (LAL-D) (123). [reviewed in (137)]

1.4.1.2 Epidemiology

The exact prevalence of LAL-D is still unknown. Reiner and colleagues (138) first reported it to be one in 40 000 to 300 000. However, the mutations vary widely depending on ethnicity and geographical location (139-142). To elucidate the true prevalence of LAL-D, analyses of the frequency of the commonly identified *LIPA* mutations have been carried out. More than 50 mutations have been described, including missense and nonsense mutations as well as splicing errors and small deletions. Different types of mutations result in variable expression and activity of LAL (143). Thirty-seven percent of the 19 known mutations causing WD are small deletions or insertions, with 26% nonsense, 21% consensus splice-site mutations, 10% missense lesions, and 5% large deletions (144). However, 50% of the 32 known CESD mutations are missense, with 25% small deletions or insertions, 16% nonsense, 6% consensus splice-site mutations, and 3% large deletions (145, 146). Usually, affected patients have either homozygous or compound heterozygous *LIPA* mutations (138, 147). The exon 8 splice junction mutation (E8SJM) (c.894G>A) is the most common one (50-70% of LAL-D patients), resulting in a mutant enzyme that retains 2–5% activity in homozygote carriers (148-151). The mutation causes a deletion of exon 8 in mRNA by presenting an alternative acceptor splice site. The presence of residual LAL activity can be explained by the fact that some mRNA is spliced properly.

1.4.1.3 Pathogenesis

LDL-C and VLDL-C are taken up by hepatocytes via LDL receptor-mediated endocytosis and are targeted to the lysosome for acid lipolysis (Figure 4). During acid lipolysis LAL plays a major role in lipid metabolism through the hydrolysis of CE and TG at an acidic pH in mammalian lysosomes (106). Other known substrates for LAL hydrolysis are RE, and diacylglycerols, however if also monoacylglycerols are a target it still under debate (108, 152, 153).

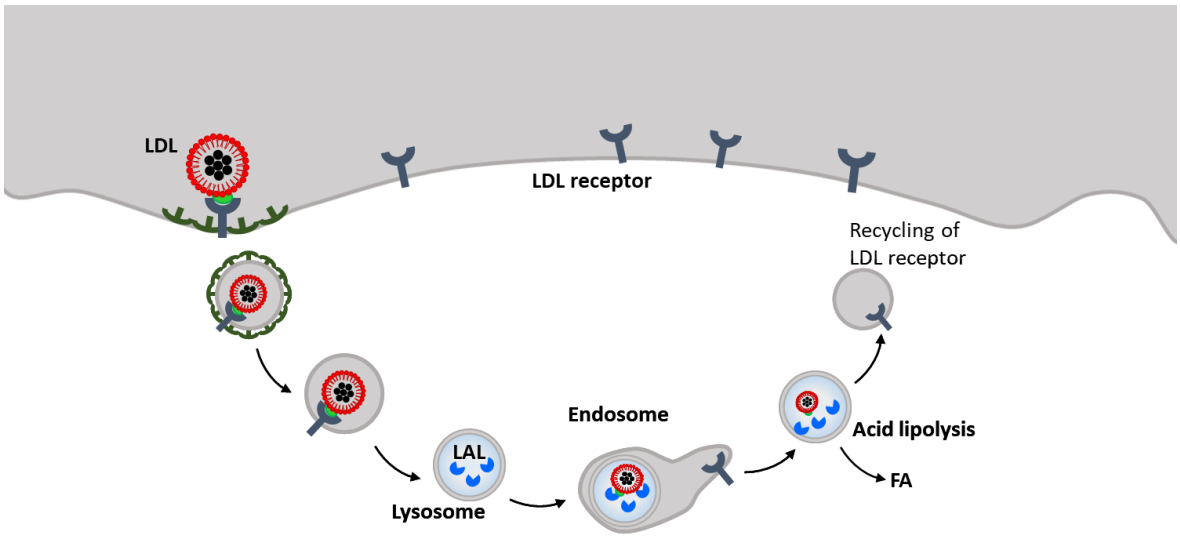

Figure 4: Acid lipolysis.

LDL particles bind to the LDL receptor and get internalized. After receptor-mediated endocytosis of the LDL particle the lysosome fuses with the endosome to degrade its cargo. During acid lipolysis CE and TG are hydrolyzed by LAL in the lysosome to release FA into the cytosol. The LDL receptor gets recycled for further uptake of lipoproteins.

The generated lipids and their precursors (e.g. FAs and un-esterified cholesterol) are important for catabolic, anabolic, and signaling pathways (154). Moreover they can also act as critical mediators of cellular cholesterol homeostasis (155). These lipids further stimulate transcription factors (e.g. SREBPs) that regulate the expression of genes controlling the synthesis and the uptake of cholesterol (156). Abundance of free cholesterol normally results in decreased entry of cholesterol into the cell as SREBP-2 downregulates LDL receptor expression. As a result, feedback inhibition of HMGCR-mediated cholesterol synthesis is decreased. Simultaneously, stimulation of ACAT results in enhanced cholesterol esterification. At the same time, abundance of intracellular FAs leads to SREBP1c-mediated downregulation of PL and TG production (47). Reduced levels or the absence of LAL activity on the other hand is associated with CE and TG accumulation within lysosomes. In addition, lack of intracellular free cholesterol leads to SREBP-mediated upregulation of endogenous cholesterol production by HMGCR and enhanced endocytosis via LDL receptor. Abnormal lipid profile (dyslipidemia) in patients with LAL-D is characterized by elevated serum total cholesterol, high LDL-C, low HDL-C, and elevated TG concentrations (157). Accumulation of CE in lysosomes of LAL-D patients leads to reduced activation of ABCA1 expression as well as decreased free cholesterol in

the subcellular compartments and in the plasma membrane that is available for HDL particle formation. Treatment with conditioned medium containing LAL from fibroblasts or with recombinant human LAL rescued ABCA1 expression, apoA-1-mediated cholesterol efflux, HDL particle formation, and the production of 27-hydroxycholesterol by CESD human skin fibroblasts (158). These observations may explain reduced HDL-C levels in patients with LAL-D and support the evidence that the rate of cholesterol release from late endosomes or lysosomes is a major regulator of ABCA1 expression and activity (158). The lipid profile of these patients is often similar to those of individuals with Fredrickson type 2a and 2b familial hyperlipidemia. However, premature death is due to liver failure and/or accelerated atherosclerotic disease rather than to chronic hyperlipidemia (147, 149, 159, 160).

1.4.1.4 Clinical features

The reported cases for WD are quite uniform. Affected patients present with symptoms within the first few days to the first month of life. Usually the first sign is persistent vomiting accompanied with watery diarrhea, occasional jaundice, and low-grade fever. These signs lead to massive weight loss, cachexia, and malnutrition (124, 127, 161), irrespective of medical or dietary interventions. Abdominal magnetic resonance imaging (MRI), computed tomography (CT), or radiography also disclose massively enlarged homogeneous livers and spleens with mesenteric and periaortic lymph node hypertrophy (136). Hepatosplenomegaly with massive liver enlargement is evident as early as the first week postpartum (162). There is even some evidence of WD in utero, including adrenal necrosis, polyhydramnios, CE accumulation, and microvesicular steatosis (163). Massive enlargement and calcification of the adrenal glands on abdominal radiographs is a hallmark of WD (127). Adrenal infiltration leading to necrosis in the fetal stage could be the precursor of the adrenal calcification described in about 50% of infants born with the condition (144, 147, 164). Adrenal glands of WD patients have punctate calcification throughout their parenchyma and are symmetrically and massively enlarged, but they retain their semilunar/pyramidal shape and children can manifest adrenal cortical insufficiency (162, 165). Intestinal malabsorption coupled with hepatic

impairment and adrenal insufficiency explain the terrible prognosis as the median life expectancy of an infant with WD is three to seven months (166).

Unlike WD, patients with CESD have residual LAL activity of 1–12% and present much later in childhood or adulthood. Clinical features are highly variable including dyslipidemia, accelerated atherosclerosis, portal hypertension, gastrointestinal disturbances, abnormal hepatic function, hepatosplenomegaly, hepatic fibrosis and cirrhosis, and decompensated liver disease (130, 135, 164, 167). This variety often leads to misdiagnosis of patients having NAFLD, NASH, hereditary dyslipidemia, or cryptogenic cirrhosis (157, 168, 169). Progressive hepatic fibrosis is associated with massive accumulation of TG and CE in lysosomes of hepatocytes, Kupffer cells, and periportal macrophages (Figure 5) (147).

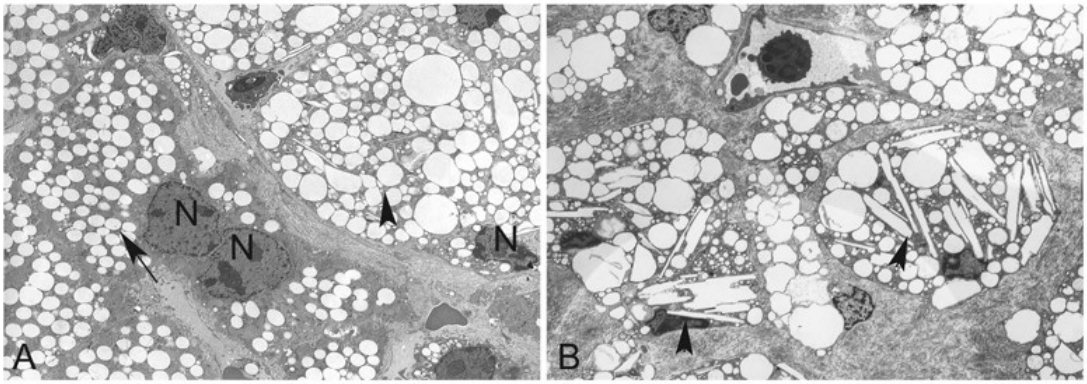

Figure 5: Electron micrographs of liver sections from a patient suffering from LAL-D.

Ultrastructural analysis of a liver showing more uniform, smaller inclusions in hepatocytes (arrow in A) compared to larger vacuoles of more variable size in Kupffer cells (arrowhead in A). Arrowheads in B show cholesterol-containing crystals/clefts in lysosomes of hepatocytes, Kupffer cells and periportal macrophages (electron lucent structures), and ceriod-containing structures (electron dense structures). N=Nucleus (147). Requisite permission to use this figure was obtained (Appendix).

Himes et al. (170) reported two children with NAFLD who managed to reduce their weight by adopting healthy diet and exercising. However, the improved body mass index was not followed by changes in hepatic biochemical markers. A liver biopsy displayed intense microvesicular steatosis, and the diagnosis of LAL-D was confirmed by measuring LAL activity and *LIPA* gene testing. These cases demonstrate the importance of increased awareness of LAL-D among clinicians and emphasize the need to consider LAL-D in the differential diagnosis of common hepatic disorders, such as NAFLD and NASH, especially when liver parameters do not improve despite appropriate life style interventions. Beside

hepatomegaly, hyperlipidemia might be the only consistent chemical abnormality in CESD. In a large case study, the clinical features of 135 patients with LAL deficiency were investigated. Hepatomegaly was identified clinically or by imaging modalities in 134 out of 135 subjects, and total cholesterol was elevated in all 110 patients for whom increased serum cholesterol concentrations were reported (144).

1.4.1.5 Diagnosis

Diagnosis of LAL-D is challenging due to the diverse clinical presentations. Beside measurement of serum transaminases, liver biopsy is commonly performed during the diagnostic process in patients who might have LAL-D. However, liver biopsy carries some morbidity and very little mortality risk (171). A less invasive approach as well as an alternative to repeated liver biopsies in patients with LAL-D is MRI. Thelwall et al. demonstrated that MRI can identify and quantify the hepatic lipid features associated with LAL-D. Following treatment with sebelipase alfa (LAL replacement therapy), a substantial reduction in hepatic CE was observed in LAL-deficient mice (172).

LAL enzyme activity can be measured in cultured liver tissue, fibroblasts, or peripheral leukocytes. Due to low sensitivity of the substrate 4-nitrophenyl palmitate, this technique might not be very accurate. A relatively new diagnostic tool is dried blood spot (DBS) testing that can measure LAL activity in peripheral leukocytes and patients with LAL-D have been successfully identified with DBS (173). LAL activity is measured using the fluorimetric substrate 4-methylumbelliferyl palmitate. As other lipases in the blood may also affect the measurement of LAL activity, two studies (173, 174) screened 40 000 different potential inhibitors of LAL. They only identified Lalistat 1 and 2 as specific competitive inhibitors of LAL. To determine LAL activity, it is measured in the presence and absence of Lalistat 2 and the total lipase activity in both situations is compared. DBS reflects the total activity in blood including peripheral leukocytes and has several advantages, including long-term stability and the requirement of only a small blood sample. Therefore, DBS is a promising diagnostic modality that can be also used in the future for newborn screening (166).

Furthermore, LAL-D can be diagnosed by comprehensive sequencing of the coding regions of *LIPA* (147). However, screening for the most common mutation E8SJM may fail

to detect affected individuals, as only 50-70% of mutant alleles carry this mutation. Moreover, E8SJM has a low prevalence in some populations, such as Asians and African Americans (141). The possibility of an intronic mutation, which is a nucleotide sequence within a gene that is removed by RNA splicing during maturation of the final RNA product, can be problematic as this type of mutation may not be detected with regular genetic screening. By determination of the genotype, WD can be distinguished from CESD, but it does not predict residual enzyme activity since varying levels of LAL enzyme activity have been reported in patients with the same genotype. Similarly, measuring residual LAL enzyme activity is not effective in predicting the course of the disease as the severity of the disease vary significantly among patients with similar enzyme level and exact parameters are still missing (156).

Histopathological analysis often reveals intense microvesicular steatosis in liver biopsies from patients with LAL-D. However, microvesicular steatosis is not specific for LAL-D as it can be associated with multiple disorders. Other specific features in LAL-D patients include hypertrophic Kupffer cells and portal macrophages with a periodic acid-Schiff-positive foamy tan-colored cytoplasm. The presence of luminal and membrane lysosomal markers around lipid vacuoles in fixed paraffin-embedded material, as well as CE crystals in unfixed samples, is pathognomonic for LAL-D (175).

1.4.1.6 Treatment

1.4.1.6.1 Lipid lowering agents

Dyslipidemia is a hallmark feature in patients with LAL-D and lipid-lowering therapies are widely used in these patients. Statins (HMG-CoA-reductase inhibitors) are the number one prescription agents in lowering LDL-C and decreasing the risk of cardiovascular disease in patients with dyslipidemia (176). Statins were also used as monotherapy or in combination with other lipid-lowering agents (e.g. Ezetimibe) in patients with LAL-D, yet mixed results were found. While Ginsberg et al. (177) reported reduced LDL and VLDL concentrations in a nine-year-old female LAL-D patient on lovastatin therapy for six months, no change or an actual increase of LDL were described in other reports (178-182). Improvement of hepatomegaly was reported in patients with LAL-D. However, statins did not improve liver histology or stop the progression of liver

fibrosis (183). Reduced LDL-C levels (15%) were reported in a 18-year-old boy affected with LAL-D after 80 months of treatment with lovastatin. After the addition of ezetimibe (10 mg), a cholesterol absorption inhibitor, to lovastatin (40 mg) an additional decline of LDL-C could be observed (179).

1.4.1.6.2 Enzyme replacement therapy

Enzyme replacement therapy (ERT) has already been shown to be effective for several metabolic disorders, such as Gaucher's disease and Fabry's disease. Sebelipase alfa (Kanuma®) is a recombinant hLAL that has been expressed in egg whites from transgenic hen oviduct cells (116). It is a glycoprotein with a molecular weight of 55 kDa, including mannose-terminated N-linked glycan structures. The glycan element enables targeted delivery of LAL to the lysosomal compartment through mannose 6-phosphate receptors and the mannose receptor on reticuloendothelial cells (184). Infusion of recombinant hLAL in a mouse model mimicking LAL-D resulted in histological improvement in several tissues, including Kupffer cells (185). To date, eight clinical investigations with sebelipase alfa have been initiated but only two investigated the effects of ERT in infants with WD (186, 187). Nine infants were treated with sebelipase alpha of whom six reached the primary endpoint of survival at one year. Five patients survived beyond two years. Preliminary data further showed improvements in liver function tests, platelets, albumin, hemoglobin, body weight, degree of hepatosplenomegaly, gastrointestinal symptoms, and developmental screening scores after treatment. [reviewed in (137)]

For late-onset CESD patients, the success of ERT is better established and there are currently six trials ongoing. Balwani and colleagues treated nine patients with four intravenous infusions of sebelipase alpha 0.35 mg/kg, 1 mg/kg and 3 mg/kg once a week (LAL-CL01) (187). Those patients, who successfully completed the LAL-CL01 study, were able to enroll in the extension trial (LAL-CL04). After a median washout period, patients resumed therapy with the same dose for another four weeks before getting infusions (1 mg/kg or 3 mg/kg) every other week for another 12 weeks (188). The seven patients who completed 12 weeks of treatment showed reductions from baseline in mean aspartate aminotransferase (AST) and alanine aminotransferase (ALT) concentrations, TG, total

cholesterol (TC), and LDL-C, as well as increases in HDL-C concentrations. All seven patients had adverse events, including headache, nausea, and diarrhea. This cohort was further treated with infusions every other week for 52 weeks, demonstrating the long-term efficacy of this treatment (188). There is also evidence for continued efficacy beyond 52 weeks, with preliminary reports showing statistically significant improvements in liver function tests and lipid profiles after 78 weeks (189) and 90 weeks (190) of this long-term extension study.

Another study investigated the effectiveness of sebelipase alfa in the phase 3, multicenter, randomized, placebo-controlled ARISE trial in 66 adults and children (NCT01757184 (191)). Patients received an infusion of 1 mg/kg every other week for 20 weeks, followed by an open-label period for 16 weeks, during which both groups received treatment. The treatment group had a significant normalization of ALT, AST, and lipid parameters as well as an improvement of hepatic fat content, steatosis, and liver volume. There were no reported deaths during the study period and the most common side-effects were headache, fever, and diarrhea. An open-label extension of this trial included 65 patients who continued treatment for up to 130 weeks. After 52 weeks of treatment with sebelipase alfa, concentrations of ALT and AST normalized in 47% and 56% of patients, respectively (192). Twenty-five% of patients showed reductions in baseline hepatic fat and 13% in hepatic volume. Twenty patients who had a biopsy at baseline and after 52 weeks were assessed for the degree of hepatic fibrosis, which was reduced with longer exposure to the drug. Regression of liver fibrosis by at least one stage was also seen in four patients with 30 weeks of exposure and in eight patients with 52 weeks of exposure (193). The long-term 76-week data from the ARISE study (LAL-CL02) suggest that improvements were sustained at 76 weeks, with normalization of ALT and AST in 52% and 65% of patients, respectively, as well as improvements in total cholesterol, LDL, and HDL concentrations (191, 194). [reviewed in (137)]

These data may indicate that Kanuma® therapy can halt or even reverse the advancement of liver damage. The importance of early recognition as well as prompt and long-term treatment with Kanuma® is evident as the greatest effect was observed in those patients with substantial liver fibrosis at baseline. However, the outcomes of long-term therapy still need to be determined. Despite significant improvements in the lipid profiles of the included subjects, the question remains if long term therapy will prevent

and/or decrease cardiovascular disease morbidity and mortality. Another question is what the effect of therapy on patients with advanced liver disease, decompensated cirrhosis, and liver comorbidities will be, as these patients were excluded (195). Currently, there is no recommendation regarding the use of sebelipase alfa during pregnancy. Although animal studies did not indicate any detrimental effects with respect to the reproductive system, it is advisable to avoid use of sebelipase alfa in pregnant women.

1.4.1.6.3 Stem cell or bone marrow transplantations

Stem cell or bone marrow transplantation can be a possible treatment for patients with LAL-D if performed early enough. Four WD patients, treated with hematopoietic stem cell transplantation (HSCT), were reported. Two of them are long-term survivors (four- and eleven-years-old) whose diarrhea resolved within weeks and also liver function and hepatosplenomegaly improved. Adrenal function was restored in one child and both children had normal adaptive functions. Unfortunately, one of the patients developed mild to moderate neurocognitive deficits (196). In another study, an infant with WD, who received unrelated HLA-mismatched umbilical cord blood-derived stem cells, survived until the age of four and LAL levels were restored back to normal (197). Other studies reported unsuccessful outcomes after HSCT mainly due to hepatic complications (198, 199).

1.4.1.6.4 Liver transplantations

Liver failure as one of the most prominent features in LAL-D can be treated with a liver transplant. In nine pediatric patients between 5 to 14 years of age, liver transplantation was reported (156). One of these children with LAL-D, who had a liver transplant did well after 4.5 years with only mild hypersplenism and elevated creatinine and blood urea nitrogen. While serum cholesterol normalized, TG concentrations remained elevated and after seven years, the patient developed end-stage renal disease. This was most likely due to glomerular sclerosis and atherosclerosis with extensive vascular lipid accumulation and tubular atrophy as well as interstitial fibrosis. By 21 years, the patient required chronic hemodialysis (200). Despite multiple different organ dysfunctions being connected with CESD, including kidney disease, (201, 202), this was

the first patient progressing to end-stage renal disease. One possible explanation might be the usage of cyclosporine, a known nephrotoxic immune suppressor, which destroyed kidney function and led to a rapid decline in renal function. In 1991, Arterburn et al. (203) reported a successful liver transplant in a 13-year-old child. In 1995, Leone et al. described a five-year-old boy who had 16% residual lysosomal acid lipase activity, severe hepatosplenomegaly, adrenal gland calcifications, hypercholesterolemia, hypertriglyceridemia, and increased ALT values. A low-fat diet, cholestyramine, and simvastatin were used as initial treatment. However, despite an improvement in lipid profile and a decrease in hepatomegaly, the patient's liver enzymes remained unchanged. He underwent successful liver transplantation after four years of medical therapy and was reported to do well ten months after, showing normal liver enzymes and lipid profile (204). In an adult woman, who was diagnosed with CESD during childhood, two liver transplantations were necessary to regain excellent liver function and a normal lipid profile without cardiovascular events. However, peripheral LAL concentrations remained low (205).

Regarding the long-term outcome of patients with LAL-D post-liver transplant information is lacking. Considering the fact that LAL activity may not normalize, the question remains whether the disease will recur in the graft. Renal failure is another concern, as it indicates that liver transplantation may only improve hepatic function but not systemic lysosomal lipid deposition. Therefore, close monitoring of cardiovascular, pulmonary, and renal functions is needed, taking into account that immunosuppressive therapy in transplanted patients may have adverse effects on multiple organs.

Summing up, many different treatment strategies are already available, which possess advantages and disadvantages, however, a lot more research is needed to finally diagnose and treat all patients with LAL-D adequately.

1.4.2 LAL-D in mice

Mouse and human LAL enzymes are encoded by ~3.2 kb and ~2.5 kb cDNA with 75% identity and 95% similarity of the amino acid sequences (116, 118, 206). Both enzymes encompass ten exons spanning 47.7 and 37 kb of genomic DNA with the same exon-intron organization (117, 207). The human gene was mapped on chromosome

10q23.2-23.3 and the mouse gene on chromosome 19 (115). In the mouse, LAL is expressed in the kidney (cortical tubes), adrenal glands (zona fasciculata and reticularis), and pancreas (acinar cells). High mRNA expression was detected in liver (hepatocytes and sinusoidal cells) and small intestine (enterocytes), while other organs with abundant LAL gene expression, showed this due to tissue-resident macrophages (spleen, thymus and uterus). Lowest expression was found in heart, tongue, ovary, and testis (206).

In contrast to humans, LAL-deficient ($Lipa^{-/-}$) mice are viable with a median life span of approximately one year. They exhibit hepatic TG and CE accumulation in various tissues and due to an abnormal lipid metabolism they show growth retardation, lack white adipose tissue (WAT) and progressively lose brown adipose tissue (BAT) (208). $Lipa^{-/-}$ mice display an enlargement of mesenteric lymph nodes with massive lipid accumulation. The hepatic phenotype is characterized by “microvesicular steatosis” and infiltration of Kupffer cells forming nests of “fatty lysosomes”. Extensive accumulation of hepatic cholesterol leads to the formation of CE crystals, which induce an inflammatory response (107). Additionally, the clearance of TG of endocytosed particles in the endosome rather than the lysosome might explain a much higher accumulation of hepatic CE vs. TG (40-fold vs 2-fold, respectively). The degree of different hepatic CE vs TG accumulation is also consistent with WD or CESD patients, who show around 50-100-fold increase in CEs, while TGs are only 7 to 10-fold increased (209).

Similar to LAL-D patients, $Lipa^{-/-}$ mice have increased LDL-C levels, while HDL-C is decreased. However, total cholesterol and TG concentrations in plasma are unchanged in $Lipa^{-/-}$ mice (208). Recently, LAL has been shown to not only degrade CE and TAG in lysosomes but also RE. Interestingly, $Lipa^{-/-}$ mice exhibit reduced and not increased hepatic RE content. This is most likely a consequence of defective intestinal absorption and/or decreased nutritional availability of vitamin A, since they exhibit lower postprandial circulating RE levels (108). Moreover, we could show that defective lysosomal hydrolysis of CE and TG decreases the availability of FA for hepatic acyl-CoA formation, thereby regulating hepatic VLDL secretion. Consequently, abolished nuclear expression of genes involved in lipoprotein assembly attenuates VLDL secretion. The decreased energy supply triggers an increase in glucose tolerance and insulin sensitivity as metabolic adaptations (107). Furthermore, LAL is important for shuttling of FAs derived from circulating lipoproteins to BAT during cold exposure (210) and the generation of lipid

mediators (211), which are critical processes to maintain energy homeostasis in Lipa$^{-/-}$ mice. Peritoneal macrophages of Lipa$^{-/-}$ mice accumulate 18:2 and 20:4 FAs, important precursors for lipid mediator generation, in the CE but not PL or TG fractions (211). Overall, global deletion of LAL in mice results in a phenotypic model for CESD and a biochemical and histopathological model for WD (185, 208, 212).

To date it is unclear, why the phenotype of LAL-D in mice is more moderate. One possibility might be additional lysosomal activities for neutral lipid ester hydrolysis, which can partially compensate for the loss of LAL activity. Furthermore, the differences in lipoprotein metabolism of mice compared to humans might contribute to the better outcome, considering a different lipoprotein profile in LDL-C and HDL-C levels.

Aim of the thesis

Numerous studies have already investigated whole-body LAL-D in detail, it remained elusive, however, why large amounts of cholesterol (crystals) accumulate in hepatocytes and Kupffer cells and both cell types massively proliferate. Hepatocytes contribute to chylomicron remnant uptake, the mobilization of neutral lipids from cytosolic LDs, as well as the secretion of neutral lipids via VLDL. We therefore hypothesized that hepatocyte-specific deletion of LAL triggers the liver phenotype in LAL-D by affecting carbohydrate and lipid metabolism. To address this question, we generated and characterized hepatocyte-specific Lipa$^{-/-}$ (Liv-Lipa$^{-/-}$) mice.

2. Material and Methods

2.1 Materials

2.1.1 Buffers and solutions

Western blotting

RIPA buffer
50 mM Tris-HCl pH 8.0
150 mM NaCl
1% Triton X-100
0.5% SDS

SDS sample buffer
2.3 g SDS
0.6 g Tris
25 ml H2O
pH 6.8 with HCl
10 ml glycerol
25 mM DTT
add H_2O to 45 ml
one drop of bromophenol blue

Ponceau S
0.2% Ponceau S
3% trichloracetic acid
diluted in 1 x PBS

10x Electrophoresis buffer
250 mM Tris
1.92 M glycine
1% SDS

10x Blotting buffer
100 mM Tris
0.38 M glycine

10x TBS-T (washing buffer)
100 mM Tris-HCl pH 7.4
1.5 M NaCl 1%
Tween 20

10x PBS pH 7.4
1.4 M NaCl
25 mM KCl
81 mM Na_2HPO_4
15 mM KH_2PO_4

Activity assays using radioactive tracers

Citrate buffer, pH4:
Solution A: 0.1M citric acid monohydrate
Solution B: 0.1M trisodium citrate, dehydrate
Mix 54ml of Solution A with 46ml of Solution B to reach pH optimum of 4.2

Phosphatidylcholine/ phosphatidylinositol (3:1, w:w)
20 mg/ml in toluene

BSA-solutions (5% and 20%)
Fatty acid-free BSA in 0.1 M citrate buffer pH 4

Stop solution
Methanol:choroform:n-heptane (10:9:7, v:v:v)

Potassium carbonate
0.1 M K_2CO_3 in H_2O
pH 10.5 with boric acid

LAL assay

Lysis buffer
100 mM NaH_2PO_4 pH 6.8
1 mM EDTA
0.5% NP-40
0.02% sodium azide
Store at 4°C →10 mM DTT and PIC will be added always fresh

Assay buffer
0.2M NaAc/0.01% Tween 20
pH 4.5
Store at 4°C

Substrate diluents
Sodium taurocholate 2.4mM dissolved in Assay Buffer
Store at 4°C.

Stop solution
0.75M Tris pH 11.0
Store at 4°C

Hepatocyte isolations

10x perfusion I
1.42 M NaCl
0.067 M KCl
0.1 M HEPES
pH to 7.4 and bring up to 1 L
Store at 4°C

1x perfusion I
50 ml of 10X to 400 ml ddH2O
Add EGTA to 2.5 mM (0.475 g) and stir to dissolve pH to 7.4
Bring up to 500 ml

10x perfusion II
66.7 mM NaCl
6.7 mM KCl
100 mM HEPES
pH to 7.6
Add $CaCl_2$ $2H_2O$ (0.706g)
Recheck pH and bring up to 1 L

Before use add to 300 ml: 150 mg collagenase (Gibco #17104-019)
3 g fatty acid-free albumin (Biowest)

Percoll
45 ml Percoll (sterile)
5 ml 10X PBS (sterile)
0.5 ml 1M HEPES (sterile)
Set pH to 7.4±0.2
Store ingredients and Percoll stock at 4°C.

2.1.2 Chemicals

4-methylumbelliferone	Santa Cruz, Dallas, USA
4-methylumbelliferyl palmitate	Santa Cruz, Dallas, USA
Acryl amide	Applichem, St.Louis, USA
Agarose	Sigma-Aldrich, St.Louis, USA
APS	Sigma-Aldrich, St.Louis, USA
β-Mercaptoethanol	Merck, Darmstadt, Germany
Bis acrylamide	Applichem, St.Louis, USA
Bromophenol blue	Merck, Darmstadt, Germany
BSA	Sigma-Aldrich, St.Louis, USA
Chloroform	Sigma-Aldrich, St.Louis, USA
DEPC	Roth, Karlsruhe, Germany
EDTA	UltraPure™, Life Technologies, Carlsbad, USA
Ethanol	Roth, Karlsruhe, Germany
Ethidium bromide	Merck, Darmstadt, Germany
Ethylacetate	Roth, Karlsruhe, Germany
Formaldehyde	Sigma-Aldrich, St.Louis, USA
Formamide	Merck, Darmstadt, Germany
Glucose	Sigma-Aldrich, St.Louis, USA
Glycerol	Sigma-Aldrich, St.Louis, USA
Glycine	Roth, Karlsruhe, Germany
^{3}H Trioleate	Perkin Elmer, Waltheim, USA
HCl	Roth, Karlsruhe, Germany
Hexane	Roth, Karlsruhe, Germany
HEPES	Roth, Karlsruhe, Germany
n-Heptane	Roth, Karlsruhe, Germany
Isopropanol	Roth, Karlsruhe, Germany
KBr	Roth, Karlsruhe, Germany
KCl	Roth, Karlsruhe, Germany
K_2CO_3 in H_2O	Sigma-Aldrich, St.Louis, USA

KH_2PO_4	Roth, Karlsruhe, Germany
M199 Medium	Thermo Fischer Scientific, Waltheim, USA
Methanol	Roth, Karlsruhe, Germany
$MgCl_2$	Merck, Darmstadt, Germany
MOPS	Roth, Karlsruhe, Germany
Na-acetate	Roth, Karlsruhe, Germany
$NaHCO_3$	Fluka Analytical, St.Louis, USA
$Na_2HPO_4*7H_2O$	Merck, Darmstadt, Germany
NaCl	Roth, Karlsruhe, Germany
NaN_3	Merck, Darmstadt, Germany
NaOH	Roth, Karlsruhe, Germany
NP-40	Fluka Analytical, St.Louis, USA
Pen-Strep	Thermo Fischer Scientific, Waltheim, USA
Percoll	Sigma-Aldrich, St.Louis, USA
Petroleumether	Roth, Karlsruhe, Germany
PIC	Sigma-Aldrich, St.Louis, USA
SDS	Serva Electrophoresis, Heidelberg, Germany
Skim-milk powder	Fluka Analytical, Sigma-Aldrich, St.Louis, USA
Sodium Taurocholate	Sigma-Aldrich, St.Louis, USA
Sucrose	Roth, Karlsruhe, Germany
Temed	Sigma-Aldrich, St.Louis, USA
Toluene	Roth, Karlsruhe, Germany
Trifast	VWR, Radnor, USA
Tris	Roth, Karlsruhe, Germany
Triton X-100	Merck, Darmstadt, Germany
Tween 20	Merck, Darmstadt, Germany
Tyloxapol	Sigma-Aldrich, St.Louis, USA

2.1.3 Kits

Kit	Company	Used for
Protein Assay	Bio-Rad	Lowry-Protein concentration determination
ECL western blotting substrate	Pierce	Western-blot development
Triglyceride FS	Diasys	TG concentration determination
Total Cholesterol FS	Diasys	TC concentration determination
Free Cholesterol FS	Diasys	FC concentration determination
NEFA C	Wako	FFA concentration determination
Ketone Bodies	Cayman	β- hxdroxybutyrate determination
Sybr Green Kit	Qiagen	Real-Time PCR
High Capacity cDNA Reverse Transcription Kit	Applied biosystems	Reverse Transcription
DirectPCR-tail	Peqlab	DNA isolation
Hot Firepol DNA Polymerase	Biodyne	Gene amplification

2.1.4 Devices

Absorption measurements:	Anthos photometer (Anthos Mikrosysteme GmbH, Krefeld, Germany)
Centrifuge:	Eppendorf Centrifuge 5417R (Eppendorf AG, Hamburg, Germany) Eppendorf 5810R (Eppendorf AG, Hamburg, Germany) Beckman Optima TLX; TLA 120.2 (Backman Coulter, Pasadena, USA)
Fecal energy content	Adiabatic oxygen bomb calorimenter C4000 A (IKA Analysentechnik, Stauffen, Germany)
FPLC:	Pharmacia FPLC system (Pfizer Pharma, Karlsruhe, Germany) with a Superose 6 column (Amersham Biosciences, Piscataway, USA)
Homogenizer:	Precellys 24 homogenizer (Peqlab GmbH, Erlangen, Germany)
Lyophilizing Device:	VirTis BenchTop K Manifold (SP Scientific, New York, USA)
pH measurement:	SCHOTT pH-meter (SCHOTT AG, Mainz, Germany)
PCR machine:	BioRad C1000 Thermal Cycler (Bio-Rad Laboratories, Inc., Berkeley, USA)
Real time PCR machine:	ROCHE Light cycler 480 (Hoffman-LaRoche, Basel, Switzerland)
RNA Gels:	FlashGel® Gel Cassette: 1.2% 12+1 Single Tier RNA and FlashGel® Gel Dock (Lonza Group AG, Basel, Switzerland)
Scintillation-counter:	Tri-Card 3100TR Liquid Scintillation Analyser (Perkin Elmer, Waltham, USA)
SDS electrophoresis chamber:	BioRad Protean System (Bio-Rad Laboratories, Inc.,Berkeley, USA)
Spectral photometer:	Nano Drop Peqlab ND1000 (Peqlab GmbH, Erlangen, Germany)
Trans-Blot Turbo®:	BioRad Protean System (Bio-Rad Laboratories, Inc., Berkeley, USA)

Ultra sonication:	Labsonic U (B.Braun Melsungen AG, Melsungen, Germany)
Water bath:	Aqualine Water Baths MD 20 (LAUDA-Brinkmann, Delran, USA)
Western blotting:	wet Tankblot system (Bio-Rad Laboratories, Inc., Berkeley, USA)
Western blot detection:	ChemiDoc™ (Bio-Rad Laboratories, Inc., Berkeley, USA)

2.2 Methods

2.2.1 Animals and diets

Experiments were performed using male and female age- and sex-matched control and Liv-Lipa$^{-/-}$ mice with ad libitum access to water and food. Mice were maintained on a regular light-dark cycle (12 h/12 h) in a clean and temperature-controlled environment. Control and Liv-Lipa$^{-/-}$ mice were either kept on a regular chow diet (11.9% caloric intake from fat; Altromin Spezialfutter GmbH, Lage, Germany) or challenged with a high-fat/high-cholesterol diet (HF/HCD; 30% caloric intake from fat plus 1% cholesterol; Ssniff, Soest, Germany) starting at the age of seven weeks. All animal experiments were performed according to the European Directive 2010/63/EU in compliance with national laws and approved by the Austrian Federal Ministry of Education, Science and Research, Vienna, Austria. (213)

2.2.2 Genotyping

At the age of four to five weeks, animals are weaned. Genotyping was performed by using a piece of ear punch that was digested in 140 µl DirectPCR-tail lysis reagent (Peqlab, Erlangen, GER) and 10 µl proteinase K (10 mg/ml; Roth, Karlsruhe, Germany) for 1-2 h at 56°C under vigorous shaking. Afterwards, the samples were incubated for 45 min at 85°C to inactivate Proteinase K. The reaction mix contained ~200 ng of the template DNA, 2.5 mM $MgCl_2$, 0.4 mM of each dNTP, 0.1 µM of each primer, 4% DMSO, 2.5 U Hot Firepol DNA Polymerase I (Solis BioDyne OU, Tartu, Estonia), and the reaction buffer system of DyNAzyme™ DNA Polymerase (Finnzymes, Espoo, Finland). For genotyping, primers listed in Table 1 were used. Genotyping was performed by Silvia Rainer and Sarah Krenn, Medical University of Graz.

Table 1: Primer sequences for genotyping of mice

Gene	Forward Primer	Reverse Primer
Lipa	TGCTGGCAGATTCTAGTAACTGGG	CCACAAGGCCAGGAATGGTA
Alb-Cre	GGGGTAGGAACCAATGAAA	TAGCTGGCTGGTGGCAGATG

The following cycle conditions, shown in Table 2, were used for the amplification of the specific DNA-products.

Table 2: PCR programs for genotyping of mice.

	Alb-Cre			**Lipa**		
	Temperature	Time	Cycles	Temperature	Time	Cycles
Initial	95°C	15 min		95°C	15 min	
Denaturation	95°C	30 min	35x	95°C	30 min	35x
Annealing	60°C	60 s		60°C	60 s	
Elongation	72°C	60 s		72°C	60 s	
Final elongation	72°C	10 min		72°C	10 min	
Cool down	4°C	∞		4°C	∞	

2.2.3 Blood biochemical analyses

Blood was collected via the facial vein from *ad libitum* fed or 12 h fasted mice, and plasma was prepared by centrifugation at 7,000 rpm for 7 min at 4°C. TG, TC (DiaSys, Holzheim, Germany), and β-hydroxybutyrate (Cayman, Ann Harbor, MI) concentrations were measured enzymatically according to manufacturer's instructions. Lipoprotein fractions were separated from 200 µl pooled plasma from each group using fast protein liquid chromatography (FPLC) (Pharmacia P-500) equipped with a Superose 6 column (Amersham Biosciences, Piscataway, NJ). TG and TC concentrations were assayed enzymatically. The liver injury markers ALT and AST were measured enzymatically (Roche Diagnostics, Mannheim, Germany). Blood glucose was determined using Accu-Chek® Active glucometer and glucose strips (Roche Diagnostics GmbH, Mannheim, Germany). Blood insulin concentrations were measured using an ELISA kit (Peprotech, Rocky Hill, CT), according to manufacturers' instructions.

2.2.4 Glucose tolerance test

Six hour-fasted mice were administered intraperitoneally with 2 g/kg body weight (BW) of glucose in PBS. Blood glucose levels were measured 0, 15, 30, 60, and 120 min after injection using Accu-Chek® Active glucometer and glucose strips (Roche Diagnostics GmbH, Mannheim, Germany). (213)

2.2.5 Insulin tolerance test

Four hour-fasted mice were injected intraperitoneally with 1 IU/kg BW of insulin in PBS (100 IU/ml stock; Actrapid Novo Nordisk, Wien, Austria). Blood glucose levels were measured 0, 15, 30, 45, 60, and 120 min post-injection using Accu-Chek® Active glucometer and glucose strips (Roche Diagnostics GmbH, Mannheim,Germany). (213)

2.2.6 Energy metabolism and fecal energy content

Assessment of energy intake and energy expenditure was performed using a climate-controlled indirect calorimetry system (TSE PhenoMaster, TSE Systems, Bad Homburg, Germany). Control and Liv-Lipa$^{-/-}$ mice fed either chow or HF/HCD were housed in computer-controlled metabolic cages in a regular light-dark cycle (12 h light, 12 h dark) with free access to food and water. Weight-matched female mice were acclimatized for 48 h before experiments. O_2 consumption, CO_2 production, and locomotor activity (using infrared sensor frames) were measured every 15 min. Carbohydrate and lipid oxidation rates were determined as described (214) and converted from mg/h into kcal/h. (210)
To measure fecal output and fecal energy content, we collected fecal pellets from five consecutive days. The pellets were dried, weighed, and grounded. For fecal energy content mesaurements, 1g of dried fecal powder was pressed into tablet form and burned in an adiabatic oxygen bomb calorimenter C4000 A (IKA Analysentechnik, Stauffen, Germany). Measurements were performed in duplicate.

2.2.7 Tissue lipid content

50 mg of tissue was homogenized in lysis buffer. Lysates containing 1 mg protein were normalized with the appropriate amount of lysis buffer to the same volume. A chloroform:methanol (2:1) solution was added to the tissue lysates in 20-fold excess and rotated for 2 h at RT. The extracts were centrifuged at 4,000 rpm for 15 min at 4 °C and the organic phase was decanted to the fresh vial. Two hundred µl 2% Triton X-100 in chloroform were added to the extracts, vortexed, and dried under the stream of nitrogen. The samples were redissolved in 100 µl of ddH_2O and TG, TC and FC concentrations were measured enzymatically according to manufacturers' instructions. CE concentrations were calculated by subtracting FC from TC concentrations.

2.2.8 Primary mouse hepatocyte isolation and culture

For primary hepatocyte isolations, mice were anesthetized by intraperitoneal injection of 100 µl of ketamin (80 mg/kg)/xylazin (12 mg/kg). Primary hepatocytes were isolated by the collagenase perfusion method as described previously (215) and seeded on collagen-coated plates. Cells were cultivated overnight in M199 medium (Sigma-Aldrich, St.Louis, MO) containing 10% FBS, 23 mM HEPES, 0.01 µM dexamethasone, 2 mM glutamine, 1% penicillin/streptomycin (P/S), 26 mM sodium bicarbonate, and 5.5 mM glucose. The following day, hepatocytes were switched to FBS-free medium for another 24 h and then used for experiments. (213)

2.2.9 Lipase activity assays

Hepatocytes from male mice were lysed in citrate buffer (100 mM citric acid monohydrate, 100 mM trisodium citrate dehydrate, pH 4) and centrifuged at 1,000 x g and 4°C for 10 min. The protein content of the supernatant was determined by a Lowry assay (Bio-Rad, Hercules, CA). The TG substrate contained 17 nmol triolein/assay and 2,000 cpm/nmol of ^{3}H-triolein (Perkin Elmer, Waltham, MA). The CE substrate contained 20 nmol cholesteryl oleate/assay and 1,000 cpm/nmol of ^{3}Hcholesteryl oleate (Amersham Biosciences, Piscataway, NJ). Fifty micrograms of protein from cell lysates were mixed with 100 µl of substrate and incubated in a water-bath for 1 h at 37°C. The reaction was

stopped by the addition of 3.25 ml stop solution (methanol:chloroform:n-heptane, 10:9:7, v:v:v) and 1 ml of 0.1 M potassium carbonate and 0.1 M boric acid (pH 10.5). The tubes were vortexed for 10-15 s and centrifuged at 800x*g* for 20 min at 4°C. In 1 ml of the upper phase the radioactivity was determined by liquid scintillation counting, and the release of FAs was calculated. In addition, livers and hepatocytes from male mice were lysed in lysis buffer (100 mM NaH_2PO_4, pH 6.8, 1 mM EDTA, 10 mM DTT, 0.5% NP-40, 0.02% sodium azid, protease inhibitors) and centrifuged for 10 min at 10,000x*g*. LAL activity was estimated using the fluorogenic substrate 4-methyl-umbelliferyl-palmitate (4-MUP) as described (211).

2.2.10 Western blot analysis

Hepatocytes were lysed in RIPA buffer and protein concentrations were quantitated (DC™ Protein assay, Bio-Rad Laboratories, Hercules, CA). Hepatocyte lysates (50 µg protein) were separated by SDS-PAGE and transferred onto a PVDF membrane. To block non-specific binding sites of the membrane, 5% solution of milk powder was used for 1 h. LAL protein expression was detected using an polyclonal anti-rabbit LAL antibody (1:1,000, Origene, Rockville, MD). Polyclonal anti-rabbit calnexin (1:1,000; Santa Cruz, Heidelberg, Germany) was used as loading control. HRP-conjugated goat anti-rabbit (1:2,500) was visualized by enhanced chemiluminescence detection on a ChemiDoc™ MP imaging system (Bio-Rad Laboratories). Thermo Scientific™ PageRuler™ Plus Prestained 10-250 kDa Protein Ladder (Thermo Fischer Scientific, Waltheim, USA) was used as MW marker. (213)

2.2.11 RNA isolation and cDNA synthesis

Primary hepatocytes were isolated and cultured for at least 24 h. Total RNA was isolated with PerfectPure RNA Cultured Cell Kit (5 Prime GmbH, Hilden, Germany) according to manufacturer's protocol. Briefly, 400 µl Lysis Solution (with freshly added 1% β-mercaptoethanol) was added per well. The cells were incubated at room temperature (RT) for 10 min, scraped, and sheared by pressing the lysate through a 25 gauge needle for at least ten times. These lysates were transferred onto purification columns and centrifuged for 1 min at 14,000 rpm at RT. Four hundred µl of Wash Solution 1 were added to the column and centrifuged again for 1 min at 14,000 rpm at RT. Thereafter, 50 µl of DNase were added. After 15 min at RT, columns were treated twice with 200 µl of Wash Solution 2 and centrifuged at 14,000 rpm at RT for 1 and 2 min, respectively. Finally, the column was transferred to a fresh tube, 30 – 50 µl of Elution solution were added per column and centrifuged at 14,000 rpm at RT for 1 min.

Total RNA from tissues was isolated using TriFast reagent according to the manufacturer's protocol (Peqlab, Erlangen, Germany). Briefly, tissues were homogenized in 1 ml of TriFast reagent using Precellys 24 bead homogenizer (Bertin technologies, Siege, France). Two hundred µl of chloroform were added per ml TriFast reagent, vortexed, and centrifuged at 8,500 rpm at 4°C for 15 min. The supernatant was transferred to a fresh tube, mixed with 500 µl of isopropanol, vortexed, and centrifuged at 8,500 rpm at 4°C for 10 min. Thereafter, supernatant was discarded, pellets were washed twice with 75% ethanol and centrifuged again at 8,500 rpm at 4°C for 5 min. Supernatant was discarded, pellets were air-dried, and resuspended in 100-500 µl DEPC water. RNA concentrations were measured at 260 nm using NanoDrop (Thermo scientific, Waltham, MA). Two µl RNA were used for concentration determination using the following equation:

$$\mathbf{C\ (ngRNA/\mu l) = OD\ 260nm \times 40}$$

2.2.12 Reverse transcription and cDNA preparation

cDNA was prepared from RNA by reverse transcription. One or two µg RNA in 10 µl (adjusted with nuclease-free ddH_2O) were reverse transcribed by using High-Capacity DNA Reverse Transcription kit (Applied Biosystems, Foster City, CA). The composition of the master mix for reverse transcription is shown in Table 3 and the thermal cycling conditions in Table 4.

Table 3: High-Capacity cDNA reverse transcription master mix composition

Component	Volume (µl) / reaction
10 x RT Buffer	2
25 x dNTP Mix (100 mM)	0.8
10 x RT Random Primers	2
Multiscribe Reverse Transcriptase	1
RNAse Inhibitor	3.5
Nuclease-free H_2O	0.7
1 or 2 µg RNA/10 µl ddH_2O	10
Total volume per reaction	20

Table 4: Reverse transcription thermal cycling conditions

	Step 1	Step 2	Step 3	Step 4
Temperature	25°C	37°C	85°C	4°C
Time	10 min	120 min	5 s	∞

2.2.13 Real time PCR

cDNA was diluted 1:50 in nuclease-free ddH_2O if 2 µg or 1:25 if 1 µg of RNA was used for reverse transcription. Three µl of diluted cDNA, 1 µl of forward and reverse primer (stock solution, 100 µM, diluted 1:10 with nuclease-free ddH_2O), and 5µl QuantiFastTM SYBR® Green were pipetted into a LightCycler 480 white Multiwell plate. The plate was centrifuged for 1 min at 800 rpm and loaded on a RocheLight Cycler 480 instrument. The real-time PCR program conditions are shown in Table 5.

Table 5: Real-time PCR program conditions

	Temperature	Time	Cycles
Denaturation	95°C	5 min	1
Amplification	95°C	10 s	40
	60°C	30 s	
Melting Curve	95°C	10 s	1
	60°C	20 s	1
	95°C	continuous	
Cool Down	40°C	20 s	1

Samples were analyzed in duplicate and normalized to the expression of cyclophilin A as a reference gene. Expression profiles and associated statistical parameters were determined using the $2^{-\Delta\Delta CT}$ method. Primer pairs are shown in Table 6.

Table 6: Primers used for real-time PCR

Gene	Forward Primer	Reverse Primer
Adipor1	AATGGGGCTCCTTCTGGTAAC	GGATGACTCTCCAACGTCCCT
Adipor 2	GCCAAACACCGATTGGGGT	GGCTCCAAATCTCCTTGGTAGTT
Asl	CCGGCATCTGTGGAATGTG	GTTGCGACTTCGTCCTGTGT

Ass	CTCCTGCATCCTCGTGTGG	GCTCACATCCTCAATGAACACC
Ccl3	TGTACCATGACACTCTGCAAC	CAACGATGAATTGGCGTGGAA
Ccl4	TTCCTGCTGTTTCTCTTACACCT	CTGTCTGCCTCTTTTGGTCAG
Ccl5	GCTGCTTTGCCTACCTCTCC	TCAGTGACAAACACGACTGC
Col3a	GGGGACCAGGGCGACCACT	CAGGTGAACCCGGCAAGAACG
Cps	TACCCGGAAGCACTTACTGAT	GCCAGCCAGTGGTTATAGTCATT
Cyclophilin A	CCATCCAGCCATTCAGTCTT	TTCCAGGATTCATGTGCCAG
F4/80	CTTTGGCTATGGGCTTCCAGTC	GCAAGGAGGACAGAGTTTATCGTG
G6Pase	CGACTCGCTATCTCCAAGTGA	GGGCGTTGTCCAAACAGAAT
Gpdh	CTCGCCATCGCCCTCACTG	ACCGCTCACTCGCTCTTTGC
Il4	TGGATCTGGGAGCATCAAGGT	TGGAAGTGCGGATGTAGTCAG
Il6	TCTATACCACTTCACAAGTCGGA	GAATTGCCATTGCACAACTCTTT
Ckt19	GTTCAGTACGCATTGGGTCAG	GAGGACGAGGTCACGAAGC
Leptr1	AATGACGCAGGGCTGTATGT	ATGGACTGTTGGGAAGTTGG
Lipa	GCAAAGGTCCCAGACCAGTT	TCATCAAAACTGAAGGCCCAGA
Mcp1	ACTGAAGCCAGCTCTCTCTTCCTC	TTCCTTCTTGGGGTCAGCACGAC
Mcsf1	ATGAGCAGGAGTATTGCCAAGG	TCCATTCCCAATCATGTGGCTA
Mdh	GAACCAATCAGAGTCCTTGTGAC	GGCACAGTCTTGCAGTTCCA
Otc	AGGGTCACACTTCTGTGGTTC	CAGAGAGCCATAGCATGTACTG
Pcx	AATGTCCGGCGTCTGGAGTA	ACGCACGAAACACTCGGAT
Pdhb	AAGAGGCGTTTTCACCGCTC	GTCACCGTATTTCTTCCACAGG
Pepck	AAGCATTCAACGCCAGGTTC	TGCAGGCACTTGATGAACTC
Pfkl	GGAGGCGAGAACATCAAGCC	GCACTGCCAATAATGGTGCC
Tgfb	CCGCTTTAAGTAGTTCTGTTCGT	AGCCGTGGGGTCCTTTCTGTG
Tnfa	CCCTCACACTCAGATCATCTTCT	GCTACGACGTGGGCTACAG

2.2.14 Nuclear magnetic resonance metabolic profiling

The phosphate buffer solution was prepared by dissolving 5.56 g of anhydrous NaH_2PO_4, 0.4 g of TSP, and 0.2 g NaN_3, in 500 ml of deionized water and adjusted to pH 7.4 with 1 M NaOH and HCl. The phosphate buffer was lyophilized and re-dissolved in D_2O. Metabolism was quenched in mouse liver samples using methanol:water solution (2:1). Tissues were homogenized using Precellys® homogenizer. After homogenization, lysates were incubated for 1 h at -20°C, then spun (10,000 rpm, 4°C, 1 h) and the supernatant containing polar metabolites was used for lyophilisation. Five hundred µl of nuclear magnetic resonance (NMR) buffer in D_2O were added to the samples, re-dissolved, and transferred to 5 mm NMR tubes.

All NMR experiments were performed at 310 K on a Bruker Avance III 500 MHz spectrometer equipped with a TXI probe head. The 1D CPMG (Carr−Purcell−Meiboom−Gill) pulse sequence (cpmgpr1d, 512 scans, 73728 points in F1, 12019.230 Hz spectral width, 1024 transients, recycle delay 4 s), with water suppression using pre-saturation, was used for ^1H 1D NMR experiments. Bruker Topspin version 3.1 was used for NMR data acquisition. The spectra for all samples were automatically processed (exponential line broadening of 0.3 Hz), phased, and referenced to TSP at 0.0 ppm using Bruker Topspin 3.1 software (Bruker GmbH, Rheinstetten, Germany). NMR data were imported to Matlab® vR2014a (Mathworks, Natick, MA), regions around the water, TSP, and remaining methanol signals excluded, and probabilistic quotient normalization (216) was performed to correct for differences in sample metabolite dilution.

To identify changes in metabolic profiles, multivariate statistical analysis was performed. Statistical analysis included Principle Component Analysis (PCA), Orthogonal Partial Least Squares Discriminant Analysis (O-PLS-DA) (217), associated data consistency checks and 7-fold cross-validation.

Cross-validation and data consistency checks are methods to determine the statistical significance of results. Hereby, 7-fold cross-validation is a re-sampling procedure to evaluate machine learning models on a limited data sample. In principle, the data set is shuffled randomly and split into 7 groups. Each group is a test data set, and the remaining groups act as a training data set. The training set is used to fit a model, which is then

evaluated on the test set. It generally results in a less biased or less optimistic estimate of the model skill than other methods, such as a simple train/test split. For data consistency checks, parameters R2 and Q2 are determined. Those parameters provide a measure of model fit to the original data (R2), and a measure of consistency between the original and cross-validation predicted data (Q2). (217)

Metabolites of interest were quantified using Chenomx NMR Suite Professional 8.2 (Chenomx Inc.) with the existing Chenomx Inc. library and processed one-dimensional CPMG spectra. This experiment was performed and analyzed by Sarah Stryeck, Medical University of Graz.

2.2.15 Fat mass quantification using micro-computed tomography

HF/HCD-fed control and Liv-Lipa$^{-/-}$ mice were anesthetized with isoflurane (Abbvie GmbH, Vienna, Austria) and transferred to a Siemens Inveon micro-computed tomography (µCT) scanner (Siemens, Erlangen, Germany). Under continuous anesthetic inhalation during scanning, fat and lean mass were detected and the obtained data were calculated using Materialise Mimics 20.0 software (Materialise HQ, Leuven, Belgium). This experiment was performed together with Ines Anders at the Core Facility for Biomedical Imaging.

2.2.16 FA composition by GC analysis

FA composition was quantitated by GC-flame ionization detection. Liver lipids were extracted twice with chloroform:methanol (2:1, v:v) and aqua dest., dried under a stream of nitrogen, and re-dissolved in 1 ml of toluol. Aliquots were separated by thin layer chromatography under argon using hexane:diethylether:acetic acid (70:30:1; v:v:v) as mobile phase. Plates were dried, standards were stained with iodine vapor, and PL, DG, free fatty acids (FFA)-, TG-, and CE-corresponding bands were scraped off the plates. After addition of the internal standard (pentadecanoic acid), lipids were transesterified (1.2 ml toluene and 1 ml boron trifluoride-methanol (20 %) directly on the silica gel at 110°C for 1 h. Reactions were stopped by the addition of 2 ml of ice-cold H_2O. FA methyl esters (FAMEs) were extracted by the addition of 200 µl of hexane and shaking for 10 min at RT. After centrifugation (1,480 g, 10 min, 4°C), the upper phase was collected. The combined

phases were evaporated under a stream nitrogen, and FAMEs were dissolved in toluol. The GC conditions were set to split injection (split flow, 15 ml/min; split ratio, 1/5; injection volume, 2 µl) using an injector temperature of 230°C and a wall-coated open tubular fused silica column (25 m, 0.32-mm inner diameter, FFA phase-coated, film thickness 0.3 µm; Agilent Technologies, Santa Clara, CA). The carrier gas consisted of helium. As a temperature gradient, two consecutive ramps from 150 to 230 °C (ramp 1, 2.5 °C/min to 215 °C hold for 10 min; ramp 2, 10 °C/min to 230 °C hold for 12.5 min) were used. Flame ionization detector (Trace-GC Ultra, Thermo- Quest Corp., Atlanta, GA) conditions were as follows: base temperature, 150 °C; gas flow, split ratio 1:7, 350 ml/min air, 35 ml/min hydrogen, and 60 kPa helium, constant pressure). Data acquisition and analysis were done with Chrom-Cad data system software. For quantitative analysis, the corresponding peaks of FAMEs were integrated, and peak areas were calculated in relation to the C15:0 peak as internal standard. FAME concentrations were calculated as percentage of total FAMEs in a given sample and/or as amounts per microgram protein (µg/ml). Separation and quantitation were performed as previously described (218). This experiment was performed by Helga Reicher, Medical University of Graz.

2.2.17 Electron microscopy

Female control and Liv-Lipa$^{-/-}$ mice challenged with a HF/HCD for 10 weeks and fasted for 12 h were used to assess liver morphology. The livers were fixed in phosphate buffer/2.5% glutaraldehyde for 2 h, washed, post-fixed in phosphate buffer/OsO_4 for 2 h and 4x10 min in phosphate buffer. After dehydration, tissues were infiltrated (acetone and agar 100 epoxy resin, pure agar 100 epoxy resin) for 4 h, placed in agar 100 epoxy resin (8 h), transferred into embedding molds, and polymerized (48 h, 60°C). Sections stained with lead citrate and platine blue were imaged at 120 kV with a Tecnai G 2 FEI microscope (FEI, Eindhoven, Netherlands) equipped with a Gatan ultrascan 1000 CCD camera. LDs from 97 electron micrographs (each having a surface of 142.09µm^2) per genotype were counted and analyzed by open source ImageJ software image processing and analysis in Java. (213) Electron microscopy was performed by Dagmar Kolb, counting and analyzing of electron micrographs was performed by Dominique Pernitsch, Medical University of Graz.

2.2.18 Histochemistry and immunohistochemistry

Tissues of male HF/HCD-fed controls and Liv-Lipa$^{-/-}$ mice were fixed in 4% neutral-buffered formaldehyde for 24 h and embedded in paraffin. Sections (5 µm) were de-paraffinized and subjected to CAB (Chromotrope Aniline Blue), PAS (periodic acid Schiff stain), Trichrome, and hematoxylin and eosin staining (H&E), respectively, using standard histopathological techniques (219, 220). For KI67 immunohisto chemistry (IHC), sections were de-paraffinized and incubated with anti-rabbit KI67 antibody (Cell signaling CS12202, Danvers, MA, 1:100 dilution). For F4/80 IHC, sections were incubated with anti-mouse F4/80 antibody (Serotec MCA 497GA, Biorad, CA, 1:50 dilution). Antibody binding was visualized using aminoethyl carbazole (AEC) substrate chromogen (cat#3464, Dako, Glostrup, Denmark). For histochemical staining with Oil Red O (ORO), 7 µm thick cryosections were prepared and stained with ORO; nuclei were counter-stained with Mayer's haematoxylin. This experiment was performed by Silvia Schauer, Medical University of Graz.

2.2.19 Statistics

Statistical analyses were performed using GraphPad Prism 5.0 software (GraphPad Software Inc, San Diego, CA). Significances were determined by Student's unpaired t-test and Welch correction (in case of unequal variances) for two group comparison and ANOVA followed by Bonferroni correction for multiple group comparison. Data are presented as mean values ± SD. Significance levels were set at $p< 0.05$ (*), $p\leq 0.01$ (**), and $p\leq 0.001$ (***).

3. Results

3.1 Generation of hepatocyte-specific Lipa$^{-/-}$ mice (Liv-Lipa$^{-/-}$)

Mice with ubiquitous Lipa gene deletion (Lipa$^{-/-}$) have already been investigated in detail. However, defective lysosomal lipolysis resulting from a global loss of LAL made this model unsuitable for studying the hepatic contributions to the overall disease contribution. The severe phenotype with hepatomegaly, microvesicular steatosis and infiltration of Kupffer cells leading to formation of "fatty lysosomes" (107) in Lipa$^{-/-}$ mice made it impossible to isolate hepatocytes and therefore prompted us to generate Liv-Lipa$^{-/-}$ mice.

A LoxP-Cre approach was used (221) to allow conditional silencing of LAL specifically in hepatocytes (222). Mice carrying the Lipa$^{tm1a(EUCOMM)Hmgu}$/Biat on a C57BL/6N background were generated using an ES cell line from the European Conditional Mouse Mutagenesis Program (EUCOMM). Injections of ES cells into founder mice was performed by Prof. Thomas Rülicke and his team of the University of Veterinary Medicine in Vienna. Floxed Lipa mice (Lipa$^{fl/fl}$) were generated by breeding Lipa$^{tm1a(EUCOMM)Hmgu}$/Biat with FLP deleter mice (Taconic #7089) to create a floxed Lipa^{tm1c} allele with restored Lipa expression. Mice heterozygous for the floxed allele were bred together to obtain homozygous Lipa$^{fl/fl}$ mice that served as controls. Lipa$^{fl/fl}$ mice were then bred with transgenic mice (Alb-Cre 003574 Magnuson JAX) expressing the Cre recombinase under the control of the albumin promoter to generate hepatocyte-specific Liv-Lipa$^{+/-}$ mice. Mice containing the hepatocyte-specific deletion were then bred to produce Liv-Lipa$^{-/-}$ mice and their respective control littermates (Figure 6). (213)

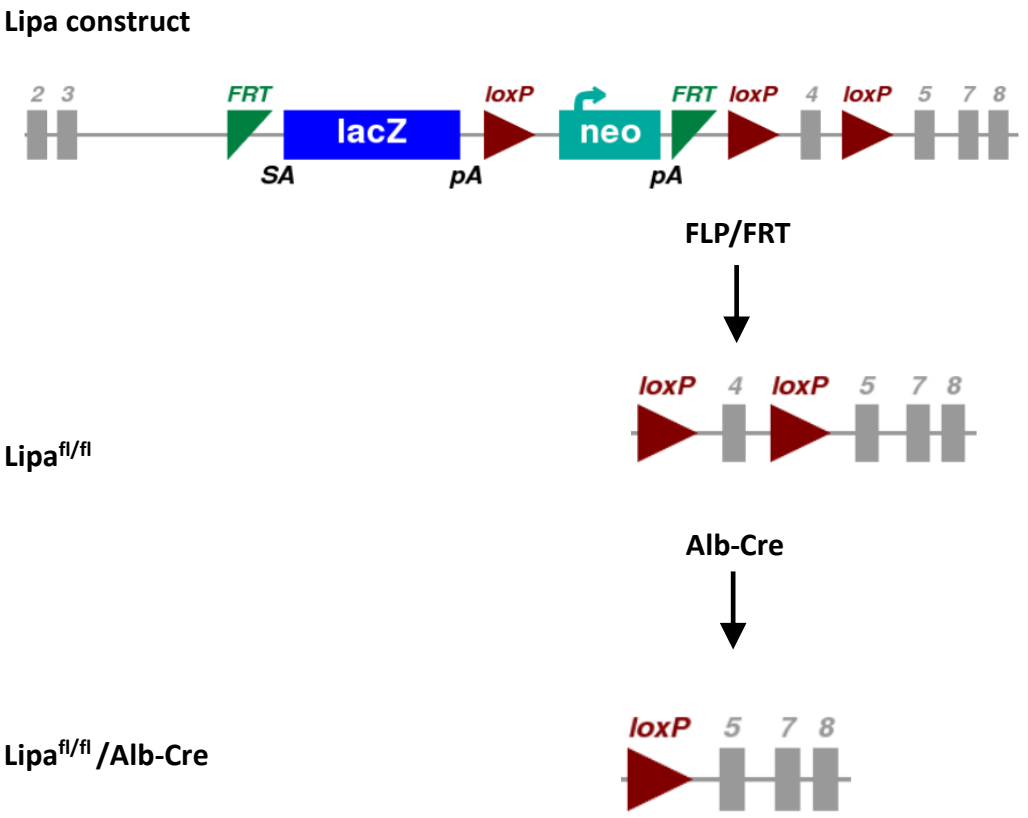

Figure 6: Generation of hepatocyte-specific Lipa$^{-/-}$ mice (Liv-Lipa$^{-/-}$).

The floxed mouse (Lipa$^{fl/fl}$) with a conditional Lipa allele was generated by breeding Lipa$^{tm1a(EUCOMM)Hmgu}$/Biat with mice expressing FLP recombinase. Mice heterozygous for the floxed allele were bred together to obtain homozygous Lipa$^{fl/fl}$ mice that served as controls. The hepatocyte-specific null allele is generated by crossing Lal$^{fl/fl}$ mice with mice expressing Cre recombinase under the control of the albumin promoter to generate Liv-Lipa$^{+/-}$ mice. Mice containing the hepatocyte-specific deletion were then bred homozygously to produce Liv-Lipa$^{-/-}$ mice. The schematic illustration is a copy from the website of EUCOMM. (213) Requisite permission to use this figure was obtained (Appendix).

3.2 Significantly reduced Lipa mRNA and protein expression in Liv-Lipa$^{-/-}$ mice

Liv-Lipa$^{-/-}$ mice are viable and born at Mendelian frequency and proportional male/female ratios (data not shown). Levels of Lipa mRNA expression in livers of Liv-Lipa$^{-/-}$ mice were reduced by 93% compared to control mice, while Lipa mRNA levels in all other tissues remained unchanged (Figure 7A). In hepatocytes, Lipa mRNA levels of Liv-Lipa$^{-/-}$ mice were reduced by 99% compared to control mice (Figure 7B). Furthermore, LAL protein expression in isolated hepatocytes revealed complete absence of LAL in Liv-Lipa$^{-/-}$ hepatocytes (Figure 7C). (213)

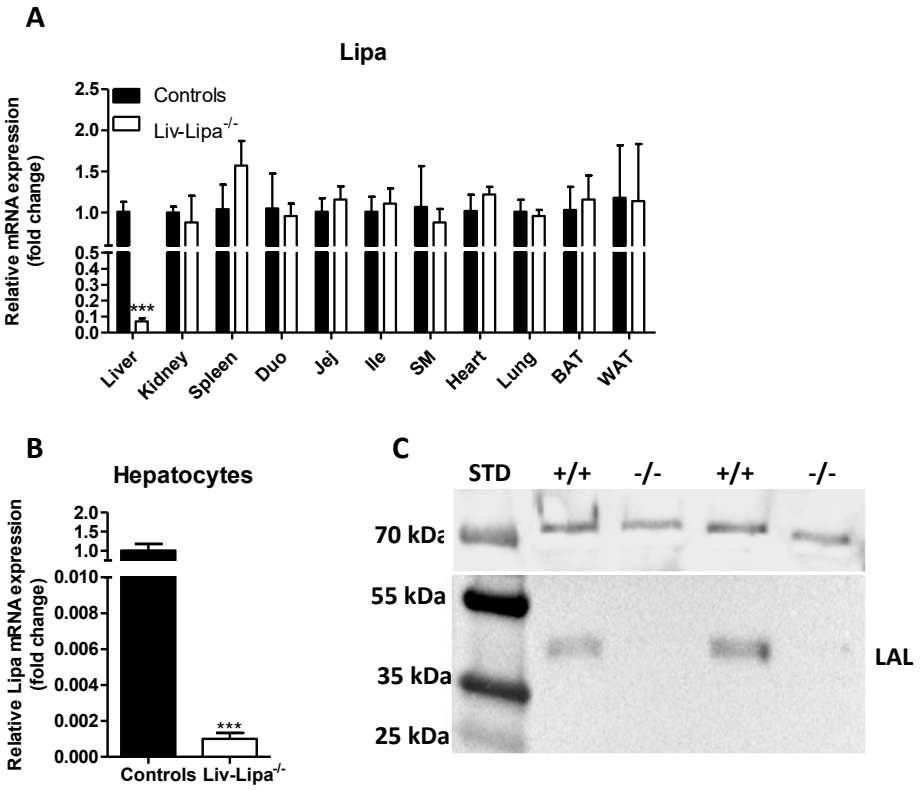

Figure 7: Significantly reduced Lipa mRNA and protein expression in Liv-Lipa$^{-/-}$ mice.

Fifteen week old male *ad libitum* chow diet-fed Lipa$^{fl/fl}$ (controls) and Liv-Lipa$^{-/-}$ mice were used. Lipa mRNA expression relative to cyclophilin A as reference gene in (A) indicated tissues (n=4) and (B) hepatocytes (n=3) (Duo, Duodenum; Jej, Jejunum; Ile, Ileum; SM, skeletal muscle; BAT, brown adipose tissue; WAT, white adipose tissue). Expression profiles were determined using the $2^{-\Delta\Delta Ct}$ method and Lipa mRNA expression in control mice was arbitrarily set to 1. (C) Immunoblotting against LAL using calnexin as loading control. Data represent mean + SD; $p < 0.05$ (*), $p \leq 0.01$ (**), $p \leq 0.001$ (***). (A,B) Student's unpaired t-test. (213) Requisite permission to use this figure was obtained (Appendix).

3.3 LAL is efficiently knocked out in hepatocytes of Liv-Lipa$^{-/-}$ mice

The selectivity of LAL deletion exclusively in hepatocytes was further verified as LAL activity in non-parenchymal cells (NPCS) of Liv-Lipa$^{-/-}$ and control mice was identical, while it was reduced by 70% in hepatocytes (Figure 8A). LAL activity levels in both Lipa$^{-/-}$ and Liv-Lipa$^{-/-}$ mice were reduced to the same extent (70%) indicating a successful tissue-specific KO (Figure 8B). By providing specific substrates for TG and CE hydrolysis at an acidic pH, we found a 70% reduction in TG hydrolase activity (Figure 8C) and an even more pronounced reduction of CE hydrolase activity (Figure 8D) of 90% in Liv-Lipa$^{-/-}$ compared to control hepatocytes. (213)

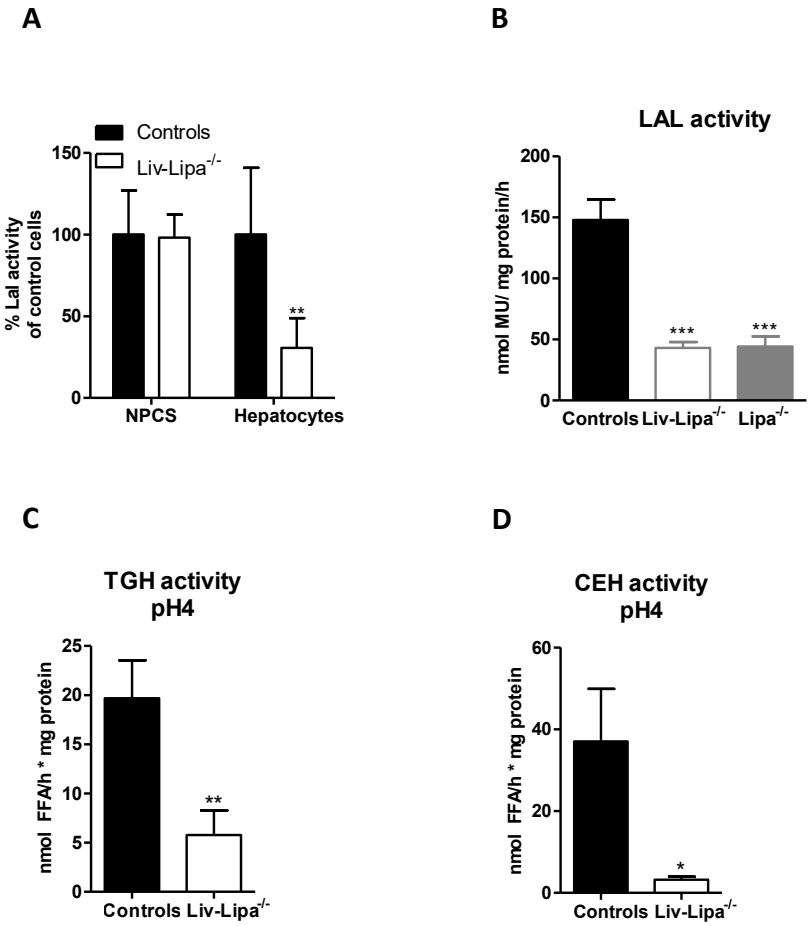

Figure 8: LAL is efficiently knocked out in hepatocytes of Liv-Lipa$^{-/-}$ mice.

LAL activity in (A) non-parenchymal cells (NPCs) (n=3) and hepatocytes (n=5), as well as in (B) livers of Lipa$^{-/-}$ and Liv-Lipa$^{-/-}$ mice (n=3-6) was determined using the fluorogenic substrate 4-MUP at pH 4 (n=5). (C) TG hydrolase activity (pH 4) and (D) CE hydrolase activity (pH 4) in hepatocytes (n=3). Data represent mean + SD; $p < 0.05$ (*), $p \leq 0.01$ (**), $p \leq 0.001$ (***). (A-D) Student's unpaired t-test. (213) Requisite permission to use this figure was obtained (Appendix).

3.4 Increased reliance on carbohydrate oxidation in Liv-Lipa$^{-/-}$ mice

To analyze the impact of hepatic LAL deficiency on whole-body energy homeostasis, I used indirect calorimetry and found that Liv-Lipa$^{-/-}$ mice fed a regular chow diet exhibited a higher respiratory exchange ratio (RER) (Figure 9A). This suggested an enhanced reliance on the breakdown and oxidation of carbohydrates for ATP generation (Figure 9B) and reduced lipid oxidation (Figure 9C), while energy expenditure remained unchanged (Figure 9D). This result was expectable as food intake (Figure 9E) and physical activity were similar in Liv-Lipa$^{-/-}$ and control mice (Figure 9F). (213)

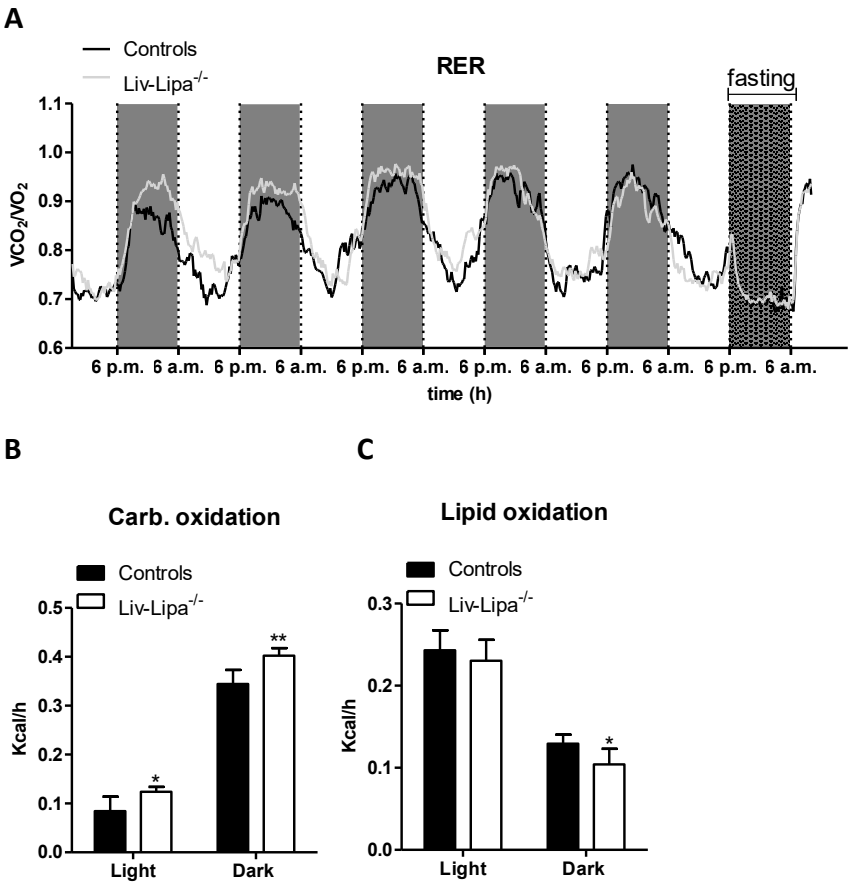

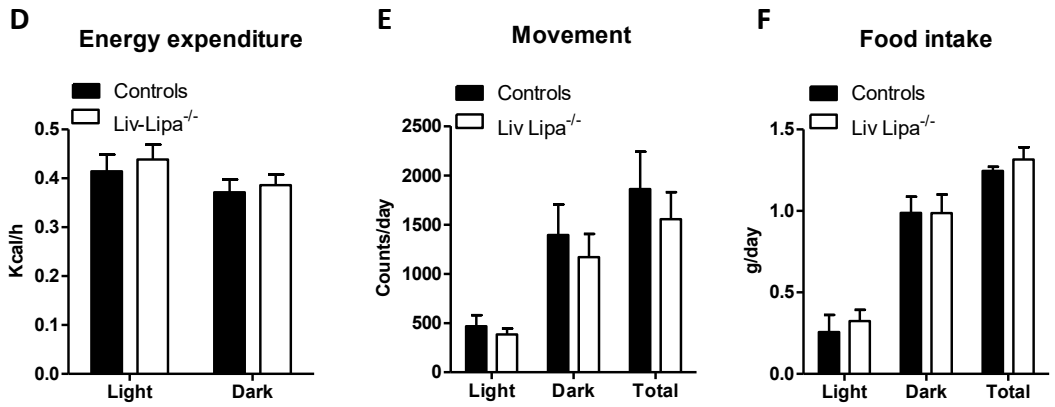

Figure 9: Increased reliance on carbohydrate oxidation in Liv-Lipa$^{-/-}$ mice.

Female control and Liv-Lipa$^{-/-}$ mice were housed at RT in metabolic cages with free access to chow diet and water. (A) Respiratory exchange ratio (RER), (B) carbohydrate oxidation, (C) lipid oxidation, and (D) energy expenditure were measured by indirect gas calorimetry. (E) Food intake and (F) daily locomotor activity (n=4-7). Gray-shaded areas represent dark phases (6 p.m. - 6 a.m.); non-shaded light phases (6 a.m. - 6 p.m.). Data represent mean (n=5-7) + SD; $p < 0.05$ (*), $p \leq 0.01$ (**); (B-F) Student's unpaired t-test (213). Requisite permission to use this figure was obtained (Appendix).

In accordance to unchanged metabolic parameters in chow diet-fed Liv-Lipa$^{-/-}$ mice also plasma lipid parameters (Figure 10A) as well as lipoprotein profiles (Figure 10B,C) were comparable between the genotypes.

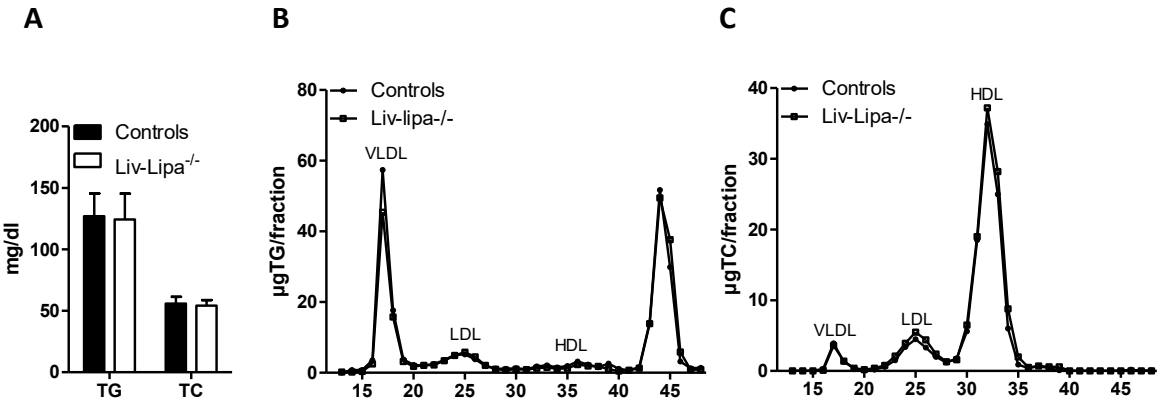

Figure 10: Similar plasma lipid parameters between chow diet-fed control and Liv-Lipa$^{-/-}$ mice.

(A) Plasma triglyceride (TG) and total cholesterol (TC) concentrations in female mice fasted for 12 h. (B,C) Lipoprotein profile of pooled plasma samples after FPLC separation. Data represent mean (n=6) + SD.

3.5 Comparable liver phenotype in chow diet-fed control and Liv-Lipa$^{-/-}$ mice

The liver damage markers ALT and AST are the first diagnostic tools to determine LAL deficiency in humans. As we could not find systemic changes in Liv-Lipa$^{-/-}$ mice fed a normal chow diet, we were wondering if livers are affected. However, we did not see differences between plasma concentrations in ALT or AST between control and Liv-Lipa$^{-/-}$ mice (Figure 11).

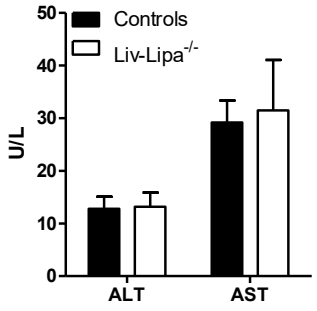

Figure 11: Comparable ALT and AST levels in plasma of chow diet-fed control and Liv-Lipa$^{-/-}$ mice.
Plasma concentrations of aspartate-aminotransferase (AST) and alanine aminotransferase (ALT) in male chow diet-fed mice. Data represent mean values (n=5) + SD.

Furthermore, the histopathological analysis of markers for glycogen storage (PAS) (Figure 12A), proliferation (KI67) (Figure 12B), collagen content (CAB) (Figure 12C), and connective tissue content (Trichrome) (Figure 12D) revealed comparable results between female control and Liv-Lipa$^{-/-}$ mice.

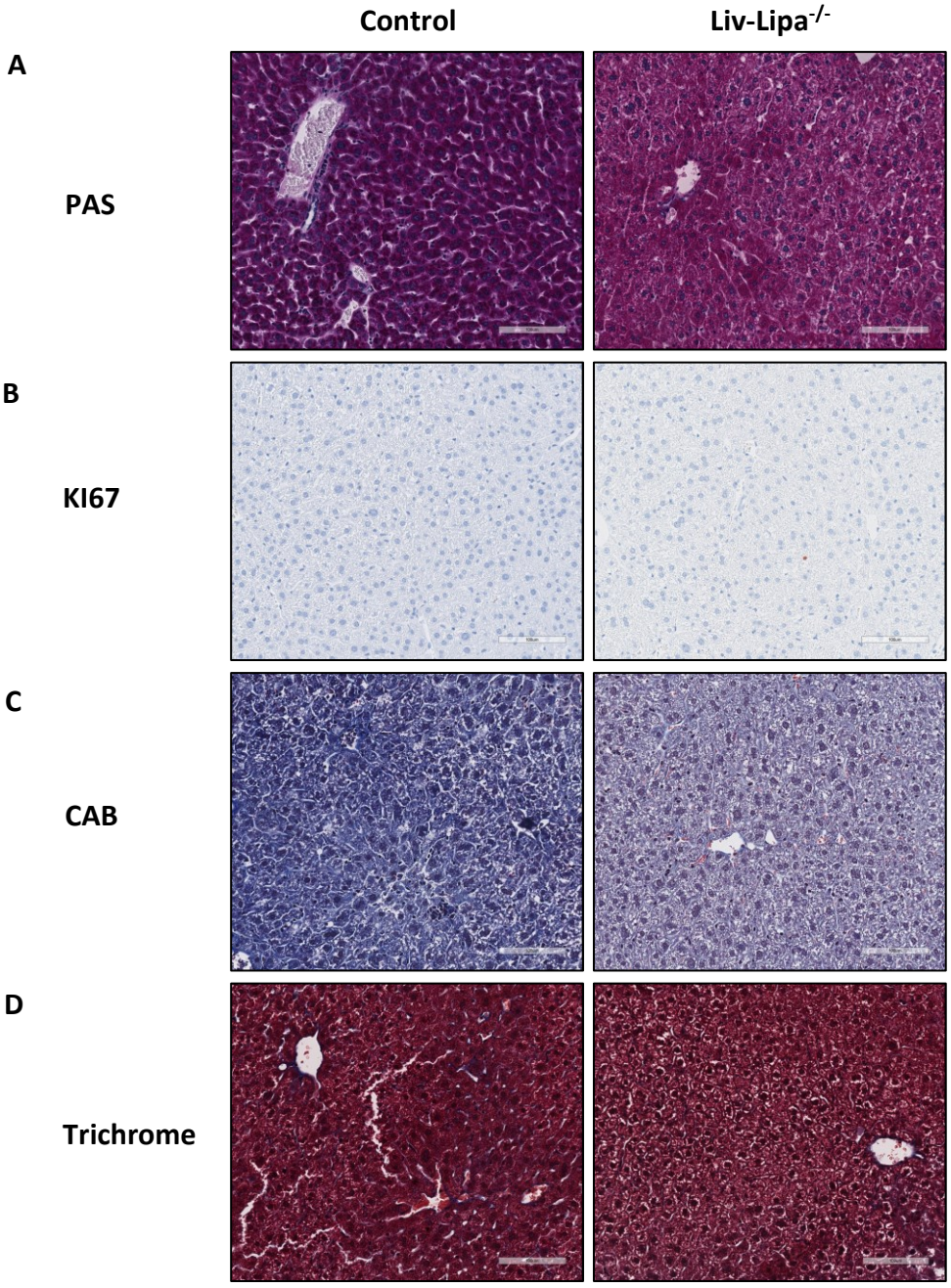

Figure 12: Comparable liver phenotype in chow diet-fed control and Liv-Lipa$^{-/-}$ mice.

Representative images of (A) PAS, (B) KI67, (C) CAB, and (D) Trichrome stainings of female control (left panel) and Liv-Lipa$^{-/-}$ (right panel) liver sections (scale bar, 100 µm).

These results imply that chow-diet fed Liv-Lipa$^{-/-}$ mice do not suffer from liver damage or fibrosis.

3.6 Increased hepatic cholesterol concentrations in Liv-Lipa$^{-/-}$ mice fed chow diet

Liv-Lipa$^{-/-}$ mice did not display any differences in body (Figure 13A) and liver weight (Figure 13B) on chow diet. However, we found a 7-fold increase of hepatic CE concentrations in 12 h-fasted Liv-Lipa$^{-/-}$ mice (Figure 13C), in accordance with increased staining of the neutral lipid dye ORO (Figure 13D). As CE accumulation is a characteristic of LAL-D in patients suffering from CESD or WD (147), these findings emphasize the suitability of this mouse model to study the direct consequences of diminished LAL activity in the liver. (213)

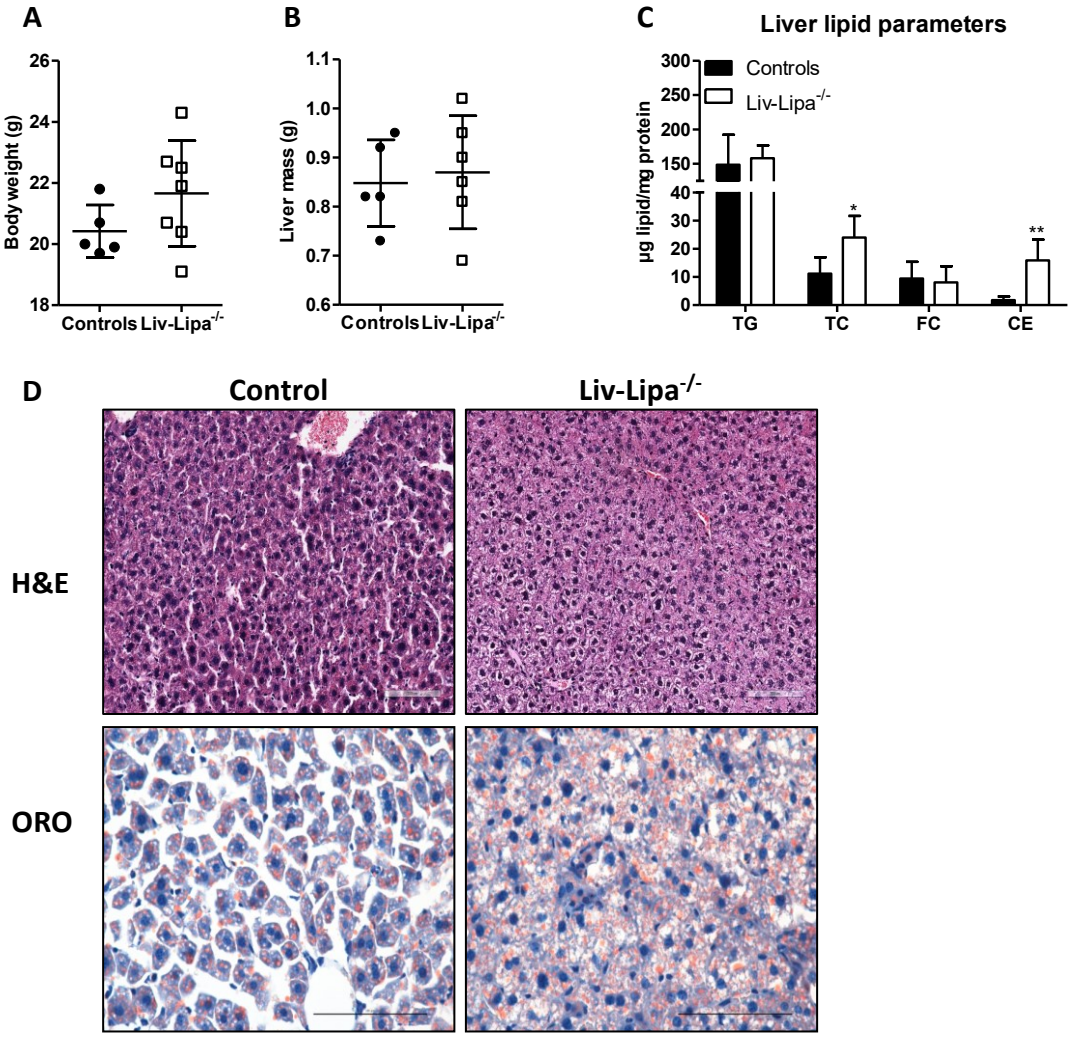

Figure 13: Increased hepatic cholesterol concentrations in Liv-Lipa$^{-/-}$ mice fed chow diet.

(A) Body weight and (B) total liver weight of chow diet-fed control and Liv-Lipa$^{-/-}$ mice. (C) Hepatic lipid parameters. (D) H&E staining (upper panel) and Oil red O (ORO) staining (lower panel) of liver sections (scale bar 100 µm). Data represent mean (n = 5-7) ± SD; $p < 0.05$ (*), $p \leq 0.01$ (**). (A-C) Student's unpaired t-test. (213) Requisite permission to use this figure was obtained (Appendix).

3.7 HF/HCD-fed Liv-Lipa$^{-/-}$ mice are resistant to diet-induced obesity

The increase in hepatic cholesterol concentrations on a regular chow diet containing only 4% fat prompted us to investigate Liv-Lipa$^{-/-}$ mice after challenging them with a HF/HCD for 20 weeks. Already after 8 weeks on diet, Liv-Lipa$^{-/-}$ mice weighed up to 8 g (35% of BW) less than their control littermates (Figure 14 A,B). In analogy to Lipa$^{-/-}$ mice (107), we expected plasma lipid parameters in the fasted state to be affected by hepatocyte-specific LAL deficiency. While Liv-Lipa$^{-/-}$ mice exhibited comparable plasma TG, we found increased TC concentrations in comparison to control mice (Figure 14C). Plasma lipoprotein profiles after separation by FPLC revealed increased LDL cholesterol levels in Liv-Lipa$^{-/-}$ mice (Figure 14D). (213)

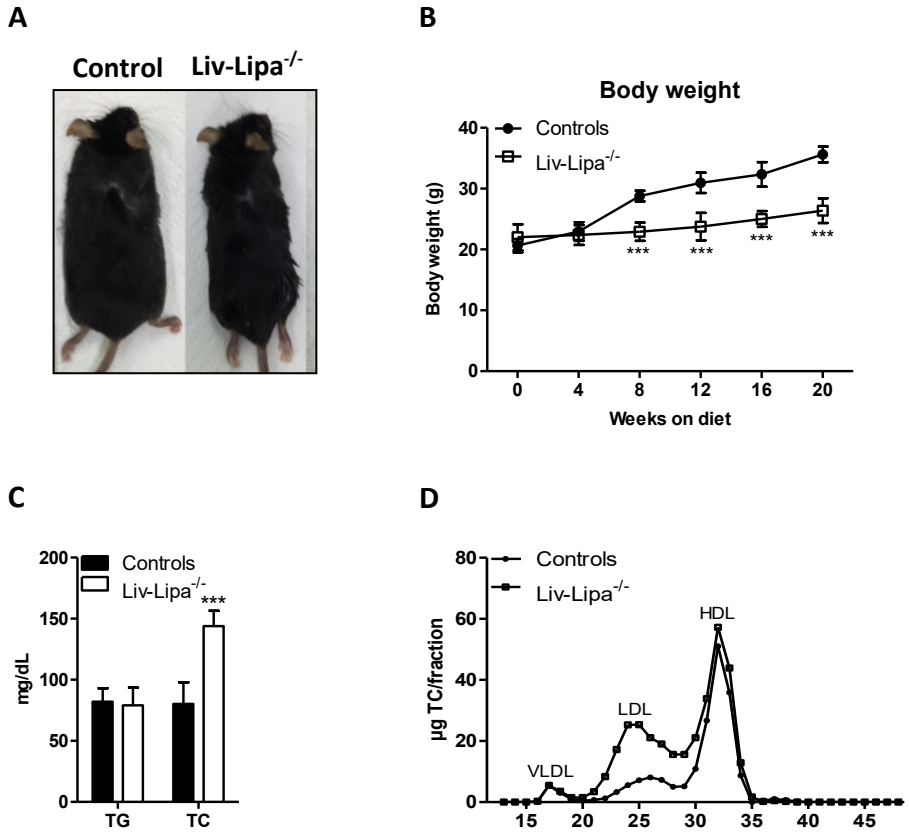

Figure 14: Liv-Lipa$^{-/-}$ mice are resistant to diet-induced obesity.

(A) Representative image of a male control and a Liv-Lipa$^{-/-}$ mouse fed HF/HCD. (**B**) Body weight curve during 20 weeks of HF/HCD feeding. (**C**) Plasma triglyceride (TG) and total cholesterol (TC) concentrations in 12 h-fasted mice fed HF/HCD for 20 weeks. (**D**) Lipoprotein profile of pooled plasma samples after FPLC separation. Data represent mean (n=8) ± SD; $p \leq 0.001$ (***). (**B**) ANOVA. (**C**) Student's unpaired t-test. (213) Requisite permission to use this figure was obtained (Appendix).

3.8 Comparable metabolic parameters between controls and Liv-Lipa$^{-/-}$ mice

Food intake (Figure 15A), movement (Figure 15B), energy expenditure (Figure 15C), fecal energy content (Figure 15D), and body temperature (Figure 15E) did not explain the body weight differences in Liv-Lipa$^{-/-}$ and control mice as all metabolic parameters measured were comparable between the genotypes. (213) Furthermore, fecal output, measured after three consecutive days, was similar in control and Liv-Lipa$^{-/-}$ mice.

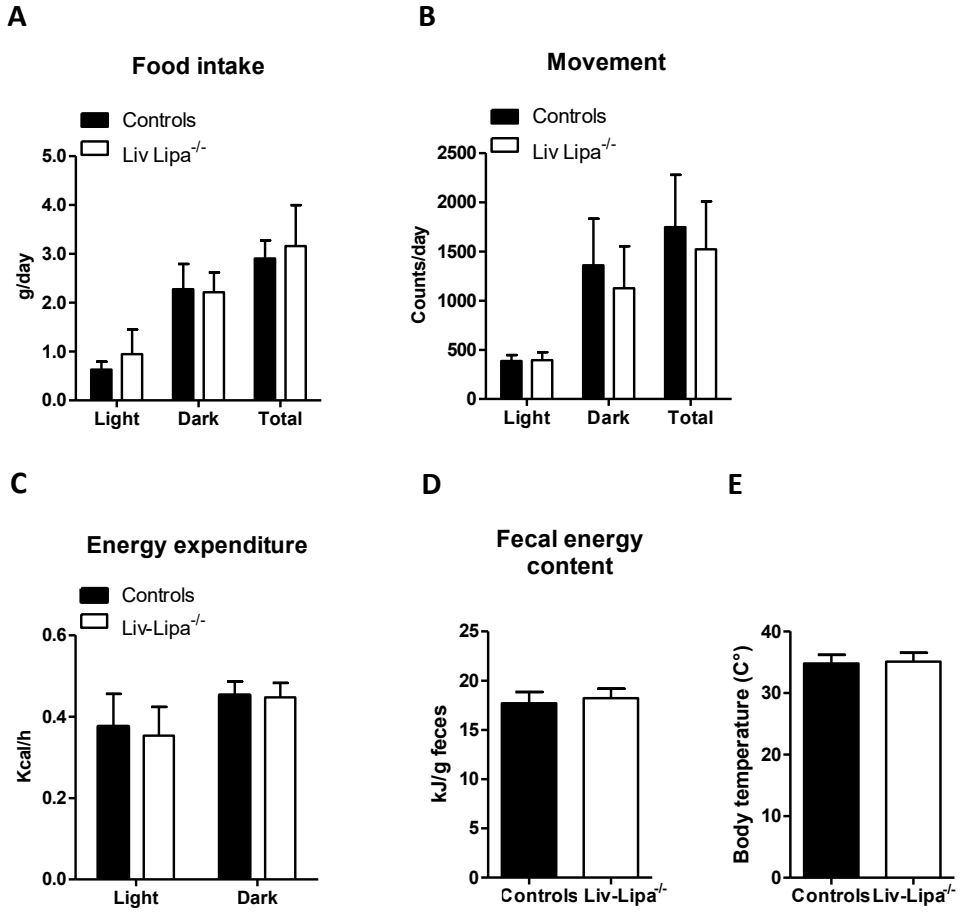

Figure 15: Comparable metabolic parameters between controls and Liv-Lipa$^{-/-}$ mice.

Female control and Liv-Lipa$^{-/-}$ mice were housed in metabolic cages with free access to HF/HCD and water (n=4-6). (A) Food intake, (B) daily locomotor activity (C), and energy expenditure were measured by indirect gas calorimetry. (D) Fecal energy content was measured using an adiabatic oxygen bomb calorimeter (n=5-7). (E) Body temperature was measured using a rectal probe in 12h-fasted control and Liv-Lipa$^{-/-}$ mice. Data represent mean + SD; (A-E) Student's unpaired t-test. (213) Requisite permission to use this figure was obtained (Appendix).

Similar to chow-diet fed Liv-Lipa$^{-/-}$ mice, also HF/HCD-fed mice exhibited a greater reliance on carbohydrate oxidation (Figure 16A), while lipid oxidation (Figure 16B) was comparable. (213)

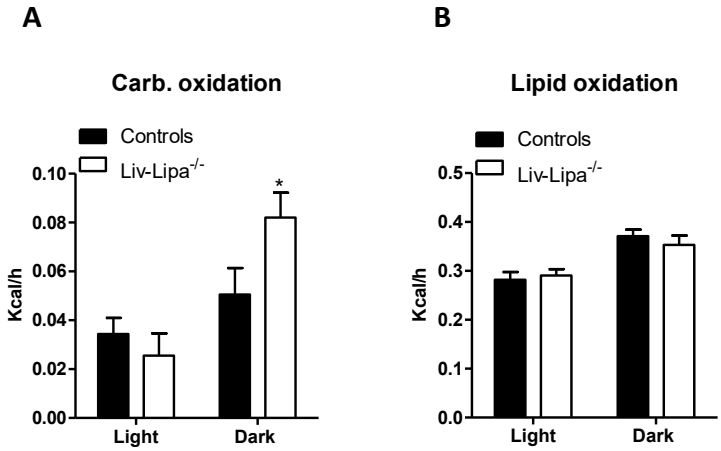

Figure 16: Increased reliance on carbohydrate oxidation in Liv-Lipa$^{-/-}$ mice fed HF/HCD.

Female control and Liv-Lipa$^{-/-}$ mice were housed in metabolic cages with free access to HF/HCD and water (n=4-6). Quantification of (A) carbohydrate oxidation and (B) lipid oxidation. Data represent mean + SD; $p < 0.05$ (*). (A,B) Student's unpaired t-test. (213) Requisite permission to use this figure was obtained (Appendix).

3.9 Reduced WAT mass but unchanged adipose tissue morphology in Liv-Lipa$^{-/-}$ mice

Despite unchanged metabolic parameters Liv-Lipa$^{-/-}$ mice had 68% reduced perigonadal WAT weight after 20 weeks of feeding (Figure 17A) with significantly smaller WAT depots. We therefore analyzed BAT and WAT morphology by H&E staining and observed comparable white and brown adipocyte size and cell appearance between genotypes (Figure 17B). (213)

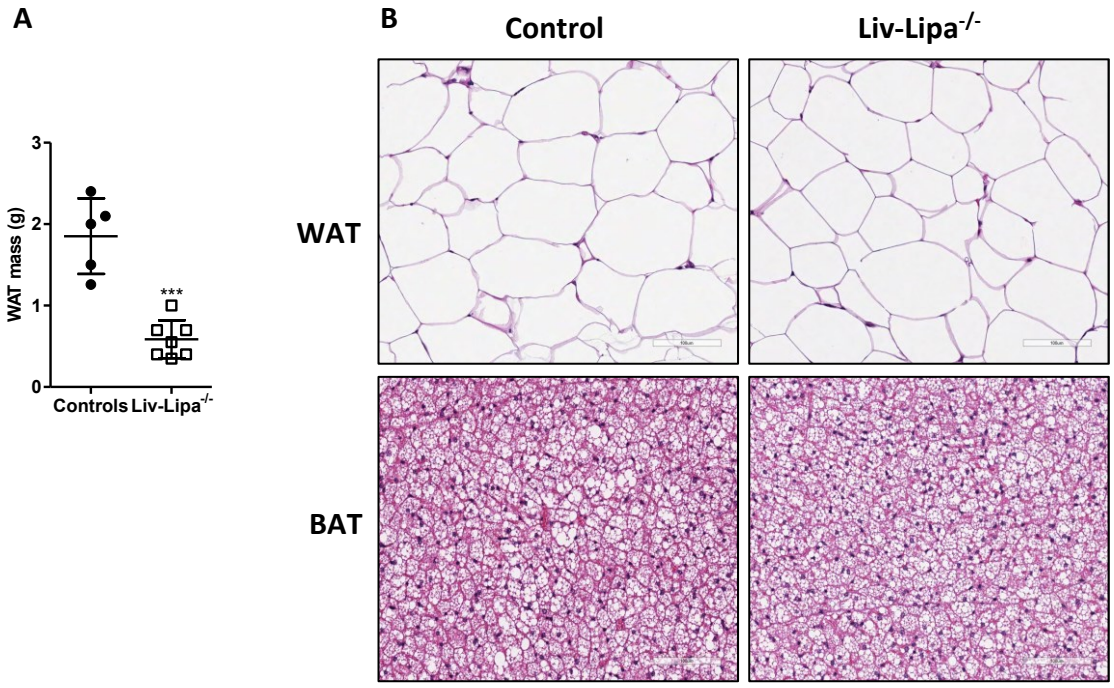

Figure 17: Reduced WAT mass but unchanged adipose tissue morphology in Liv-Lipa$^{-/-}$ mice.

(A) WAT weight of controls and Liv-Lipa$^{-/-}$ mice after 20 weeks of HF/HCD. (B) H&E staining of WAT and BAT sections of 10 week HF/HCD-fed Liv-Lipa$^{-/-}$ and control mice (scale bar 100 µm). Data represent mean (n=5-7) ± SD; $p \leq 0.001$ (***) (A) Student's unpaired t-test. (213) Requisite permission to use this figure was obtained (Appendix).

The significantly reduced WAT depots were further verified by fat mass quantification using µCT, which revealed comparable lean mass (Figure 18A) but 67% reduced fat mass (Figure 18B) with a concomitant reduction in fat/body mass ratio of 48% (Figure 18C) in Liv-Lipa$^{-/-}$ compared to control animals. The scans futher showed that the reduction in WAT mass was not only present in inguinal fat depots but also in subcutaneous fat depots (Figure 18D).

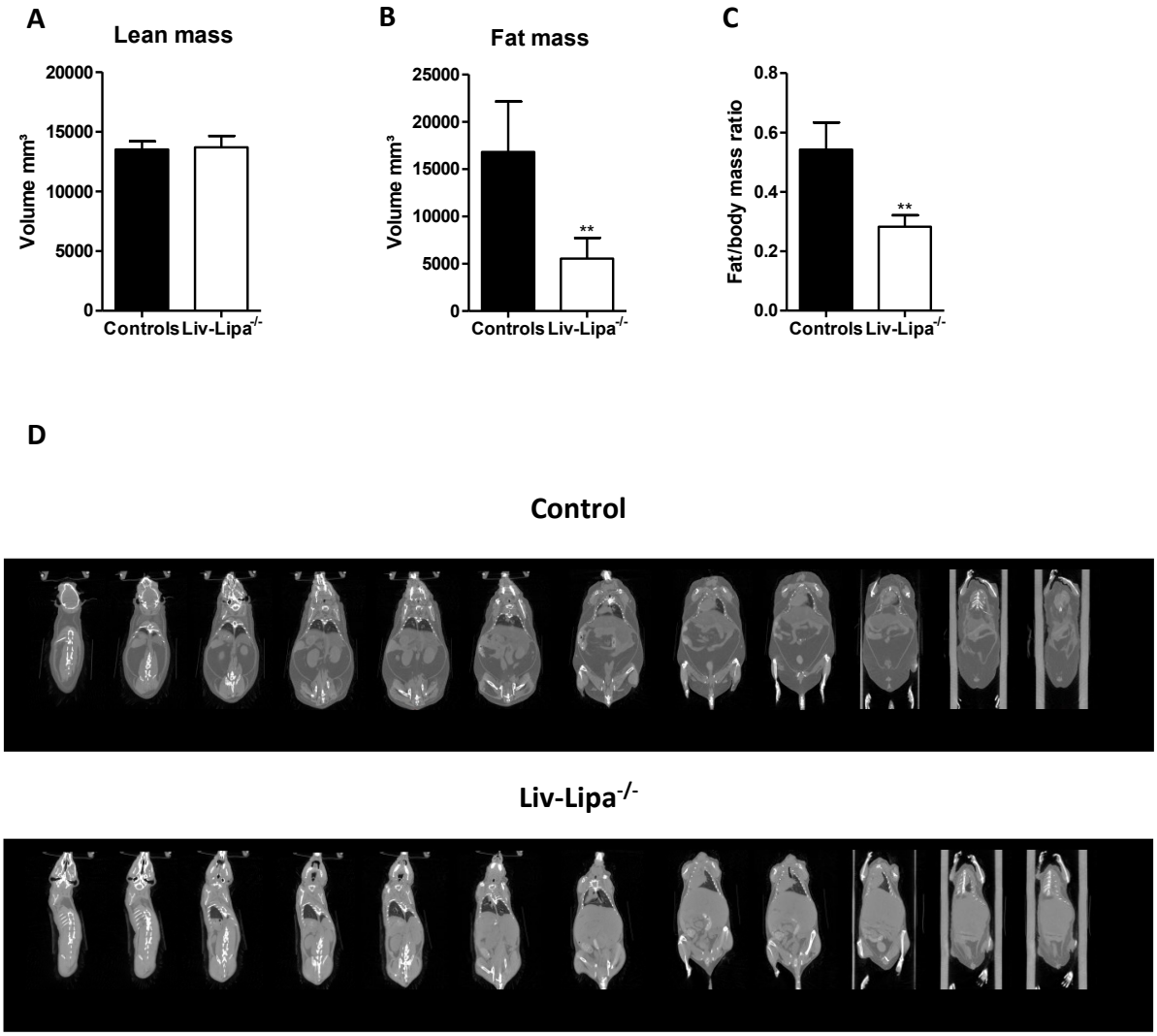

Figure 18: Fat mass quantification using µCT

Female mice were fed HF/HCD for 25 weeks. (A) Lean mass, (B) fat mass, and (C) fat/body mass ratio. (D) µCT scan of a representative control and Liv-Lipa$^{-/-}$ mouse. Data represent mean (n=5) + SD. (A-C) $p \leq 0.01$ (**). Student's unpaired t test.

Collectively, these findings demonstrate that loss of hepatic LAL leads to changes in metabolism and preserves the ability to adapt to energetic requirements in response to different dietary challenges.

3.10 Improved glucose clearance in HF/HCD-fed Liv-Lipa$^{-/-}$ mice

The hepatic accumulation of lipids and the reduced fat mass of Liv-Lipa$^{-/-}$ mice as well as the higher reliance on carbohydrate catabolism (Figure 16A) prompted us to further investigate glucose metabolism-related changes. While glucose tolerance as well as insulin sensitivity were not altered in chow diet-fed Liv-Lipa$^{-/-}$ and control mice (Figure 19A,B), we observed improved glucose clearance (Figure 19C) in Liv-Lipa$^{-/-}$ mice fed a HF/HCD compared to controls. Furthermore, Liv-Lipa$^{-/-}$ mice displayed a significant drop and delay in the normalization of blood glucose levels after an insulin challenge (Figure 19D). (213)

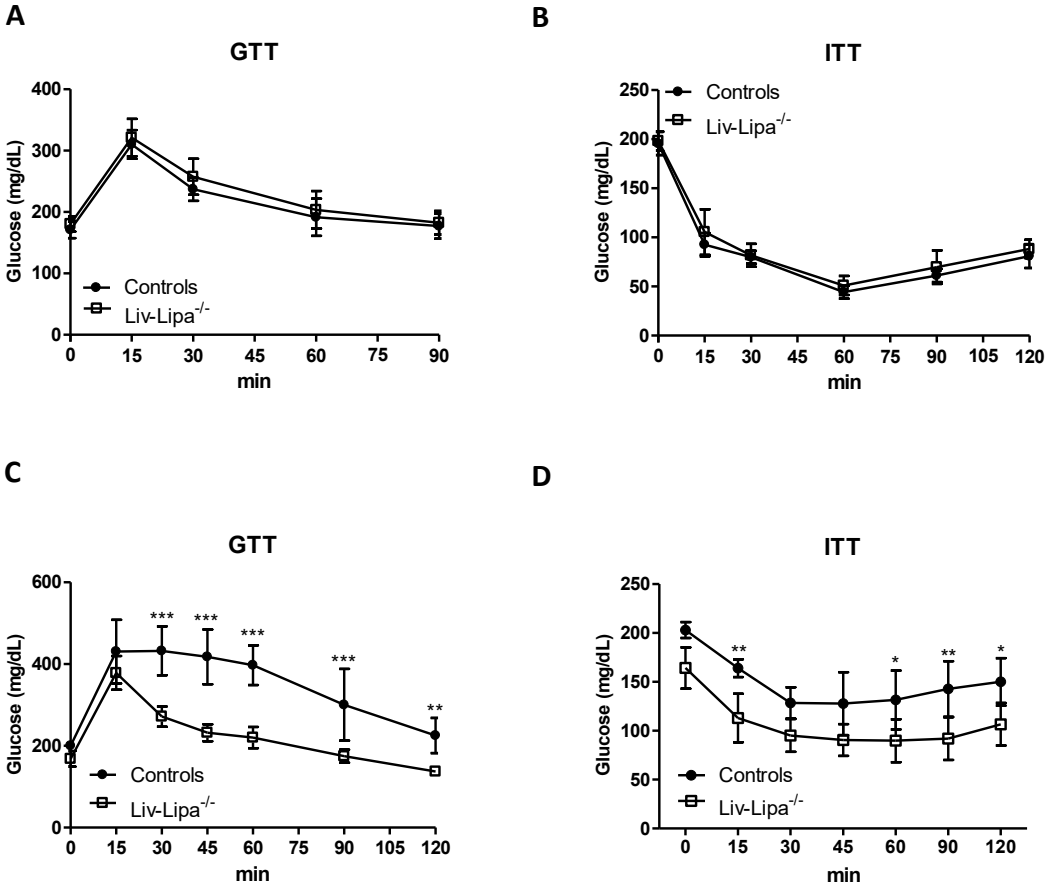

Figure 19: Improved glucose clearance in HF/HCD-fed Liv-Lipa$^{-/-}$ mice.

Plasma glucose concentrations after i.p. injection of (A,C) glucose (2 g/kg) or (B,D) insulin (0.25 U/kg), respectively. (A,C) 6 h-fasted and (B,D) 4 h-fasted control and Liv-Lipa$^{-/-}$ mice fed either (A,B) chow (n=4-5) or (C,D) HF/HCD (n=8) were used to determine (A,C) glucose and (B,D) insulin tolerance, respectively. Data represent mean ± SD; $p < 0.05$ (*), $p \leq 0.01$ (**), $p \leq 0.001$ (***). (A-D) ANOVA. (213) Requisite permission to use this figure was obtained (Appendix).

3.11 Increased insulin resistance in Liv-Lipa$^{-/-}$ mice

When HF/HCD-fed Liv-Lipa$^{-/-}$ mice were fasted for 12 h and blood was taken, we found unchanged plasma glucose concentrations (Figure 20A). Plasma insulin concentrations however, were 55-fold increased (Figure 20B). The high plasma insulin levels associated with a 19.7 -fold increase in the homeostasis model assessment (HOMA) index (Figure 20C) suggest extensive insulin resistance in Liv-Lipa$^{-/-}$ mice. In WAT mRNA expression levels of adiponectin receptor 1 and 2 were significantly upregulated (1.7 and 1.5-fold, respectively), while leptin receptor 1 mRNA expression was markedly decreased (76%) in Liv-Lipa$^{-/-}$ compared to control animals (Figure 20D).

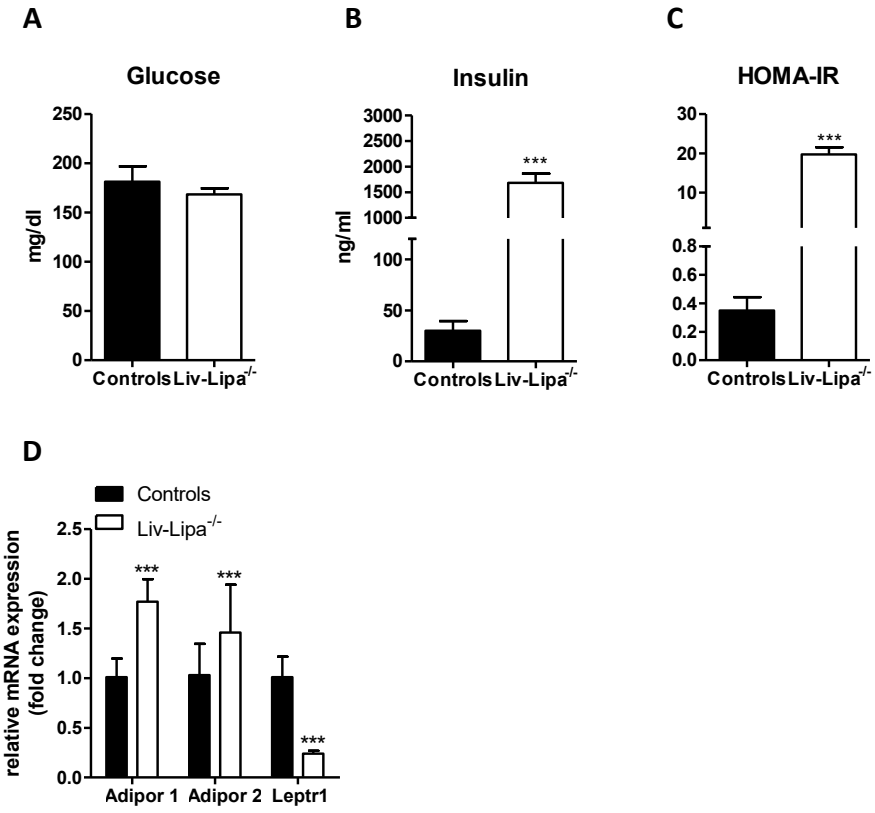

Figure 20: Increased insulin resistance in Liv-Lipa$^{-/-}$ mice.

(A) Plasma glucose and (B) insulin consentrations of female control and Liv-Lipa$^{-/-}$ mice fed HF/HCD for 20 weeks (n=8). (C) Calculation of the HOMA-IR to determine hepatic insulin resistance. (D) WAT mRNA expression of adiponectin receptor 1 and 2 and leptin receptor 1 relative to cyclophilin A as reference gene in 12 h-fasted female mice fed a HF/HCD for 20 weeks (n=3). Data represent mean + SD; $p \leq 0.001$ (***) (A-D) Student's unpaired t-test.

3.12 Reduced gluconeogenesis and switch to ketone body formation in Liv-Lipa$^{-/-}$ mice

Impairment in glucose clearance and insulin resistance prompted us to assess mRNA expression of genes involved in gluconeogenesis and found a significant reduction in *Pcx* (pyruvate carboxylase, 34%), *Mdh* (malate dehydrogenase, 32%), *Pepck* (59%), and *G6pase* (64%) expression (Figure 21A). In line, mRNA levels of the TCA cycle genes *Cs* (citrate synthase), *Suclg2* (succinate-Coenzyme A ligase), *Fh* (fumarate hydratase), and *Pdhb* (pyruvate dehydrogenase) were also reduced (41%, 44%, 23%, and 35%, respectively) (Figure 21B). mRNA expression of urea cycle genes (Figure 21C) showed a trend toward an increase but failed to reach statistical significance. Also β-hydroxybutyrate (Figue 21D) concentrations were increased in plasma of HF/HCD-fed Liv-Lipa$^{-/-}$ mice. (213)

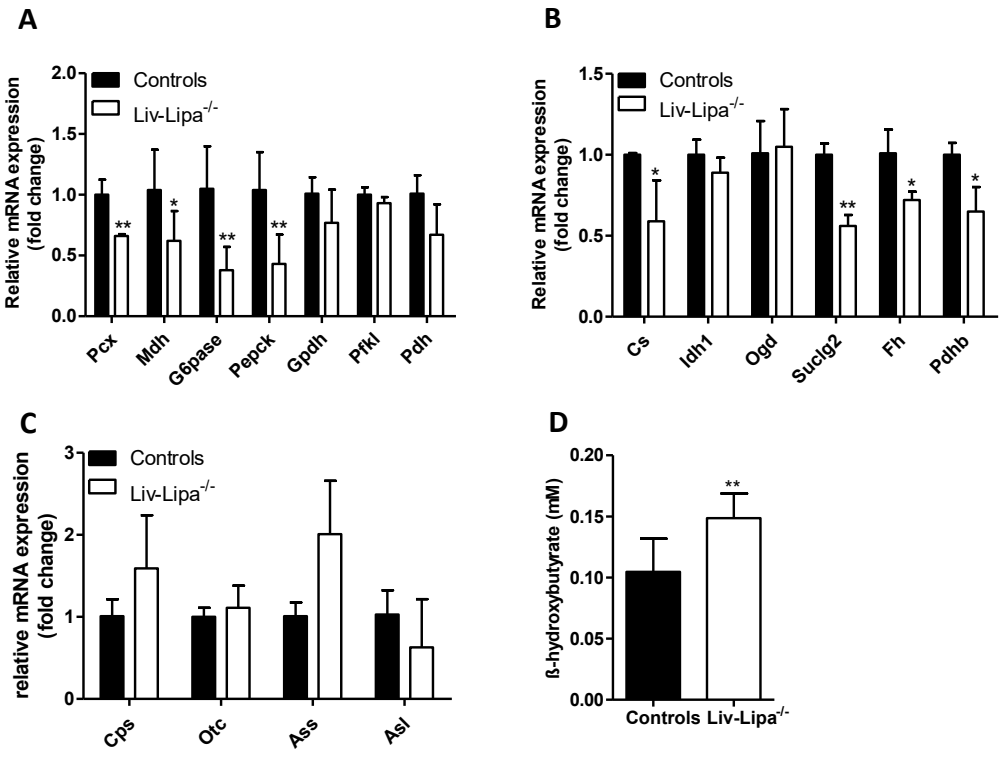

Figure 21: Reduced gluconeogenesis and switch to ketone body formation in Liv-Lipa$^{-/-}$ mice.

Hepatic mRNA expression of genes involved in (A) gluconeogenesis, (B) tricarboxylic acid cycle, and (C) urea cycle genes relative to cyclophilin A as reference gene in female mice fed HF/HCD for 20 weeks (n=3-7). (D) Plasma ß-hydroxybuyrate concentrations in male mice fed HF/HCD for 10 weeks (n=5-7). Data represent mean + SD; $p < 0.05$ (*), $p \leq 0.01$ (**), $p \leq 0.001$ (***). (A-C) Student's unpaired t-test. (213) Requisite permission to use this figure was obtained (Appendix).

3.13 Increased hepatic glutamine, glutamate, and creatine concentrations in HF/HCD-fed Liv-Lipa$^{-/-}$ mice

To further identify metabolic differences between control and Liv-Lipa$^{-/-}$ livers, we performed NMR metabolic profiling. Hereby, a metabolic fingerprint of each liver sample was obtained. When comparing differences between tissues of Liv-Lipa$^{-/-}$ and control mice, PCA analysis revealed a clustering of the samples (Figure 22A). Using a supervised multivariate statistical method called orthogonal-partial least square-discriminant analysis (O-PLS-DA), intra-group variances were removed and a well-defined clustering of Liv-Lipa$^{-/-}$compared to control animals was observed with correlation coefficients R^2 of 0.879 and Q^2 of 0.557 (Figure 22B).

By using a data reduction approach, reduced NMR spectra revealed altered metabolites in Liv-Lipa$^{-/-}$ mice (Figure 22C) including reductions in total lipid content, glycogen, NAD^+ and $NADP^+$ as well as an increase in creatine, glutamine, and glutamate. Polar metabolites were quantified and normalized using probabilistic quotient normalization and fold changes as logarithm to base 2 for metabolites of interest were determined (Figure 22D). However, when performing the same analysis in plasma samples we could not detect differences between control and Liv-Lipa$^{-/-}$ mice (data not shown).

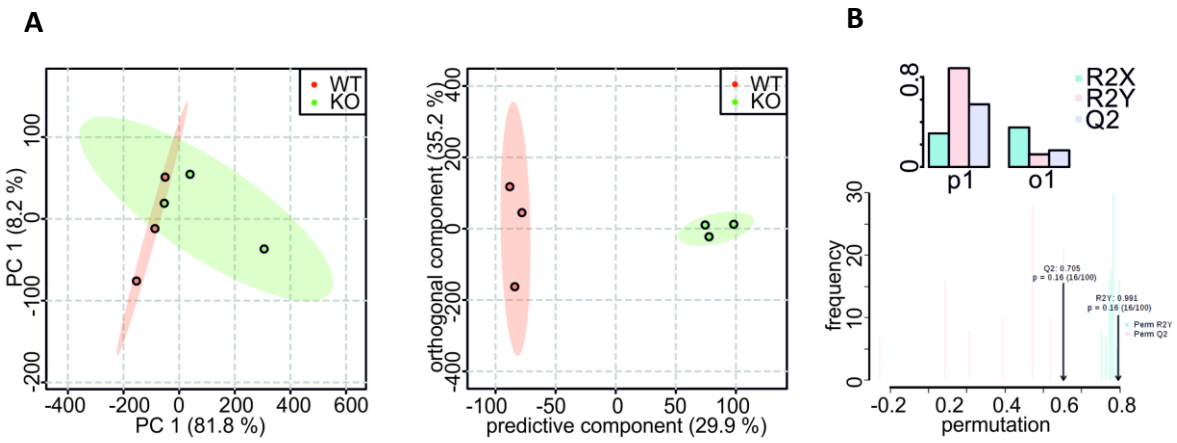

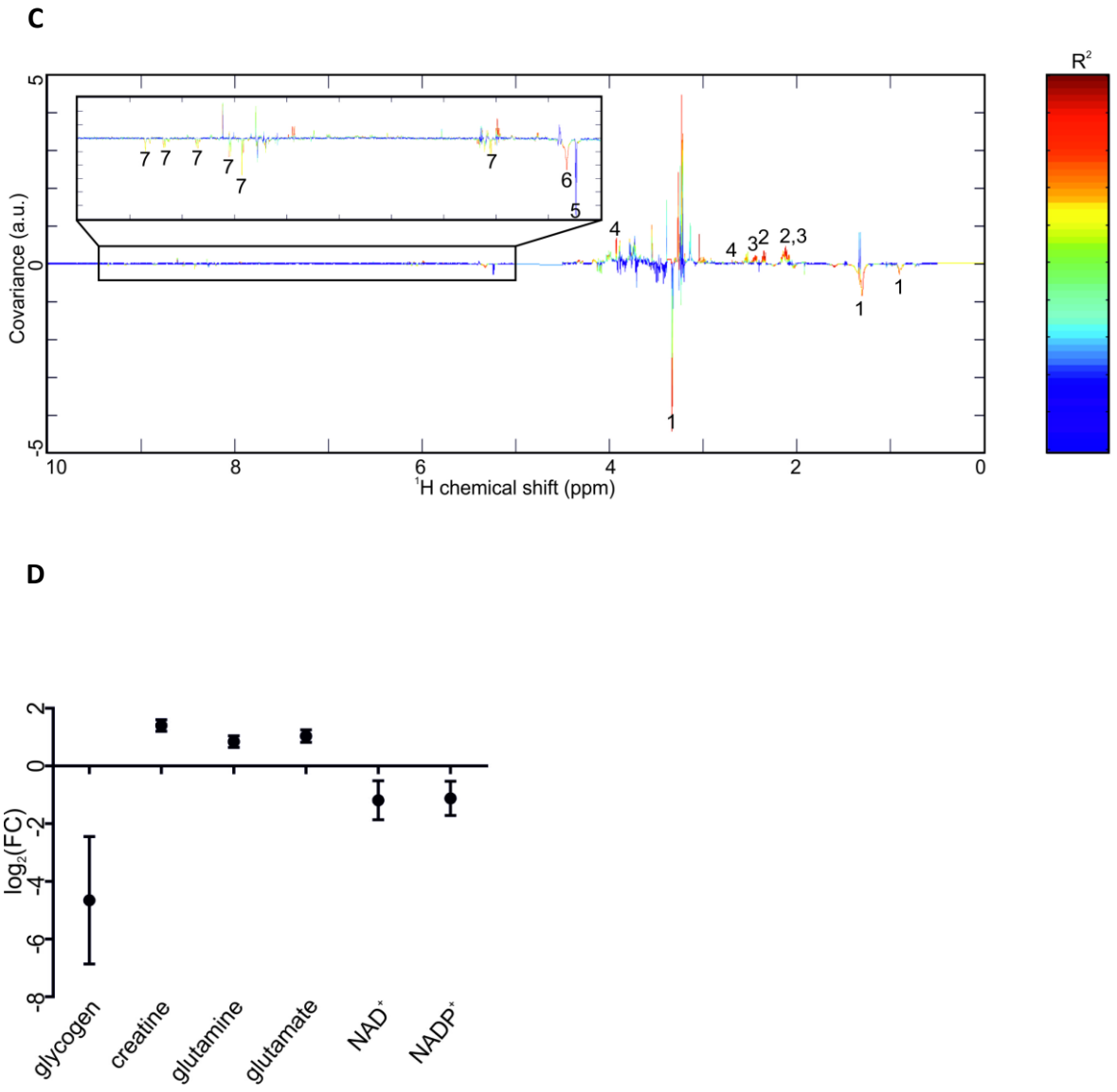

Figure 22: Metabolic phenotyping of liver tissue in control and Liv-Lipa$^{-/-}$ mice.

Mice were fed HF/HCD for 10 weeks. (A) PCA plot of control vs Liv-Lipa$^{-/-}$ mice. (B) Multivariate O-PLS-DA plot of control vs Liv-Lipa$^{-/-}$ mice. (C) Reduced NMR spectra reveal altered metabolites in control vs. Liv-Lipa$^{-/-}$ mice. Positive covariance corresponds to metabolites present at increased concentrations in Liv-Lipa$^{-/-}$ mice, whereas negative covariance corresponds to decreased metabolite concentrations in Liv-Lipa$^{-/-}$ mice. Predictivity of the model is represented by R2. 1… total lipids, 2… glutamate, 3… glutamine, 4… creatine, 5… glucose, 6… glycogen, 7…NAD$^+$, NADP$^+$. (D) Normalized metabolite fold changes as logarithm to the base 2.

3.14 Increased liver size in Liv-Lipa$^{-/-}$ mice fed HF/HCD

Liv-Lipa$^{-/-}$ mice display enlarged and discolored livers (Figure 23A). Hepatocytes from Liv-Lipa$^{-/-}$ mice contained fewer cytosolic LD. Cytosolic LD and the overall lipid load seemed to be reduced (Figure 23A), whereas total liver mass (Figure 23B) was significantly increased in Liv-Lipa$^{-/-}$ mice (213).

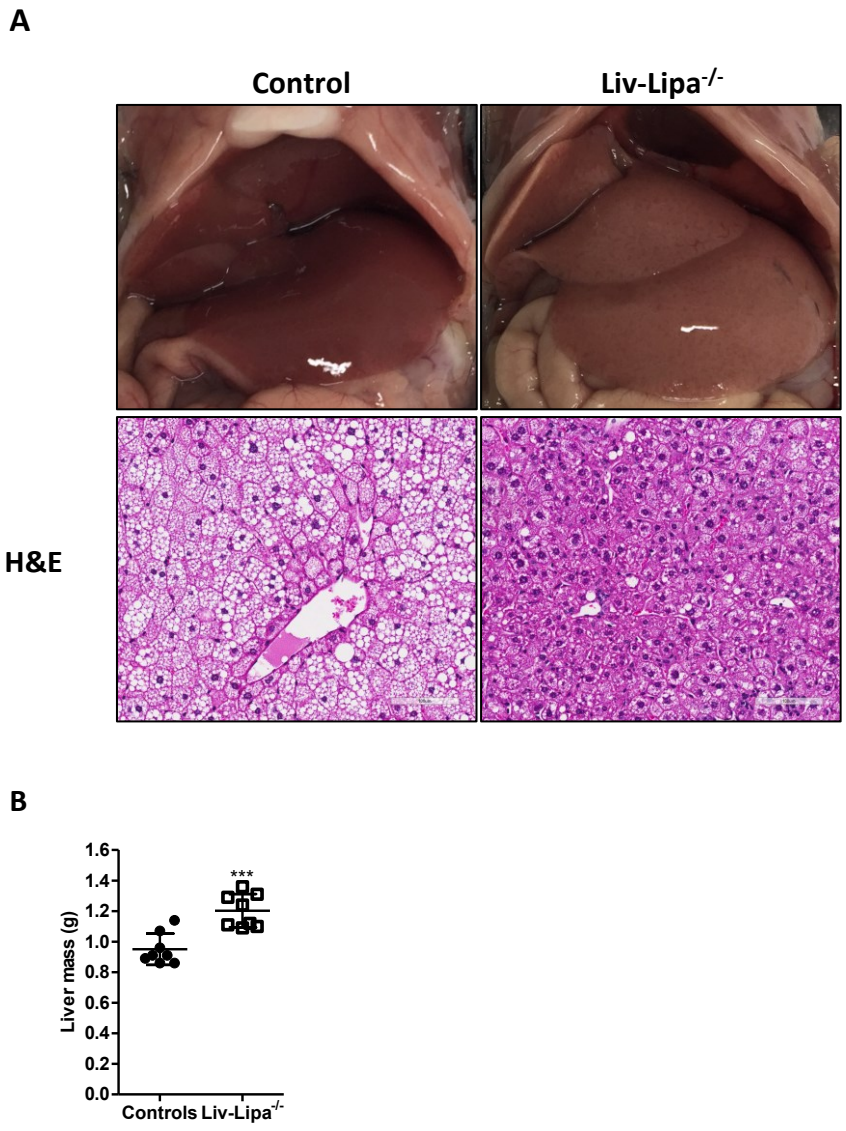

Figure 23: Increased liver size in Liv-Lipa$^{-/-}$ mice.

(A) Representative images of livers and representative H&E staining of liver sections (scale bar, 100 µm). (B) Total liver weight from male control and Liv-Lipa$^{-/-}$ mice fed HF/HCD for 10 weeks. Data represent mean (n = 8) ± SD; p ≤ 0.001 (***). (B) Student's unpaired t-test. (213) Requisite permission to use this figure was obtained (Appendix).

3.15 Lysosomal lipid accumulation and cholesterol crystal formation in Liv-Lipa$^{-/-}$ mice fed HF/HCD

To evaluate the intracellular location of the lipid stored in hepatocytes, we performed electron microscopy. Comparable to our findings in Lipa$^{-/-}$ mice (107), ultrastructural analysis confirmed that the majority of lipid present in Liv-Lipa$^{-/-}$ livers accumulate inside lysosomes with less cytosolic LD, while littermate controls only accumulate cytosolic LD. Furthermore, we observed cholesterol (or CE) crystals in the cytoplasm of Liv-Lipa$^{-/-}$ hepatocytes (Figure 24A). Detailed size distribution analysis of the cytosolic LD proved that predominantly small LD particles are present in the livers of Liv-Lipa$^{-/-}$ mice (Figure 24B) resulting in a reduced total LD area (Figure 24C) (213).

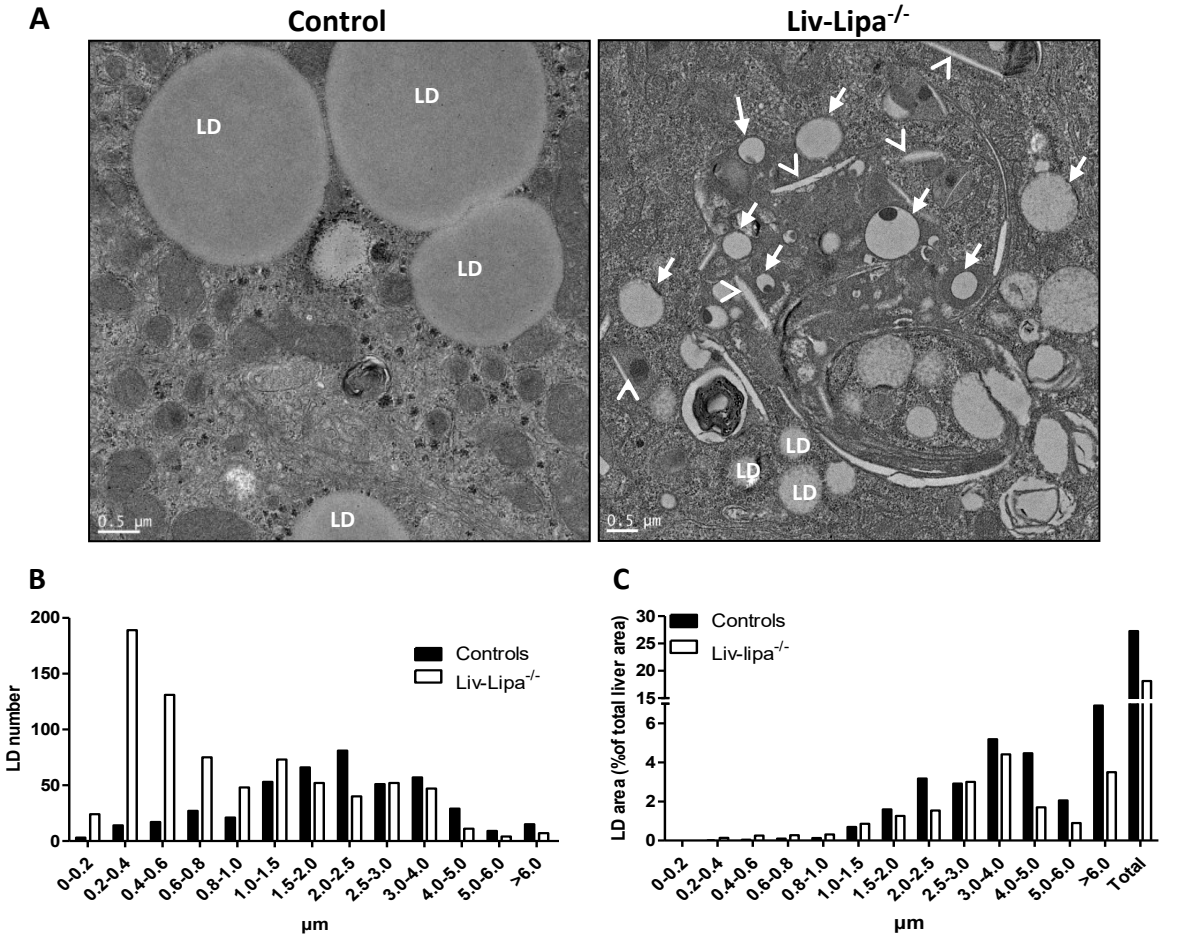

Figure 24: Lysosomal lipid accumulation and cholesterol/CE crystal formation Liv-Lipa$^{-/-}$ mice fed HF/HCD. (A) Representative electron micrographs of livers (scale bar 0,5 µm) from mice fed HF/HCD for 10 weeks; LD indicates cytosolic lipid droplets, arrows indicate lipid-laden lysosomes, arrow heads indicate cholesterol/CE crystals. (B) LD distribution and (C) % of LD area calculated from 60 electron micrographs (each 142.09 µm2) per genotype. (213) Requisite permission to use this figure was obtained (Appendix).

3.16 Similar tissue weights and H&E morphology in HF/HCD-fed Liv-Lipa$^{-/-}$ mice

While lipid accumulation in intestine and kidney as well as splenomegaly can be observed in Lipa$^{-/-}$ mice (208), we only found significant changes in relative liver weight (Figure 25A) but not in other tissues (Figure 25B-D). Morphology of these tissues (Figure 25E) was also comparable between control and Liv-Lipa$^{-/-}$ mice fed a HF/HCD for 10 weeks. (213)

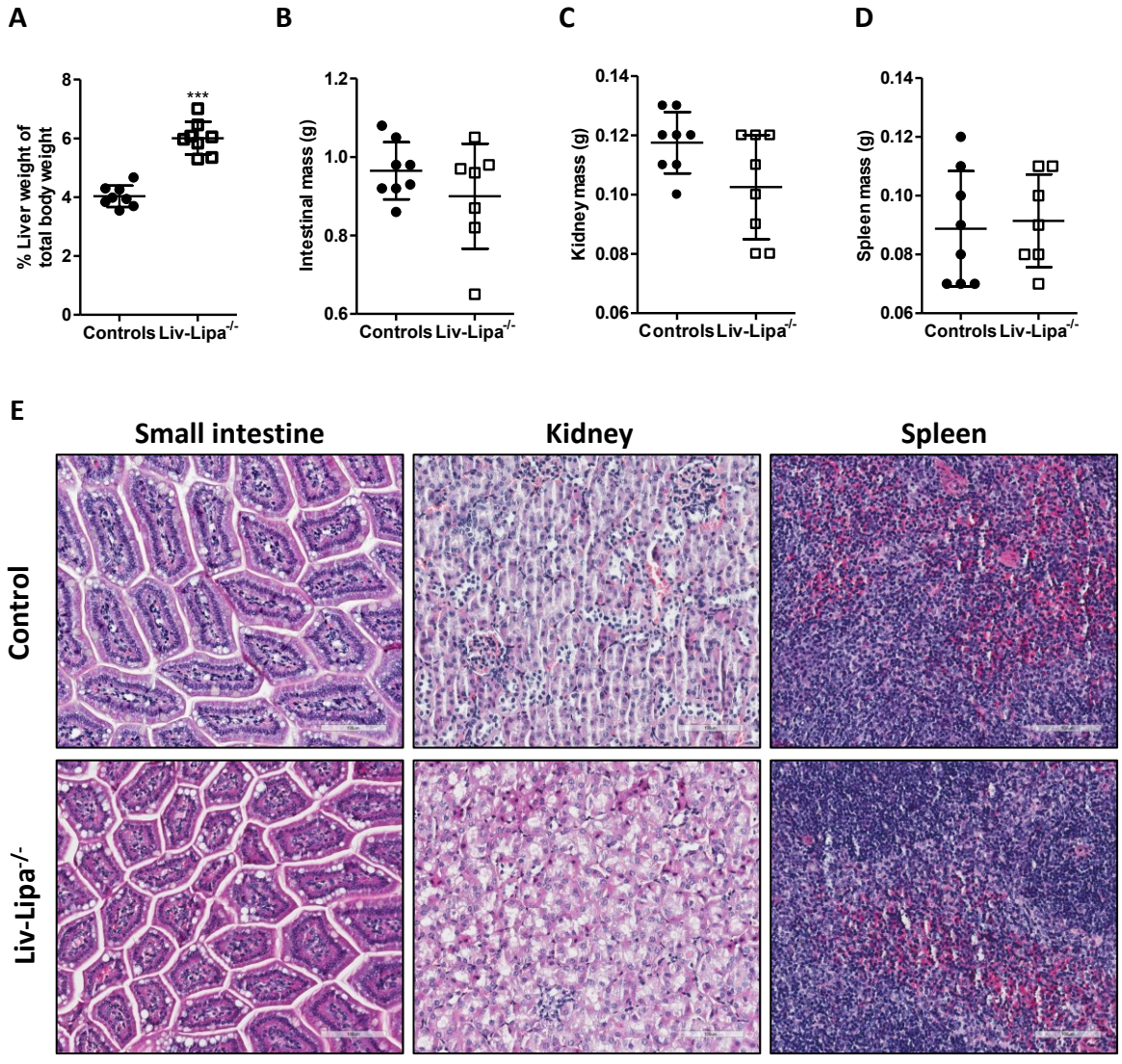

Figure 25: Tissue weight and morphology in HF/HCD-fed Liv-Lipa$^{-/-}$ and control mice.

(A) Liver weight relative to body weight. (B) Total intestine, (C) kidney, and (D) spleen weight of female control and Liv-Lipa$^{-/-}$ mice fed HF/HCD for 10 weeks. (E) Representative H&E stainings of small intestine (jejunum), kidney, and spleen sections from 10 week HF/HCD-fed male control (upper panel) and Liv-Lipa$^{-/-}$ (lower panel) mice (scale bar, 100 µm). Data represent mean (n=8) ± SD; $p \leq 0.001$ (***). (A-C) Student's unpaired t-test. (213) Requisite permission to use this figure was obtained (Appendix).

3.17 Accumulation of fatty acid species in the CE fraction of HF/HCD-fed Liv-Lipa$^{-/-}$ mice

Next, we determined the PL and neutral lipid composition of Liv-Lipa$^{-/-}$ livers by GC analysis. We found a 6.9-fold increase in CE concentrations in livers of HF/HCD-fed Liv-Lipa$^{-/-}$ mice. Interestingly, DG and TG concentrations were reduced by 40% and 62%, respectively, whereas other lipid species were unaffected (Figure 26A). Despite unchanged total hepatic FFA concentrations (Figure 26A), 16:1 and 20:4 FA were reduced in Liv-Lipa$^{-/-}$ mice (Figure 26B) by 47% and 30%, respectively. FA composition of PL was comparable between genotypes (Figure 26C). In DG (Figure 26D) and TG (Figure 26E) fractions, the unsaturated FA species 16:1, 18:1, 18:2, 20:4, and 22:6 were significantly reduced by more than 50%. In contrast, all FAs analyzed in the CE fraction were increased in Liv-Lipa$^{-/-}$ livers, with most pronounced changes in 18:0, 18:1, 18:2, 20:4, and 22:6 (Figure 26F) (213).

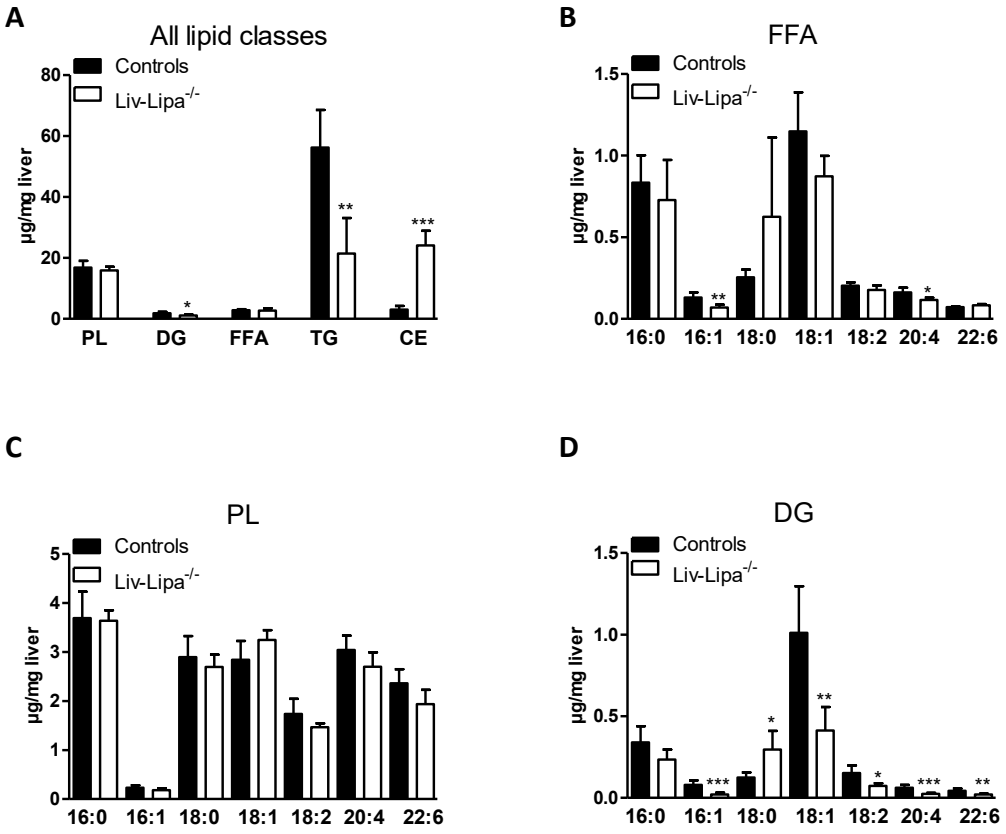

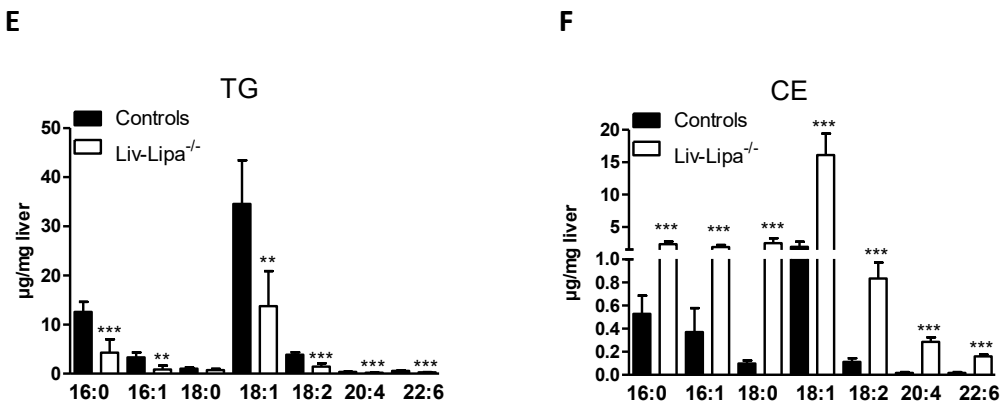

Figure 26: Accumulation of various FA species in hepatic CE fraction of HF/HCD-fed Liv-Lipa$^{-/-}$ mice.

Female control and Liv-Lipa$^{-/-}$ mice were fed HF/HCD for 10 weeks. (A) GC analysis of hepatic lipid species after TLC separation. (B-F) GC analysis of FA composition for each major lipid class (FA-, PL-, DG-, TG-, and CE-corresponding bands after TLC separation). Data represent mean (n = 5-6) + SD; $p < 0.05$ (*), $p \leq 0.01$ (**), $p \leq 0.001$ (***). (A-F) Student's unpaired t-test. (213) Requisite permission to use this figure was obtained (Appendix).

These findings indicate that liver lipid accumulations are due to the incomplete CE hydrolysis in Liv-Lipa$^{-/-}$ mice.

3.18 Comparable VLDL secretion in HF/HCD-fed Liv-Lipa$^{-/-}$ mice

Despite a substantial decrease in hepatic TG concentrations in Liv-Lipa$^{-/-}$ mice, VLDL secretion after inhibition of peripheral lipolysis by tyloxapol was unchanged (Figure 27). (213)

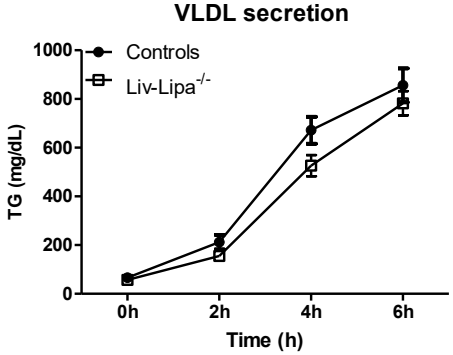

Figure 27: Comparable VLDL secretion in HF/HCD-fed Liv-Lipa$^{-/-}$ mice.

Female control and Liv-Lipa$^{-/-}$ mice were fed HF/HCD for 8 weeks prior to the experiment. VLDL secretion was measured in 8 h-fasted mice after tyloxapol injection. Data represent mean (n=8) ± SD; ANOVA. (213) Requisite permission to use this figure was obtained (Appendix).

3.19 Increased hepatic inflammation in Liv-Lipa$^{-/-}$ mice fed HF/HCD

Increase in CE concentrations as wells as hepatic cholesterol crystal formation are known to be involved in liver inflammation and hepatic steatosis (223). mRNA expression of cytokeratine 19 *(Ckt19),* macrophage colony stimulating factor (*Mcsf),* transforming growth factor beta *(Tgfb),* and collagen type III alpha *(Col3a),* indicating liver injury, inflammation, and fibrosis, were significantly upregulated (Figure 28A). Together with the upregulation of all chemokines and cytokines known to be involved in hepatic inflammation (Figure 28B), these data indicate that deficiency of hepatic LAL is associated with liver inflammation and incipient fibrosis as a response to HF/HCD feeding. Accordingly, plasma concentrations of the liver damage markers AST and ALT were increased by 11- and 28-fold, respectively (Figure 28C). (213)

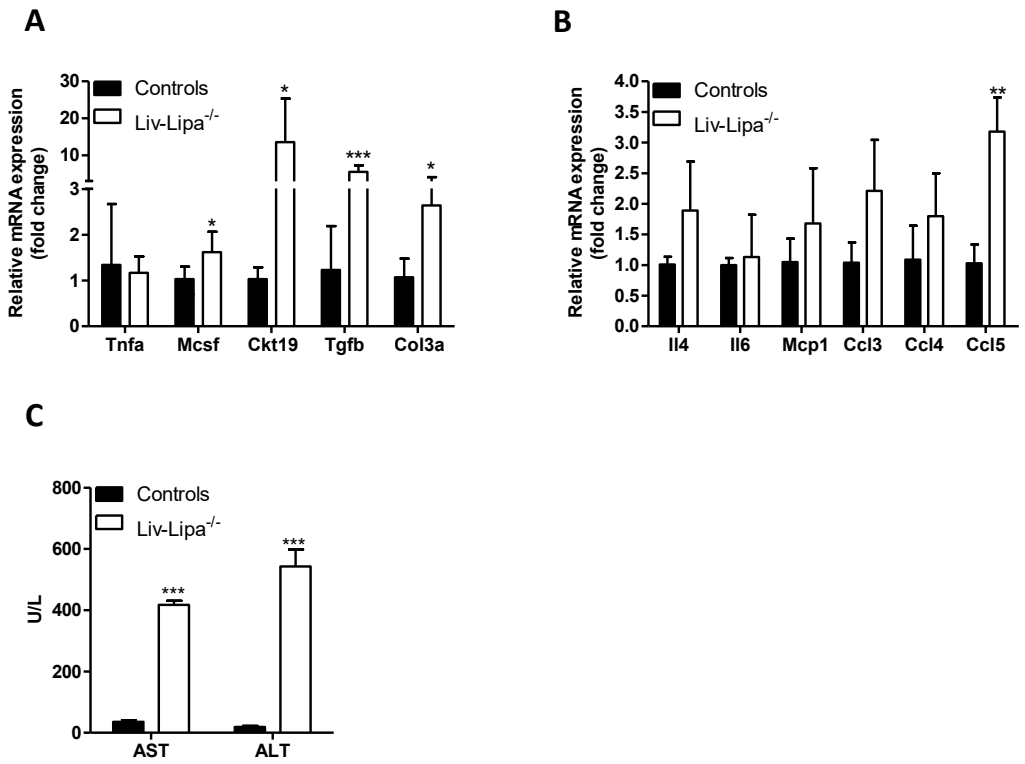

Figure 28: Increased hepatic inflammation markers in Liv-Lipa$^{-/-}$ mice fed HF/HCD.

(A, B) Hepatic mRNA expression levels of liver injury markers, chemokines, and cytokines relative to cyclophilin A as reference gene in female mice fed HF/HCD for 20 weeks (n=5-7). (C) Plasma concentrations of aspartate aminotransferase (AST) and alanine aminotransferase (ALT) in female mice fed HF/HCD for 10 weeks. Data represent mean values (n = 3–4) + SD; *p<0.05, **p≤0.01, ***p≤0.001. (A-C) Student's unpaired t-test. (213) Requisite permission to use this figure was obtained (Appendix).

LAL-D patients show hypertrophic Kupffer cells and portal macrophages with PAS-positive foamy tan-colored cytoplasm. We therefore analyzed liver sections from 20 week HF/HCD-fed Liv-Lipa$^{-/-}$ and control mice to determine liver damage in these mice. PAS staining (Figure 29A) revealed a foamy cytoplasm in Liv-Lipa$^{-/-}$ compared to control sections, while the glycogen and polysaccharide content did not change between the genotypes. To determine if the enlagement in liver size was due to increased proliferation or due to the lipid accumulation in Liv-Lipa$^{-/-}$ livers, we performed immunohistochemical analysis using an antibody against KI67 (Figure 29B). However, we could not detect differences between sections from control or Liv-Lipa$^{-/-}$ mice, which argues against induced proliferation. CAB (Figure 29C) staining proved an increased collagen content and Trichrome (Figure 29D) staining, which was used to clearly distinguish between connective tissue and liver tissue, indicated massive liver fibrosis in Liv-Lipa$^{-/-}$ mice. Immunohistochemical analysis using an antibody against the macrophage marker F4/80 exhibited a drastically increased number of positive cells compared to control mice (Figure 29E).

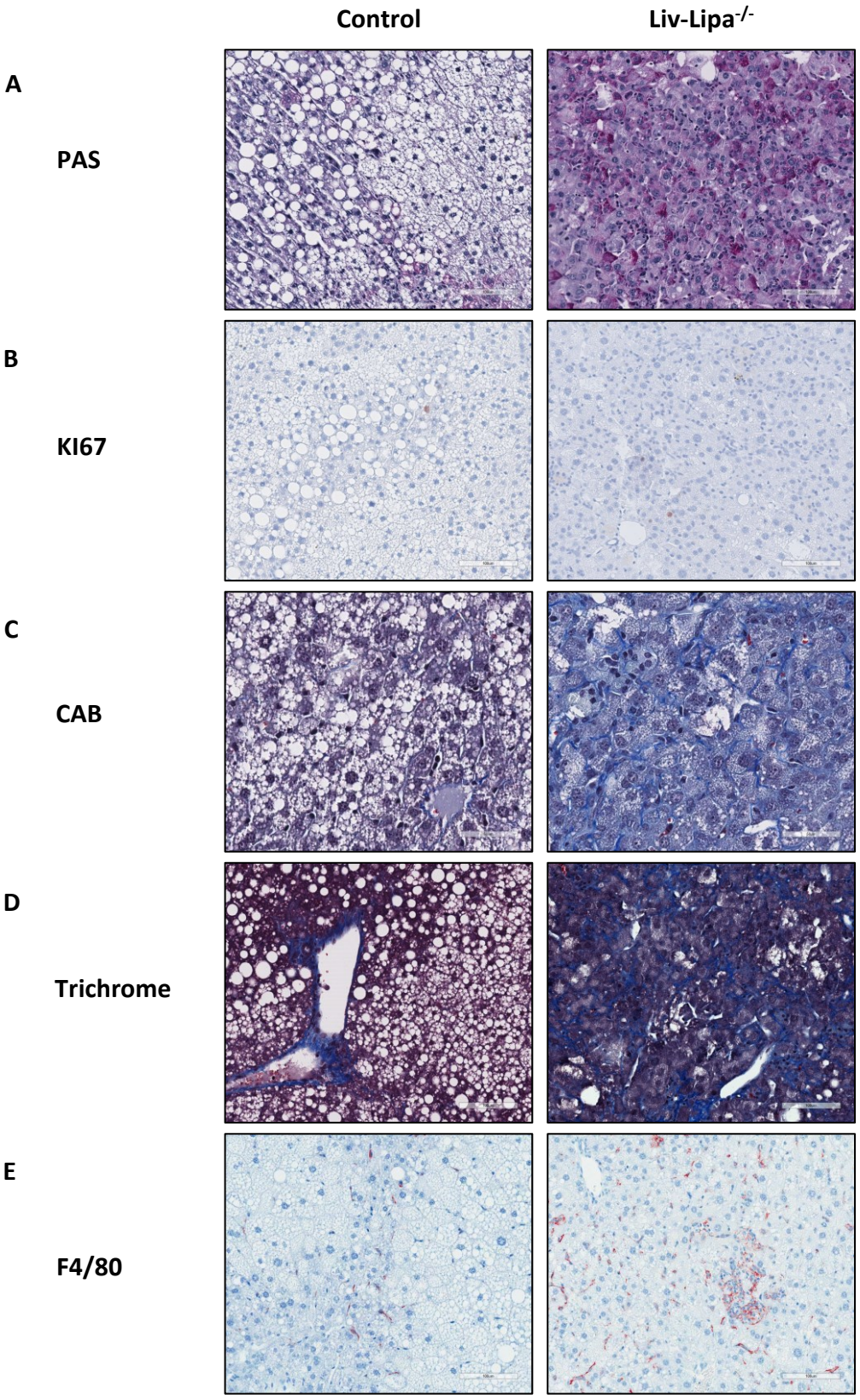

Figure 29: Increased liver fibrosis and macrophage infiltration in Liv-Lipa$^{-/-}$ livers.

Representative images for (A) PAS, (B) KI67, (C) CAB, (D) Trichrome, and (E) F4/80 stainings of control (left panel) and Liv-Lipa$^{-/-}$ (right panel) liver sections (scale bar, 100 µm). (213) Requisite permission to use this figure was obtained (Appendix).

4. Discussion

LAL hydrolyzes CE and TG within lysosomes to release FA and cholesterol for catabolic, anabolic, and signaling purposes (154). In humans and mice, LAL-D causes major metabolic changes leading to hepatomegaly, shortened life span, and hypercholesterolemia (144, 208). Recently, ERT as new therapeutic approach brought some hope for treating LAL-D patients (195). Despite its rapid approval by Drug Agencies in the USA, Europe, and Japan (195, 224), however, it is not covered by the state medical insurance in the UK, due to its unjustified high treatment price (500,000 £, according to guidance from National Institute for Health and Care Excellence). Another drawback is the fact that the human LAL, which is used for the treatment of LAL-D patients is produced in eggs from genetically modified chickens. The enzyme is then purified from the egg white and formulated as concentrate solution for infusion. Especially egg whites are known drivers of allergic reactions and it will therefore be even more important to develop better strategies to diagnose, treat, and manage this rare disease in the future.

In contrast to humans, Lipa$^{-/-}$ mice are viable with a median life span of approximately one year. They show hepatic TG and CE accumulation and due to an abnormal lipid metabolism they exhibit growth retardation, lack WAT and progressively lose BAT. Lipa$^{-/-}$ mice display an enlargement of mesenteric lymph nodes with massive lipid accumulation. Interestingly, Lipa$^{-/-}$ mice are a phenotypic model for CESD and a biochemical and histopathological model for WD (185, 208, 212). Lipa$^{-/-}$ mice, similar to humans, exhibit hepatomegaly with microvesicular steatosis and infiltration of Kupffer cells forming nests of “fatty lysosomes” (107). However, the role of LAL deficiency in lipid and carbohydrate metabolism, especially in the liver, has not been fully resolved as it still remained elusive whether hepatocytes or Kupffer cells contribute to the observed phenotype in Lipa$^{-/-}$ mice. We therefore generated hepatocyte-specific LAL-deficient mice and characterized them.

The current study demonstrates the physiological importance of hepatic LAL on whole body lipid homeostasis and provides strong evidence that hepatic ablation of LAL leads to the phenotype observed in Lipa$^{-/-}$ mice in regard to hepatic CE accumulation, inflammation, and fibrosis. The 7-fold increase in hepatic cholesterol levels in Liv-Lipa$^{-/-}$ is in line with previous studies of Lipa$^{-/-}$ mice (107, 208, 212). However, ALT and AST plasma concentrations, which are well-know markers for liver fibrosis and liver damage, were

comparable between control and Liv-Lipa$^{-/-}$ mice fed a chow diet. Moreover, liver sections were stained with different markers to determine if hyperproliferation, fibrosis or glycogen storage is visible in Liv-Lipa$^{-/-}$ mice, as it is known for LAL-D patients (144, 170) as well as for Lipa$^{-/-}$ mice (107, 208, 212). None of the used standard markers showed differences between control and Liv-Lipa$^{-/-}$ mice, implicating that chow diet-fed Liv-Lipa$^{-/-}$ mice do not develop liver damage or fibrosis. As Liv-Lipa$^{-/-}$ mice only show a mild phenotype compared to Lipa$^{-/-}$ mice and hyperproliferation is a rather late response in fibrotic/necrotic tissue it was not surprising that on chow diet we did not see differences in the stained liver sections.

Moreover, body weights were also comparable, most probably due to similar food intake, energy expenditure, and physical activity between the genotypes. Interestingly, our results are neither sex- nor age-dependent as we found similar results in all cohorts investigated. Also very old mice did not develop fibrosis (data not shown). We therefore speculate that an additional challenge is needed to reveal metabolic disturbances resulting from a lack of hepatic LAL.

Hypercholesterolemia is a hallmark in LAL-D but to date statin treatments brought little benefit in ameliorating dyslipidemia in these patients (144, 225). The rationale of statin treatments is, that they reduce cholesterol biosynthesis via inhibition of HMGCR. The reduced availability of cholesterol in the cells in turn leads to an upregulation of LDLR and promotes enhanced uptake of LDL particels. In LAL-D LDL particles can not be cleared by the lysosome and therefore the phenotype gets worse, which argues against a statin therapy in these patients. Similar to Lipa$^{-/-}$ mice (107, 208, 210), we expected plasma lipid parameters in Liv-Lipa$^{-/-}$ mice to be changed. We found increased cholesterol concentrations, especially in the LDL fraction, in plasma of HF/HCD-fed Liv-Lipa$^{-/-}$ mice, while relevant cholesterol transporters (ABCG5/8, ABCA1, SR-BI) and cholesterol biosynthesis genes (LDL-R, HMGCR) were comparable between the genotypes (data not shown). These findings indicate that cholesterol entrapped in lysosomes cannot initiate a feedback loop via the SREBP-mediated pathway and subsequent upregulation of LDLR and downregulation of HMGCR. The increased plasma cholesterol concentrations most likely derive from the excess cholesterol in the diet, which cannot be cleared.

When challenged with a HF/HCD, Liv-Lipa$^{-/-}$ mice were resistant to diet-induced obesity with reduced body weight gain starting already after 4 weeks of feeding despite unaltered food intake, movement, and energy expenditure. While both the resting metabolic ratio and the activity-related energy expenditure account for total energy expenditure, only small changes in either of them can already have huge impact on total energy expenditure (226). Unlike this study, however, we did not see a correlation between body weight and physical activity. The observed reduction in body weight can be made accountable by a 68% reduction in perigonadal WAT weight after 20 weeks of HF/HCD feeding. µCT imaging revealed signigficantly reduced fat mass and fat/body mass ratios, while lean mass was similar between the genotypes. In addition, the scans not only showed reductions in visceral, but also in subcutaneous WAT, again comparable to the situation in Lipa$^{-/-}$ mice (208). Accordingly, we speculate that the energy derived from the diet is not stored in WAT to the same extent as in control mice, but might be used immediately for other metabolic pathways. Increased fecal output and/or energy content or reduced body temperature could have been an explanation for the reduction in WAT mass as they massively impact whole body energy homeostasis and are primary contributors to metabolic regulation. However, fecal output and energy content as well as body temperature were unchanged in HF/HCD-fed Liv-Lipa$^{-/-}$ mice. To date we do not know what makes Liv-Lipa$^{-/-}$ mice resistant to diet-induced obesity but the cross-talk between liver and WAT in these mice needs to be further elucidated in the future. It is possible that secretory factors affect adipogenesis or adipocyte metabolism and by that inhibit WAT mass gain in Liv-Lipa$^{-/-}$ mice.

The reduced WAT weight together with the greater reliance on carbohydrates, as already seen in Lipa$^{-/-}$ mice (107), hinted to changes in glucose metabolism and we found improved glucose clearance in Liv-Lipa$^{-/-}$ mice fed HF/HCD. In accordance, after insulin challenge, HF/HCD-fed Liv-Lipa$^{-/-}$ mice exhibited a drop in blood glucose with a delayed normalization, indicating a defect in hepatic gluconeogenesis generally activated to prevent hypoglycemia. In line, mRNA levels of *G6Pase*, *Pepck* as well as other important genes involved in gluconeogenesis were reduced in Liv-Lipa$^{-/-}$ mice fed HF/HCD. Dephosphorylation of *G6Pase* is a rate-limiting step common for both glycogenolysis and gluconeogenesis. Mice with hepatocyte-specific deletion of *G6Pase* develop

hyperlipidemia, hepatomegaly with glycogen accumulation, and hepatic steatosis (227). The conversion of oxaloacetate to phosphoenolpyruvate by *Pepck* is the other rate-limiting step of gluconeogenesis. Mice with hepatocyte-specific deletion of *Pepck* are viable but unable to produce glucose from lactate and amino acids via gluconeogenesis (228). Gluconeogenesis is also a driver of ketogenesis and leads to a direct loss of oxaloacetate from the TCA cycle. Without oxaloacetate, the TCA cycle is not able to continue, leading mainly to ketone body formation for energy supply. Liv-Lipa$^{-/-}$ mice fed HF/HCD for 10 weeks exhibited reduced mRNA expression of TCA cycle genes (*Suclg2*, *Fh,* and *Pdhb)* and an increase in hepatic glutamine, glutamate and creatine levels, suggesting replenishment of the TCA cycle via urea cycle intermediates, thereby contributing to a normal energy homeostasis in Liv-Lipa$^{-/-}$ mice. At the same time higher plasma levels of β-hdroxybutyrate point toward a shift to ketone body formation for energy supply. In fact, chronic treatment with butyrate keeps mice essentially metabolically normal on a high-fat diet (229). Butyrate treatment is further associated with lower glucose and insulin levels, higher glucose tolerance, reduced weight gain, and improved respiratory efficiency (229). Hepatocytes oxidize FA to generate ketone bodies or incorporate TG into VLDL particles. VLDL and ketone bodies are secreted from the liver and utilized by extrahepatic tissues. Thus, the increase in β-hydroxybutyrate secretion and the replenishment of the TCA cycle intermediates in Liv-Lipa$^{-/-}$ mice ensure a constant availability of substrates for extra-hepatic tissues which also explains comparable adipocyte sizes in WAT and BAT of Liv-Lipa$^{-/-}$ and control mice. Together with the lack of effects in other tissues known to be affected in Lipa$^{-/-}$ mice (208, 212), we conclude that the observed changes are exclusively the consequences of LAL deficiency in hepatocytes.

While a previous study from our group found reduced VLDL secretion in Lipa$^{-/-}$ mice leading to improved insulin sensitivity (107), Liv-Lipa$^{-/-}$ mice, however, do not share this insulin sensitive phenotype. In contrast, Liv-Lipa$^{-/-}$ mice displayed a significant increase in plasma insulin concentrations and the HOMA index, which is in line with the fact that lipodystrophy is generally associated with insulin resistance (230). Systemic insulin sensitivity and glucose metabolism are further fundamentally influenced by WAT via the adipokines leptin and adiponectin (231). These receptors likely have an insulin-sensitizing action, but paradoxically, they are at the same time downregulated in

overweight and obese patients, potentially also linking them to insulin resistance (232). Leptin affects insulin secretion and further progression to insulin resistance (233) and fasting significantly decreases basal leptin levels (234). Although we did not measure plasma leptin concentrations we found almost abolished *Leptr1* mRNA expression in 12h-fasted Liv-Lipa$^{-/-}$ mice fed a HF/HCD and would therefore assume to also find reduced plasma leptin levels. It is known that leptin levels correlate with WAT mass as in both, humans and mice plasma and mRNA concentrations of leptin were increased in obese subjects and reduced after a weight loss regime (235). Additionally, administration of leptin to lipoatrophic mice was shown to improve metabolic abnormalities, including insulin resistance and hyperlipidaemia (236). Together with the significantly increased mRNA expression of *Adipor1* and *2* in WAT of fasted Liv-Lipa$^{-/-}$ mice this could, at least in part, explain the changes in metabolism as well as the ability of Liv-Lipa$^{-/-}$ mice to adapt to energetic requirements on a HF/HCD. Morover, adiponectin was shown to inhibit endogenous glucose production (237), and gluconeogenesis in mouse hepatocytes (238) and improves hepatic TG accumulations and protects from hepatic steatosis (239).

Recently, reduced LAL activity in adult patients was linked to NAFLD (240), indicating a possible correlation between impaired LAL activity and fatty liver disease. In particular, the known abnormalities of hepatomegaly, elevated liver enzymes and/or fatty liver and dyslipidemia, may be confused with more common disorders such as NAFLD, NASH, metabolic syndrome, and/or familial hypercholesterolemia (241). By using a targeted deletion in hepatocytes, we aimed to better understand the mechanisms leading to the observed liver phenotype in patients suffering from LAL-D. Liver size, weight, and color were similar to Lipa$^{-/-}$ mice (147, 212) and liver sections showed markedly reduced abundance and size of cytosolic LD. Significantly reduced FA levels in the DG and TG fraction may explain the reduced total LD area in livers of Liv-Lipa$^{-/-}$ mice. Despite a substantial decrease in TG concentrations, VLDL secretion was unchanged in Liv-Lipa$^{-/-}$ mice. This can be explained by a comparable mRNA expression of MTP as well as enzymes important for *de novo* synthesis of TG (e.g.DGATs) (data not shown). DGAT1$^{-/-}$ mice, similar to Liv-Lipa$^{-/-}$ mice, show normal fasting plasma TG levels despite a decrease in hepatic TG concentrations (242). Hepatic VLDL assembly and secretion is also markedly influenced by alterations in the *de novo* biosynthesis of phospholipids catalyzed by

phosphatidyletanolamine N-methyltransferase (PEMT) (243). As we found no differences in hepatic FA levels in the PL fraction this pathway may also contribute to TG synthesis for VLDL assembly.

Similar to previous findings in Lipa$^{-/-}$ mice (107), we observed cholesterol/CE crystal formation and the majority of lipid was stored in hepatic lysosomes of Liv-Lipa$^{-/-}$ mice. In a human LAL-D patient the examination of fresh-frozen tissues under polarized light revealed birefringent CE crystals in Kupffer cells (244). This finding is pathognomonic for the deficiency of LAL and we speculate that the structures observed in Liv-Lipa$^{-/-}$ mice are also CE crystals rather than cholesterol crystals. Cholesterol/CE crystal formation is known to activate Kupffer cells, leading to inflammation and liver damage (223). Previous studies using Lipa$^{-/-}$ mice provided evidence for a significant role of LAL in the regulation of inflammation-relevant functions in various tissues (107, 208, 245). LAL-D in mice causes a severe phenotype with elevated activities of transaminases, which are well-established indicators of liver damage. Systematically increased pro-inflammatory cytokines and the massive abundance of macrophages in various organs, predominantly in lung, intestine, liver, and spleen, suggest systemic inflammation (208).

In Liv-Lipa$^{-/-}$ mice we saw increased plasma transaminases as well as upregulation of liver cytokines and chemokines, known to drive inflammation, leading to Kupffer cell activation and liver damage. Kupffer cells produce cytokines and chemokines that directly influence hepatic stellate cell (HSC) activation, including TGFβ, platelet-derived growth factor (PDGF), TNF, IL-1β, monocyte chemoattractant protein 1 (MCP1), chemokine (C-C motif) ligand 3 and 5 (CCL3,CCL5). CCL3 (also known as MIP1α) is a ligand for C-C chemokine receptor 1 and 5 (CCR1, CCR5), which promote hepatic fibrosis in mice (246). In mice, deletion of CCL3 leads to reduced liver fibrosis induced by carbon tetrachloride (CCl_4) or methionine and choline-deficient (MCD) diet, which is associated with reduced HSC activation and liver immune cell infiltration in these models (247). CCL5 (also known as RANTES) is a ligand for CCR1, CCR3 and CCR5. CCL5-deficient mice also exhibit decreased hepatic fibrosis with reduced HSC activation and hepatic immune cell infiltration in response to either CCl_4 administration or MCD diet. Treatment with the CCL5 receptor antagonist Met-CCL5 further inhibits HSC migration, proliferation and

collagen secretion in vitro (248). Increased mRNA expression of both *Ccl3* and *Ccl5* as well as *Mcp1*, and *Tgfb* explain enhanced fibrosis formation in Liv-Lipa$^{-/-}$ mice. In accordance, the expression of human LAL in hepatocytes of Lipa$^{-/-}$ mice almost completely corrected liver inflammation (249), while in myeloid cells it mainly ameliorated lysosomal lipid accumulation in Kupffer cells with only minor effects in other liver cell types and the small intestine (245). Together these findings indicate that LAL in hepatocytes plays a critical role in maintaining liver homeostasis and function.

Conclusion

Until now, it has been speculated that macrophages drive lipid accumulation in various tissues of Lipa$^{-/-}$ mice and are responsible for the pathology of LAL-D. From our study, we conclude that macrophages infiltrate the liver as a consequence of impaired hepatocyte LAL activity to clear dietary lipids. The accumulation of lipids in the lysosome of Liv-Lipa$^{-/-}$ mice and the subsequent CE crystal accumulation promotes chemokine and cytokine release with a subsequent recruitment of macrophages. This macrophage activation drives fibrosis and liver damage. The metabolic changes resulting from reduced LD storage and improved glucose metabolism confirm the important role in maintaining energy balance in Liv-Lipa$^{-/-}$ mice (Figure 30).

Our data provide evidence that the pathology of LAL-D (at least in mice) is mainly driven by hepatocytes, leading to an alteration in hepatic energy homeostasis and resistance to diet-induced obesity. Consequently, our findings clearly demonstrate that hepatocyte-specific LAL deletion leads to hepatic CE accumulation and CE crystal formation, which induces Kupffer cell activation, causing inflammation and liver damage in HF/HCD-fed Liv-Lipa$^{-/-}$ mice (213).

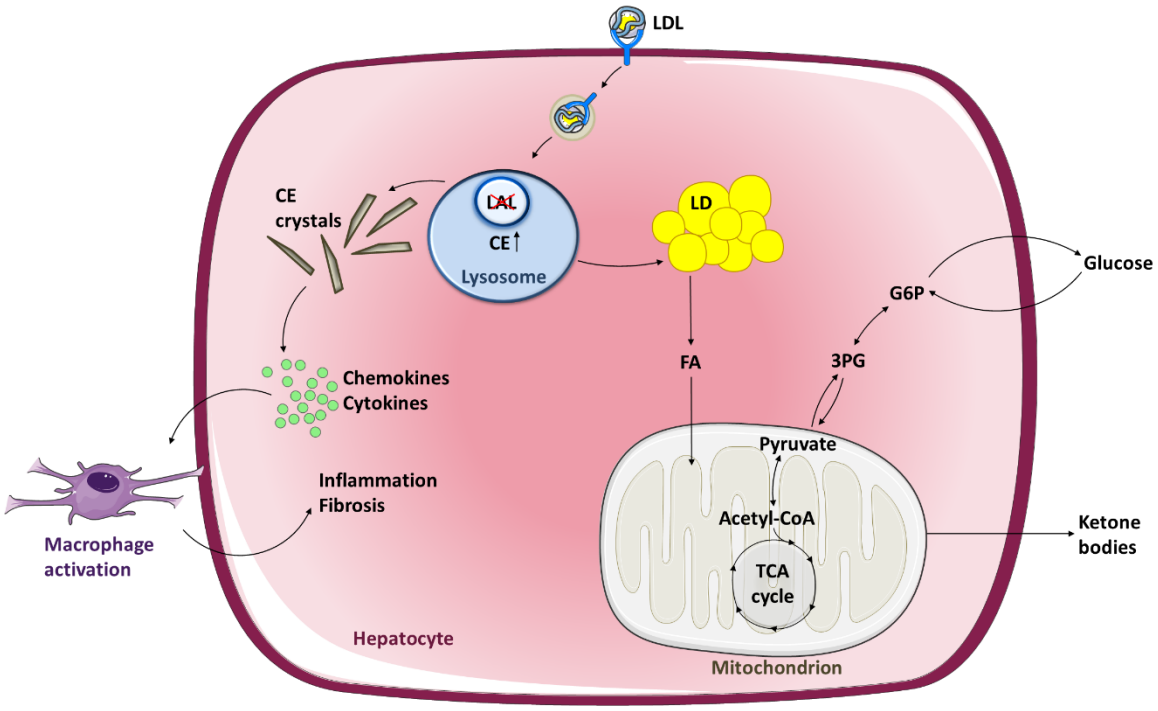

Figure 30: Proposed model of metabolic alterations resulting from hepatocyte-specific LAL deficiency.

LAL plays a key role in lipid metabolism through the hydrolysis of CE and TG in lysosomes. Absent or reduced LAL activity leads to lack of degradation of LDL-derived neutral lipids with subsequent accumulation within lysosomes. CE accumulation leads to CE crystal formation and increased signaling of hepatic chemokines and cytokines, which further activate macrophages and induce liver damage and fibrosis in Liv-Lipa$^{-/-}$ mice. Together with the reduced abundance of cytosolic LD, the improved glucose clearance, and the switch to ketone body formation for energy supply in Liv-Lipa$^{-/-}$ mice substantiate the crucial role of hepatocyte-specific LAL in lipid and energy homeostasis. LAL, lysosomal acid lipase; LD, lipid droplet; CE, cholesteryl ester; 3-PG, 3-phosphoglycerate; G6P, glucose-6-phosphate; LDL, low-density lipoprotein, TCA, tricarboxylic acid. (213) Requisite permission to use this figure was obtained (Appendix).

5. References

1. Agius L. (2008) Glucokinase and molecular aspects of liver glycogen metabolism. *Biochem J*.414(1):1-18.

2. Bechmann LP, Hannivoort RA, Gerken G, Hotamisligil GS, Trauner M, Canbay A. (2012) The interaction of hepatic lipid and glucose metabolism in liver diseases. *J Hepatol*.56(4):952-64.

3. Towle HC, Kaytor EN, Shih HM. (1997) Regulation of the expression of lipogenic enzyme genes by carbohydrate. *Annu Rev Nutr*.17:405-33.

4. Pilkis SJ, Claus TH. (1991) Hepatic gluconeogenesis/glycolysis: regulation and structure/function relationships of substrate cycle enzymes. *Annu Rev Nutr*.11:465-515.

5. Pilkis SJ, Claus TH, el-Maghrabi MR. (1988) The role of cyclic AMP in rapid and long-term regulation of gluconeogenesis and glycolysis. *Adv Second Messenger Phosphoprotein Res*.22:175-91.

6. Pilkis SJ, el-Maghrabi MR, Claus TH. (1988) Hormonal regulation of hepatic gluconeogenesis and glycolysis. *Annu Rev Biochem*.57:755-83.

7. Dentin R, Girard J, Postic C. (2005) Carbohydrate responsive element binding protein (ChREBP) and sterol regulatory element binding protein-1c (SREBP-1c): two key regulators of glucose metabolism and lipid synthesis in liver. *Biochimie*.87(1):81-6.

8. Roach PJ. (2002) Glycogen and its metabolism. *Curr Mol Med*.2(2):101-20.

9. Kim YM, Seo YH, Park CB, Yoon SH, Yoon G. (2010) Roles of GSK3 in metabolic shift toward abnormal anabolism in cell senescence. *Ann N Y Acad Sci*.1201:65-71.

10. Raddatz D, Ramadori G. (2007) Carbohydrate metabolism and the liver: actual aspects from physiology and disease. *Z Gastroenterol*.45(1):51-62.

11. Conti R, Mannucci E, Pessotto P, Tassoni E, Carminati P, Giannessi F, et al. (2011) Selective reversible inhibition of liver carnitine palmitoyl-transferase 1 by teglicar reduces gluconeogenesis and improves glucose homeostasis. *Diabetes*.60(2):644-51.

12. Puigserver P, Rhee J, Donovan J, Walkey CJ, Yoon JC, Oriente F, et al. (2003) Insulin-regulated hepatic gluconeogenesis through FOXO1-PGC-1alpha interaction. *Nature*.423(6939):550-5.

13. Cao R, Cronk ZX, Zha W, Sun L, Wang X, Fang Y, et al. (2010) Bile acids regulate hepatic gluconeogenic genes and farnesoid X receptor via G(alpha)i-protein-coupled receptors and the AKT pathway. *J Lipid Res*.51(8):2234-44.

14. Hakimi P, Johnson MT, Yang J, Lepage DF, Conlon RA, Kalhan SC, et al. (2005) Phosphoenolpyruvate carboxykinase and the critical role of cataplerosis in the control of hepatic metabolism. *Nutr Metab (Lond)*.2:33.

15. Knight BL, Hebbachi A, Hauton D, Brown AM, Wiggins D, Patel DD, et al. (2005) A role for PPARalpha in the control of SREBP activity and lipid synthesis in the liver. *Biochem J*.389(Pt 2):413-21.

16. Schadinger SE, Bucher NL, Schreiber BM, Farmer SR. (2005) PPARgamma2 regulates lipogenesis and lipid accumulation in steatotic hepatocytes. *Am J Physiol Endocrinol Metab*.288(6):E1195-205.

17. Shen LL, Liu H, Peng J, Gan L, Lu L, Zhang Q, et al. (2011) Effects of farnesoid X receptor on the expression of the fatty acid synthetase and hepatic lipase. *Mol Biol Rep*.38(1):553-9.

18. Schwarz JM, Linfoot P, Dare D, Aghajanian K. (2003) Hepatic de novo lipogenesis in normoinsulinemic and hyperinsulinemic subjects consuming high-fat, low-carbohydrate and low-fat, high-carbohydrate isoenergetic diets. *Am J Clin Nutr*.77(1):43-50.

19. Strable MS, Ntambi JM. (2010) Genetic control of de novo lipogenesis: role in diet-induced obesity. *Crit Rev Biochem Mol Biol*.45(3):199-214.

20. Jump DB, Clarke SD, Thelen A, Liimatta M. (1994) Coordinate regulation of glycolytic and lipogenic gene expression by polyunsaturated fatty acids. *J Lipid Res*.35(6):1076-84.

21. Neuschwander-Tetri BA. (2010) Hepatic lipotoxicity and the pathogenesis of nonalcoholic steatohepatitis: the central role of nontriglyceride fatty acid metabolites. *Hepatology*.52(2):774-88.

22. Wilfling F, Haas JT, Walther TC, Farese RV, Jr. (2014) Lipid droplet biogenesis. *Curr Opin Cell Biol*.29:39-45.

23. McFie PJ, Banman SL, Kary S, Stone SJ. (2011) Murine diacylglycerol acyltransferase-2 (DGAT2) can catalyze triacylglycerol synthesis and promote lipid droplet formation independent of its localization to the endoplasmic reticulum. *J Biol Chem*.286(32):28235-46.

24. Straub BK, Gyoengyoesi B, Koenig M, Hashani M, Pawella LM, Herpel E, et al. (2013) Adipophilin/perilipin-2 as a lipid droplet-specific marker for metabolically active cells and diseases associated with metabolic dysregulation. *Histopathology*.62(4):617-31.

25. Aon MA, Bhatt N, Cortassa SC. (2014) Mitochondrial and cellular mechanisms for managing lipid excess. *Front Physiol*.5:282.

26. Thiam AR, Farese RV, Jr., Walther TC. (2013) The biophysics and cell biology of lipid droplets. *Nat Rev Mol Cell Biol*.14(12):775-86.

27. Arner P. (2005) Human fat cell lipolysis: biochemistry, regulation and clinical role. *Best Pract Res Clin Endocrinol Metab*.19(4):471-82.

28. Delarue J, Magnan C. (2007) Free fatty acids and insulin resistance. *Curr Opin Clin Nutr Metab Care*.10(2):142-8.

29. Samuel VT, Shulman GI. (2016) The pathogenesis of insulin resistance: integrating signaling pathways and substrate flux. *J Clin Invest*.126(1):12-22.

30. Berk PD. (2008) Regulatable fatty acid transport mechanisms are central to the pathophysiology of obesity, fatty liver, and metabolic syndrome. *Hepatology*.48(5):1362-76.

31. Ge F, Zhou S, Hu C, Lobdell Ht, Berk PD. (2010) Insulin- and leptin-regulated fatty acid uptake plays a key causal role in hepatic steatosis in mice with intact leptin signaling but not in ob/ob or db/db mice. *Am J Physiol Gastrointest Liver Physiol*.299(4):G855-66.

32. Silverstein RL, Febbraio M. (2009) CD36, a scavenger receptor involved in immunity, metabolism, angiogenesis, and behavior. *Sci Signal*.2(72):re3.

33. Gimeno RE. (2007) Fatty acid transport proteins. *Curr Opin Lipidol*.18(3):271-6.

34. Berlanga A, Guiu-Jurado E, Porras JA, Auguet T. (2014) Molecular pathways in non-alcoholic fatty liver disease. *Clin Exp Gastroenterol*.7:221-39.

35. Reddy JK, Hashimoto T. (2001) Peroxisomal beta-oxidation and peroxisome proliferator-activated receptor alpha: an adaptive metabolic system. *Annu Rev Nutr*.21:193-230.

36. McGarry JD, Brown NF. (1997) The mitochondrial carnitine palmitoyltransferase system. From concept to molecular analysis. *Eur J Biochem*.244(1):1-14.

37. Akkaoui M, Cohen I, Esnous C, Lenoir V, Sournac M, Girard J, et al. (2009) Modulation of the hepatic malonyl-CoA-carnitine palmitoyltransferase 1A partnership creates a metabolic switch allowing oxidation of de novo fatty acids. *Biochem J*.420(3):429-38.

38. Nguyen P, Leray V, Diez M, Serisier S, Le Bloc'h J, Siliart B, et al. (2008) Liver lipid metabolism. *J Anim Physiol Anim Nutr (Berl)*.92(3):272-83.

39. Mandard S, Muller M, Kersten S. (2004) Peroxisome proliferator-activated receptor alpha target genes. *Cell Mol Life Sci*.61(4):393-416.

40. Harano Y, Yasui K, Toyama T, Nakajima T, Mitsuyoshi H, Mimani M, et al. (2006) Fenofibrate, a peroxisome proliferator-activated receptor alpha agonist, reduces hepatic steatosis and lipid peroxidation in fatty liver Shionogi mice with hereditary fatty liver. *Liver Int*.26(5):613-20.

41. Buhman KK, Chen HC, Farese RV, Jr. (2001) The enzymes of neutral lipid synthesis. *J Biol Chem*.276(44):40369-72.

42. Tobin KA, Ulven SM, Schuster GU, Steineger HH, Andresen SM, Gustafsson JA, et al. (2002) Liver X receptors as insulin-mediating factors in fatty acid and cholesterol biosynthesis. *J Biol Chem*.277(12):10691-7.

43. Tobin KA, Steineger HH, Alberti S, Spydevold O, Auwerx J, Gustafsson JA, et al. (2000) Cross-talk between fatty acid and cholesterol metabolism mediated by liver X receptor-alpha. *Mol Endocrinol*.14(5):741-52.

44. Jones PJ, Schoeller DA. (1990) Evidence for diurnal periodicity in human cholesterol synthesis. *J Lipid Res*.31(4):667-73.

45. Goldstein JL, Brown MS. (1990) Regulation of the mevalonate pathway. *Nature*.343(6257):425-30.

46. Xu X, So JS, Park JG, Lee AH. (2013) Transcriptional control of hepatic lipid metabolism by SREBP and ChREBP. *Semin Liver Dis*.33(4):301-11.

47. Horton JD, Goldstein JL, Brown MS. (2002) SREBPs: activators of the complete program of cholesterol and fatty acid synthesis in the liver. *J Clin Invest*.109(9):1125-31.

48. Wojcicka G, Jamroz-Wisniewska A, Horoszewicz K, Beltowski J. (2007) Liver X receptors (LXRs). Part I: structure, function, regulation of activity, and role in lipid metabolism. *Postepy Hig Med Dosw (Online)*.61:736-59.

49. Kidambi S, Patel SB. (2008) Cholesterol and non-cholesterol sterol transporters: ABCG5, ABCG8 and NPC1L1: a review. *Xenobiotica*.38(7-8):1119-39.

50. Enjoji M, Machida K, Kohjima M, Kato M, Kotoh K, Matsunaga K, et al. (2010) NPC1L1 inhibitor ezetimibe is a reliable therapeutic agent for non-obese patients with nonalcoholic fatty liver disease. *Lipids Health Dis*.9:29.

51. Fielding CJ, Shore VG, Fielding PE. (1972) Lecithin: cholesterol acyltransferase: effects of substrate composition upon enzyme activity. *Biochim Biophys Acta*.270(4):513-8.

52. Wang N, Silver DL, Costet P, Tall AR. (2000) Specific binding of ApoA-I, enhanced cholesterol efflux, and altered plasma membrane morphology in cells expressing ABC1. *J Biol Chem*.275(42):33053-8.

53. Rigotti A, Trigatti B, Babitt J, Penman M, Xu S, Krieger M. (1997) Scavenger receptor BI--a cell surface receptor for high density lipoprotein. *Curr Opin Lipidol*.8(3):181-8.

54. Jauhiainen M, Metso J, Pahlman R, Blomqvist S, van Tol A, Ehnholm C. (1993) Human plasma phospholipid transfer protein causes high density lipoprotein conversion. *J Biol Chem*.268(6):4032-6.

55. Timlin MT, Parks EJ. (2005) Temporal pattern of de novo lipogenesis in the postprandial state in healthy men. *Am J Clin Nutr*.81(1):35-42.

56. Hui DY, Howles PN. (2005) Molecular mechanisms of cholesterol absorption and transport in the intestine. *Semin Cell Dev Biol*.16(2):183-92.

57. Merkel M, Eckel RH, Goldberg IJ. (2002) Lipoprotein lipase: genetics, lipid uptake, and regulation. *J Lipid Res*.43(12):1997-2006.

58. Goldberg IJ. (1996) Lipoprotein lipase and lipolysis: central roles in lipoprotein metabolism and atherogenesis. *J Lipid Res*.37(4):693-707.

59. Redgrave TG, Vassiliou GG, Callow MJ. (1987) Cholesterol is necessary for triacylglycerol-phospholipid emulsions to mimic the metabolism of lipoproteins. *Biochim Biophys Acta*.921(1):154-7.

60. Hebbachi AM, Gibbons GF. (2001) Microsomal membrane-associated apoB is the direct precursor of secreted VLDL in primary cultures of rat hepatocytes. *J Lipid Res*.42(10):1609-17.

61. Kobayashi K, Oka K, Forte T, Ishida B, Teng B, Ishimura-Oka K, et al. (1996) Reversal of hypercholesterolemia in low density lipoprotein receptor knockout mice by adenovirus-mediated gene transfer of the very low density lipoprotein receptor. *J Biol Chem*.271(12):6852-60.

62. Herz J, Qiu SQ, Oesterle A, DeSilva HV, Shafi S, Havel RJ. (1995) Initial hepatic removal of chylomicron remnants is unaffected but endocytosis is delayed in mice lacking the low density lipoprotein receptor. *Proc Natl Acad Sci U S A*.92(10):4611-5.

63. Ginsberg HN. (1994) Lipoprotein metabolism and its relationship to atherosclerosis. *Med Clin North Am*.78(1):1-20.

64. Browning JD, Horton JD. (2004) Molecular mediators of hepatic steatosis and liver injury. *J Clin Invest*.114(2):147-52.

65. Evans RM, Barish GD, Wang YX. (2004) PPARs and the complex journey to obesity. *Nat Med*.10(4):355-61.

66. Alberti KG, Eckel RH, Grundy SM, Zimmet PZ, Cleeman JI, Donato KA, et al. (2009) Harmonizing the metabolic syndrome: a joint interim statement of the International Diabetes Federation Task Force on Epidemiology and Prevention; National Heart, Lung, and Blood Institute; American Heart Association; World Heart Federation; International Atherosclerosis Society; and International Association for the Study of Obesity. *Circulation*.120(16):1640-5.

67. Simmons RK, Alberti KG, Gale EA, Colagiuri S, Tuomilehto J, Qiao Q, et al. (2010) The metabolic syndrome: useful concept or clinical tool? Report of a WHO Expert Consultation. *Diabetologia*.53(4):600-5.

68. Hamaguchi M, Kojima T, Takeda N, Nakagawa T, Taniguchi H, Fujii K, et al. (2005) The metabolic syndrome as a predictor of nonalcoholic fatty liver disease. *Ann Intern Med*.143(10):722-8.

69. Anstee QM, Targher G, Day CP. (2013) Progression of NAFLD to diabetes mellitus, cardiovascular disease or cirrhosis. *Nat Rev Gastroenterol Hepatol*.10(6):330-44.

70. Choi JH, Rhee EJ, Bae JC, Park SE, Park CY, Cho YK, et al. (2013) Increased risk of type 2 diabetes in subjects with both elevated liver enzymes and ultrasonographically diagnosed nonalcoholic fatty liver disease: a 4-year longitudinal study. *Arch Med Res*.44(2):115-20.

71. Park SK, Seo MH, Shin HC, Ryoo JH. (2013) Clinical availability of nonalcoholic fatty liver disease as an early predictor of type 2 diabetes mellitus in Korean men: 5-year prospective cohort study. *Hepatology*.57(4):1378-83.

72. Browning JD, Szczepaniak LS, Dobbins R, Nuremberg P, Horton JD, Cohen JC, et al. (2004) Prevalence of hepatic steatosis in an urban population in the United States: impact of ethnicity. *Hepatology*.40(6):1387-95.

73. Williams CD, Stengel J, Asike MI, Torres DM, Shaw J, Contreras M, et al. (2011) Prevalence of nonalcoholic fatty liver disease and nonalcoholic steatohepatitis among a largely middle-aged population utilizing ultrasound and liver biopsy: a prospective study. *Gastroenterology*.140(1):124-31.

74. Allen AM, Therneau TM, Larson JJ, Coward A, Somers VK, Kamath PS. (2018) Nonalcoholic fatty liver disease incidence and impact on metabolic burden and death: A 20 year-community study. *Hepatology*.67(5):1726-36.

75. Chalasani N, Younossi Z, Lavine JE, Diehl AM, Brunt EM, Cusi K, et al. (2012) The diagnosis and management of non-alcoholic fatty liver disease: practice Guideline by the American Association for the Study of Liver Diseases, American College of Gastroenterology, and the American Gastroenterological Association. *Hepatology*.55(6):2005-23.

76. Matteoni CA, Younossi ZM, Gramlich T, Boparai N, Liu YC, McCullough AJ. (1999) Nonalcoholic fatty liver disease: a spectrum of clinical and pathological severity. *Gastroenterology*.116(6):1413-9.

77. Day CP, James OF. (1998) Steatohepatitis: a tale of two "hits"? *Gastroenterology*.114(4):842-5.

78. Cheung O, Sanyal AJ. (2008) Abnormalities of lipid metabolism in nonalcoholic fatty liver disease. *Semin Liver Dis*.28(4):351-9.

79. Tilg H, Moschen AR. (2010) Evolution of inflammation in nonalcoholic fatty liver disease: the multiple parallel hits hypothesis. *Hepatology*.52(5):1836-46.

80. Cohen DE, Fisher EA. (2013) Lipoprotein metabolism, dyslipidemia, and nonalcoholic fatty liver disease. *Semin Liver Dis*.33(4):380-8.

81. Latorre J, Moreno-Navarrete JM, Mercader JM, Sabater M, Rovira O, Girones J, et al. (2017) Decreased lipid metabolism but increased FA biosynthesis are coupled with changes in liver microRNAs in obese subjects with NAFLD. *Int J Obes (Lond)*.41(4):620-30.

82. Shojaee-Moradie F, Cuthbertson DJ, Barrett M, Jackson NC, Herring R, Thomas EL, et al. (2016) Exercise Training Reduces Liver Fat and Increases Rates of VLDL Clearance But Not VLDL Production in NAFLD. *J Clin Endocrinol Metab*.101(11):4219-28.

83. Lewis GF, Murdoch S, Uffelman K, Naples M, Szeto L, Albers A, et al. (2004) Hepatic lipase mRNA, protein, and plasma enzyme activity is increased in the insulin-resistant, fructose-fed Syrian golden hamster and is partially normalized by the insulin sensitizer rosiglitazone. *Diabetes*.53(11):2893-900.

84. Miksztowicz V, Lucero D, Zago V, Cacciagiu L, Lopez G, Gonzalez Ballerga E, et al. (2012) Hepatic lipase activity is increased in non-alcoholic fatty liver disease beyond insulin resistance. *Diabetes Metab Res Rev*.28(6):535-41.

85. Tzotzas T, Desrumaux C, Lagrost L. (2009) Plasma phospholipid transfer protein (PLTP): review of an emerging cardiometabolic risk factor. *Obes Rev*.10(4):403-11.

86. Xiao C, Watanabe T, Zhang Y, Trigatti B, Szeto L, Connelly PW, et al. (2008) Enhanced cellular uptake of remnant high-density lipoprotein particles: a mechanism for high-density lipoprotein lowering in insulin resistance and hypertriglyceridemia. *Circ Res*.103(2):159-66.

87. Donnelly KL, Smith CI, Schwarzenberg SJ, Jessurun J, Boldt MD, Parks EJ. (2005) Sources of fatty acids stored in liver and secreted via lipoproteins in patients with nonalcoholic fatty liver disease. *J Clin Invest*.115(5):1343-51.

88. Sato N. (2007) Central role of mitochondria in metabolic regulation of liver pathophysiology. *J Gastroenterol Hepatol*.22 Suppl 1:S1-6.

89. Sunny NE, Parks EJ, Browning JD, Burgess SC. (2011) Excessive hepatic mitochondrial TCA cycle and gluconeogenesis in humans with nonalcoholic fatty liver disease. *Cell Metab*.14(6):804-10.

90. Perez-Carreras M, Del Hoyo P, Martin MA, Rubio JC, Martin A, Castellano G, et al. (2003) Defective hepatic mitochondrial respiratory chain in patients with nonalcoholic steatohepatitis. *Hepatology*.38(4):999-1007.

91. Hotamisligil GS. (2010) Endoplasmic reticulum stress and the inflammatory basis of metabolic disease. *Cell*.140(6):900-17.

92. Spector AA, Yorek MA. (1985) Membrane lipid composition and cellular function. *J Lipid Res*.26(9):1015-35.

93. Crespo J, Cayon A, Fernandez-Gil P, Hernandez-Guerra M, Mayorga M, Dominguez-Diez A, et al. (2001) Gene expression of tumor necrosis factor alpha and TNF-receptors, p55 and p75, in nonalcoholic steatohepatitis patients. *Hepatology*.34(6):1158-63.

94. Endo M, Masaki T, Seike M, Yoshimatsu H. (2007) TNF-alpha induces hepatic steatosis in mice by enhancing gene expression of sterol regulatory element binding protein-1c (SREBP-1c). *Exp Biol Med (Maywood)*.232(5):614-21.

95. Hotamisligil GS, Shargill NS, Spiegelman BM. (1993) Adipose expression of tumor necrosis factor-alpha: direct role in obesity-linked insulin resistance. *Science*.259(5091):87-91.

96. Kern PA, Saghizadeh M, Ong JM, Bosch RJ, Deem R, Simsolo RB. (1995) The expression of tumor necrosis factor in human adipose tissue. Regulation by obesity, weight loss, and relationship to lipoprotein lipase. *J Clin Invest*.95(5):2111-9.

97. Tailleux A, Wouters K, Staels B. (2012) Roles of PPARs in NAFLD: potential therapeutic targets. *Biochim Biophys Acta*.1821(5):809-18.

98. Vanden Berghe W, Vermeulen L, Delerive P, De Bosscher K, Staels B, Haegeman G. (2003) A paradigm for gene regulation: inflammation, NF-kappaB and PPAR. *Adv Exp Med Biol*.544:181-96.

99. Lesmana CR, Hasan I, Budihusodo U, Gani RA, Krisnuhoni E, Akbar N, et al. (2009) Diagnostic value of a group of biochemical markers of liver fibrosis in patients with non-alcoholic steatohepatitis. *J Dig Dis*.10(3):201-6.

100. Singh R, Kaushik S, Wang Y, Xiang Y, Novak I, Komatsu M, et al. (2009) Autophagy regulates lipid metabolism. *Nature*.458(7242):1131-5.

101. Yang Z, Klionsky DJ. (2010) Mammalian autophagy: core molecular machinery and signaling regulation. *Curr Opin Cell Biol*.22(2):124-31.

102. Schneider JL, Suh Y, Cuervo AM. (2014) Deficient chaperone-mediated autophagy in liver leads to metabolic dysregulation. *Cell Metab*.20(3):417-32.

103. Yang L, Li P, Fu S, Calay ES, Hotamisligil GS. (2010) Defective hepatic autophagy in obesity promotes ER stress and causes insulin resistance. *Cell Metab*.11(6):467-78.

104. Wang Y, Singh R, Xiang Y, Czaja MJ. (2010) Macroautophagy and chaperone-mediated autophagy are required for hepatocyte resistance to oxidant stress. *Hepatology*.52(1):266-77.

105. Levine B, Kroemer G. (2008) Autophagy in the pathogenesis of disease. *Cell*.132(1):27-42.

106. Sheriff S, Du H, Grabowski GA. (1995) Characterization of lysosomal acid lipase by site-directed mutagenesis and heterologous expression. *J Biol Chem*.270(46):27766-72.

107. Radovic B, Vujic N, Leopold C, Schlager S, Goeritzer M, Patankar JV, et al. (2016) Lysosomal acid lipase regulates VLDL synthesis and insulin sensitivity in mice. *Diabetologia*.59(8):1743-52.

108. Grumet L, Eichmann TO, Taschler U, Zierler KA, Leopold C, Moustafa T, et al. (2016) Lysosomal Acid Lipase Hydrolyzes Retinyl Ester and Affects Retinoid Turnover. *J Biol Chem*.291(34):17977-87.

109. Appelmans F, De Duve C. (1955) Tissue fractionation studies. 3. Further observations on the binding of acid phosphatase by rat-liver particles. *Biochem J*.59(3):426-33.

110. Saftig P, Klumperman J. (2009) Lysosome biogenesis and lysosomal membrane proteins: trafficking meets function. *Nat Rev Mol Cell Biol*.10(9):623-35.

111. Schulze H, Kolter T, Sandhoff K. (2009) Principles of lysosomal membrane degradation: Cellular topology and biochemistry of lysosomal lipid degradation. *Biochim Biophys Acta*.1793(4):674-83.

112. Platt FM, d'Azzo A, Davidson BL, Neufeld EF, Tifft CJ. (2018) Lysosomal storage diseases. *Nat Rev Dis Primers*.4(1):27.

113. Braulke T, Bonifacino JS. (2009) Sorting of lysosomal proteins. *Biochim Biophys Acta*.1793(4):605-14.

114. Ghosh P, Dahms NM, Kornfeld S. (2003) Mannose 6-phosphate receptors: new twists in the tale. *Nat Rev Mol Cell Biol*.4(3):202-12.

115. Anderson RA, Rao N, Byrum RS, Rothschild CB, Bowden DW, Hayworth R, et al. (1993) In situ localization of the genetic locus encoding the lysosomal acid lipase/cholesteryl esterase (LIPA) deficient in Wolman disease to chromosome 10q23.2-q23.3. *Genomics*.15(1):245-7.

116. Anderson RA, Sando GN. (1991) Cloning and expression of cDNA encoding human lysosomal acid lipase/cholesteryl ester hydrolase. Similarities to gastric and lingual lipases. *J Biol Chem*.266(33):22479-84.

117. Anderson RA, Byrum RS, Coates PM, Sando GN. (1994) Mutations at the lysosomal acid cholesteryl ester hydrolase gene locus in Wolman disease. *Proc Natl Acad Sci U S A*.91(7):2718-22.

118. Ameis D, Merkel M, Eckerskorn C, Greten H. (1994) Purification, characterization and molecular cloning of human hepatic lysosomal acid lipase. *Eur J Biochem*.219(3):905-14.

119. Sando GN, Rosenbaum LM. (1985) Human lysosomal acid lipase/cholesteryl ester hydrolase. Purification and properties of the form secreted by fibroblasts in microcarrier culture. *J Biol Chem*.260(28):15186-93.

120. Du H, Cameron TL, Garger SJ, Pogue GP, Hamm LA, White E, et al. (2008) Wolman disease/cholesteryl ester storage disease: efficacy of plant-produced human lysosomal acid lipase in mice. *J Lipid Res*.49(8):1646-57.

121. Sando GN, Ma GP, Lindsley KA, Wei YP. (1990) Intercellular transport of lysosomal acid lipase mediates lipoprotein cholesteryl ester metabolism in a human vascular endothelial cell-fibroblast coculture system. *Cell Regul*.1(9):661-74.

122. Sando GN, Henke VL. (1982) Recognition and receptor-mediated endocytosis of the lysosomal acid lipase secreted by cultured human fibroblasts. *J Lipid Res*.23(1):114-23.

123. Aslanidis C, Ries S, Fehringer P, Buchler C, Klima H, Schmitz G. (1996) Genetic and biochemical evidence that CESD and Wolman disease are distinguished by residual lysosomal acid lipase activity. *Genomics*.33(1):85-93.

124. Abramov A, Schorr S, Wolman M. (1956) Generalized xanthomatosis with calcified adrenals. *AMA J Dis Child*.91(3):282-6.

125. Wolman M, Sterk VV, Gatt S, Frenkel M. (1961) Primary familial xanthomatosis with involvement and calcification of the adrenals. Report of two more cases in siblings of a previously described infant. *Pediatrics*.28:742-57.

126. Alexander WS. (1946) Niemann-Pick disease; report of a case showing calcification in the adrenal glands. *N Z Med J*.45:43-5.

127. Crocker AC, Vawter GF, Neuhauser EB, Rosowsky A. (1965) Wolman's Disease: Three New Patients with a Recently Described Lipidosis. *Pediatrics*.35:627-40.

128. Schiff L, Schubert WK, McAdams AJ, Spiegel EL, O'Donnell JF. (1968) Hepatic cholesterol ester storage disease, a familial disorder. I. Clinical aspects. *Am J Med*.44(4):538-46.

129. Partin JC, Schubert WK. (1969) Small intestinal mucosa in cholesterol ester storage disease. A light and electron microscope study. *Gastroenterology*.57(5):542-58.

130. D'Agostino D, Bay L, Gallo G, Chamoles N. (1988) Cholesterol ester storage disease: clinical, biochemical, and pathological studies of four new cases. *J Pediatr Gastroenterol Nutr*.7(3):446-50.

131. Hanak J, Elleder M. (1984) [Cholesterol ester storage disease (CESD)]. *Cesk Pediatr*.39(12):721-5.

132. Lageron A, Gautier M, Scotto J. (1985) [Clinical and histoenzymological peculiarities of cholesterol storage in 2 children of the same family]. *Arch Fr Pediatr*.42 Suppl 1:605-11.

133. Kunnert B, Pohlandt K, Ruschke I, Keller E. (1987) [Cholesterol ester storage disease and sea-blue histiocytes]. *Zentralbl Allg Pathol*.133(6):517-25.

134. Besley GT, Broadhead DM, Lawlor E, McCann SR, Dempsey JD, Drury MI, et al. (1984) Cholesterol ester storage disease in an adult presenting with sea-blue histiocytosis. *Clin Genet*.26(3):195-203.

135. Edelstein RA, Filling-Katz MR, Pentchev P, Gal A, Chandra R, Shawker T, et al. (1988) Cholesteryl ester storage disease: a patient with massive splenomegaly and splenic abscess. *Am J Gastroenterol*.83(6):687-92.

136. Hill SC, Hoeg JM, Dwyer AJ, Vucich JJ, Doppman JL. (1983) CT findings in acid lipase deficiency: wolman disease and cholesteryl ester storage disease. *J Comput Assist Tomogr*.7(5):815-8.

137. Pericleous M, Kelly C, Wang T, Livingstone C, Ala A. (2017) Wolman's disease and cholesteryl ester storage disorder: the phenotypic spectrum of lysosomal acid lipase deficiency. *Lancet Gastroenterol Hepatol*.2(9):670-79.

138. Reiner Z, Guardamagna O, Nair D, Soran H, Hovingh K, Bertolini S, et al. (2014) Lysosomal acid lipase deficiency--an under-recognized cause of dyslipidaemia and liver dysfunction. *Atherosclerosis*.235(1):21-30.

139. Saito S, Ohno K, Suzuki T, Sakuraba H. (2012) Structural bases of Wolman disease and cholesteryl ester storage disease. *Mol Genet Metab*.105(2):244-8.

140. Lohse P, Maas S, Lohse P, Elleder M, Kirk JM, Besley GT, et al. (2000) Compound heterozygosity for a Wolman mutation is frequent among patients with cholesteryl ester storage disease. *J Lipid Res*.41(1):23-31.

141. Scott SA, Liu B, Nazarenko I, Martis S, Kozlitina J, Yang Y, et al. (2013) Frequency of the cholesteryl ester storage disease common LIPA E8SJM mutation (c.894G>A) in various racial and ethnic groups. *Hepatology*.58(3):958-65.

142. Stitziel NO, Fouchier SW, Sjouke B, Peloso GM, Moscoso AM, Auer PL, et al. (2013) Exome sequencing and directed clinical phenotyping diagnose cholesterol ester storage disease presenting as autosomal recessive hypercholesterolemia. *Arterioscler Thromb Vasc Biol*.33(12):2909-14.

143. vom Dahl S, Harzer K, Rolfs A, Albrecht B, Niederau C, Vogt C, et al. (1999) Hepatosplenomegalic lipidosis: what unless Gaucher? Adult cholesteryl ester storage disease (CESD) with anemia, mesenteric lipodystrophy, increased plasma chitotriosidase activity and a homozygous lysosomal acid lipase -1 exon 8 splice junction mutation. *J Hepatol*.31(4):741-6.

144. Bernstein DL, Hulkova H, Bialer MG, Desnick RJ. (2013) Cholesteryl ester storage disease: review of the findings in 135 reported patients with an underdiagnosed disease. *J Hepatol*.58(6):1230-43.

145. Reynolds T. (2013) Cholesteryl ester storage disease: a rare and possibly treatable cause of premature vascular disease and cirrhosis. *J Clin Pathol*.66(11):918-23.

146. A-Kader HH. (2017) Lysosomal acid lipase deficiency: a form of non-obese fatty liver disease (NOFLD). *Expert Rev Gastroenterol Hepatol*.11(10):911-24.

147. Grabowski DA, Du H, Charnas L. (2002) Lysosomal Acid Lipase Deficiencies: The Wolman Disease/Cholesteryl Ester Storage Disease Spectrum *The Online Metabolic and Molecular Bases of Inherited Disease*.

148. Muntoni S, Wiebusch H, Funke H, Ros E, Seedorf U, Assmann G. (1995) Homozygosity for a splice junction mutation in exon 8 of the gene encoding lysosomal acid lipase in a Spanish kindred with cholesterol ester storage disease (CESD). *Hum Genet*.95(5):491-4.

149. Seedorf U, Wiebusch H, Muntoni S, Christensen NC, Skovby F, Nickel V, et al. (1995) A novel variant of lysosomal acid lipase (Leu336-->Pro) associated with acid lipase deficiency and cholesterol ester storage disease. *Arterioscler Thromb Vasc Biol*.15(6):773-8.

150. Fasano T, Pisciotta L, Bocchi L, Guardamagna O, Assandro P, Rabacchi C, et al. (2012) Lysosomal lipase deficiency: molecular characterization of eleven patients with Wolman or cholesteryl ester storage disease. *Mol Genet Metab*.105(3):450-6.

151. Gasche C, Aslanidis C, Kain R, Exner M, Helbich T, Dejaco C, et al. (1997) A novel variant of lysosomal acid lipase in cholesteryl ester storage disease associated with mild phenotype and improvement on lovastatin. *J Hepatol*.27(4):744-50.

152. Warner TG, Dambach LM, Shin JH, O'Brien JS. (1981) Purification of the lysosomal acid lipase from human liver and its role in lysosomal lipid hydrolysis. *J Biol Chem*.256(6):2952-7.

153. Hayase K, Tappel AL. (1970) Specificity and other properties of lysosomal lipase of rat liver. *J Biol Chem*.245(1):169-75.

154. Zechner R, Madeo F, Kratky D. (2017) Cytosolic lipolysis and lipophagy: two sides of the same coin. *Nat Rev Mol Cell Biol*.18(11):671-84.

155. Brown MS, Faust JR, Goldstein JL. (1975) Role of the low density lipoprotein receptor in regulating the content of free and esterified cholesterol in human fibroblasts. *J Clin Invest*.55(4):783-93.

156. Jeon TI, Osborne TF. (2012) SREBPs: metabolic integrators in physiology and metabolism. *Trends Endocrinol Metab*.23(2):65-72.

157. Fouchier SW, Defesche JC. (2013) Lysosomal acid lipase A and the hypercholesterolaemic phenotype. *Curr Opin Lipidol*.24(4):332-8.

158. Bowden KL, Bilbey NJ, Bilawchuk LM, Boadu E, Sidhu R, Ory DS, et al. (2011) Lysosomal acid lipase deficiency impairs regulation of ABCA1 gene and formation of high density lipoproteins in cholesteryl ester storage disease. *J Biol Chem*.286(35):30624-35.

159. Tylki-Szymanska A, Jurecka A. (2014) Lysosomal acid lipase deficiency: wolman disease and cholesteryl ester storage disease. *Pril (Makedon Akad Nauk Umet Odd Med Nauki)*.35(1):99-106.

160. Pisciotta L, Fresa R, Bellocchio A, Pino E, Guido V, Cantafora A, et al. (2009) Cholesteryl Ester Storage Disease (CESD) due to novel mutations in the LIPA gene. *Mol Genet Metab*.97(2):143-8.

161. Marshall WC, Ockenden BG, Fosbrooke AS, Cumings JN. (1969) Wolman's disease. A rare lipidosis with adrenal calcification. *Arch Dis Child*.44(235):331-41.

162. Lough J, Fawcett J, Wiegensberg B. (1970) Wolman's disease. An electron microscopic, histochemical, and biochemical study. *Arch Pathol*.89(2):103-10.

163. Desai PK, Astrin KH, Thung SN, Gordon RE, Short MP, Coates PM, et al. (1987) Cholesteryl ester storage disease: pathologic changes in an affected fetus. *Am J Med Genet*.26(3):689-98.

164. Anderson RA, Bryson GM, Parks JS. (1999) Lysosomal acid lipase mutations that determine phenotype in Wolman and cholesterol ester storage disease. *Mol Genet Metab*.68(3):333-45.

165. Burton BK, Remy WT, Rayman L. (1984) Cholesterol ester and triglyceride metabolism in intact fibroblasts from patients with Wolman's disease and cholesterol ester storage disease. *Pediatr Res*.18(12):1242-5.

166. Jones SA, Valayannopoulos V, Schneider E, Eckert S, Banikazemi M, Bialer M, et al. (2016) Rapid progression and mortality of lysosomal acid lipase deficiency presenting in infants. *Genet Med*.18(5):452-8.

167. Elleder M, Chlumska A, Hyanek J, Poupetova H, Ledvinova J, Maas S, et al. (2000) Subclinical course of cholesteryl ester storage disease in an adult with hypercholesterolemia, accelerated atherosclerosis, and liver cancer. *J Hepatol*.32(3):528-34.

168. Zhang B, Porto AF. (2013) Cholesteryl ester storage disease: protean presentations of lysosomal acid lipase deficiency. *J Pediatr Gastroenterol Nutr*.56(6):682-5.

169. Kostner GM, Hadorn B, Roscher A, Zechner R. (1985) Plasma lipids and lipoproteins of a patient with cholesteryl ester storage disease. *J Inherit Metab Dis*.8(1):9-12.

170. Himes RW, Barlow SE, Bove K, Quintanilla NM, Sheridan R, Kohli R. (2016) Lysosomal Acid Lipase Deficiency Unmasked in Two Children With Nonalcoholic Fatty Liver Disease. *Pediatrics*.138(4).

171. Bravo AA, Sheth SG, Chopra S. (2001) Liver biopsy. *N Engl J Med*.344(7):495-500.

172. Thelwall PE, Smith FE, Leavitt MC, Canty D, Hu W, Hollingsworth KG, et al. (2013) Hepatic cholesteryl ester accumulation in lysosomal acid lipase deficiency: non-invasive identification and treatment monitoring by magnetic resonance. *J Hepatol*.59(3):543-9.

173. Hamilton J, Jones I, Srivastava R, Galloway P. (2012) A new method for the measurement of lysosomal acid lipase in dried blood spots using the inhibitor Lalistat 2. *Clin Chim Acta*.413(15-16):1207-10.

174. Rosenbaum AI, Cosner CC, Mariani CJ, Maxfield FR, Wiest O, Helquist P. (2010) Thiadiazole carbamates: potent inhibitors of lysosomal acid lipase and potential Niemann-Pick type C disease therapeutics. *J Med Chem*.53(14):5281-9.

175. Hulkova H, Elleder M. (2012) Distinctive histopathological features that support a diagnosis of cholesterol ester storage disease in liver biopsy specimens. *Histopathology*.60(7):1107-13.

176. Reiner Z. (2013) Statins in the primary prevention of cardiovascular disease. *Nat Rev Cardiol*.10(8):453-64.

177. Ginsberg HN, Le NA, Short MP, Ramakrishnan R, Desnick RJ. (1987) Suppression of apolipoprotein B production during treatment of cholesteryl ester storage disease with lovastatin. Implications for regulation of apolipoprotein B synthesis. *J Clin Invest*.80(6):1692-7.

178. Tarantino MD, McNamara DJ, Granstrom P, Ellefson RD, Unger EC, Udall JN, Jr. (1991) Lovastatin therapy for cholesterol ester storage disease in two sisters. *J Pediatr*.118(1):131-5.

179. Tadiboyina VT, Liu DM, Miskie BA, Wang J, Hegele RA. (2005) Treatment of dyslipidemia with lovastatin and ezetimibe in an adolescent with cholesterol ester storage disease. *Lipids Health Dis*.4:26.

180. Yokoyama S, McCoy E. (1992) Long-term treatment of a homozygous cholesteryl ester storage disease with combined cholestyramine and lovastatin. *J Inherit Metab Dis*.15(2):291-2.

181. McCoy E, Yokoyama S. (1991) Treatment of cholesteryl ester storage disease with combined cholestyramine and lovastatin. *Ann N Y Acad Sci*.623:453-4.

182. Leone L, Ippoliti PF, Antonicelli R. (1991) Use of simvastatin plus cholestyramine in the treatment of lysosomal acid lipase deficiency. *J Pediatr*.119(6):1008-9.

183. Levy R, Ostlund RE, Jr., Schonfeld G, Wong P, Semenkovich CF. (1992) Cholesteryl ester storage disease: complex molecular effects of chronic lovastatin therapy. *J Lipid Res*.33(7):1005-15.

184. Stahl PD, Rodman JS, Miller MJ, Schlesinger PH. (1978) Evidence for receptor-mediated binding of glycoproteins, glycoconjugates, and lysosomal glycosidases by alveolar macrophages. *Proc Natl Acad Sci U S A*.75(3):1399-403.

185. Du H, Schiavi S, Levine M, Mishra J, Heur M, Grabowski GA. (2001) Enzyme therapy for lysosomal acid lipase deficiency in the mouse. *Hum Mol Genet*.10(16):1639-48.

186. Jones SA, Rojas-Caro S, Quinn AG, Friedman M, Marulkar S, Ezgu F, et al. (2017) Survival in infants treated with sebelipase Alfa for lysosomal acid lipase deficiency: an open-label, multicenter, dose-escalation study. *Orphanet J Rare Dis*.12(1):25.

187. Balwani M, Breen C, Enns GM, Deegan PB, Honzik T, Jones S, et al. (2013) Clinical effect and safety profile of recombinant human lysosomal acid lipase in patients with cholesteryl ester storage disease. *Hepatology*.58(3):950-7.

188. Valayannopoulos V, Malinova V, Honzik T, Balwani M, Breen C, Deegan PB, et al. (2014) Sebelipase alfa over 52 weeks reduces serum transaminases, liver volume and improves serum lipids in patients with lysosomal acid lipase deficiency. *J Hepatol*.61(5):1135-42.

189. Whitley C, Valayannopoulos V, Malinova V, Sharmad R, Bourdone C, Boyadjiev S, et al. (2014) Long-term clinical effect and safety of sebelipase alfa in adults with lysosomal acid lipase deficiency. *Mol Genet Metab*.111:S113–14.

190. Valayannopoulos V, Malinová V, Sharma R, Bourdon C, Boyadjiev S, Kessler B, et al. (2014) Effect of sebelipase alfa after 90 weeks in adults with lysosomal acid lipase deficiency. *Atherosclerosis*.235(2):e19

191. Burton BK, Balwani M, Feillet F, Baric I, Burrow TA, Camarena Grande C, et al. (2015) A Phase 3 Trial of Sebelipase Alfa in Lysosomal Acid Lipase Deficiency. *N Engl J Med*.373(11):1010-20.

192. Furuya K, Marulkar S, Friedman M, Tripuraneni R, Burton K. (2016) Long-term benefit of sebelipase alfa over 52 weeks in children and adults with lysosomal acid lipase deficiency (ARISE trial). *J Pediatr Gastroenterol Nutr*.63.

193. Goodman Z, Burton B, Alaparthi L, Monge F, Friedman M, Soni P. (2016) Change in liver fibrosis in children and adults with lysosomal acid lipase deficiency after 52 weeks of sebelipase alfa (ARISE trial). *Hepatology*.64:S274.

194. Furuya K, Marulkar S, Friedman M. (2016) Long-term benefit of sebelipase alfa over 76 weeks in children and adults with lysosomal acid lipase deficiency (ARISE trial). *Hepatology*.64:S281.

195. Su K, Donaldson E, Sharma R. (2016) Novel treatment options for lysosomal acid lipase deficiency: critical appraisal of sebelipase alfa. *Appl Clin Genet*.9:157-67.

196. Tolar J, Petryk A, Khan K, Bjoraker KJ, Jessurun J, Dolan M, et al. (2009) Long-term metabolic, endocrine, and neuropsychological outcome of hematopoietic cell transplantation for Wolman disease. *Bone Marrow Transplant*.43(1):21-7.

197. Stein J, Garty BZ, Dror Y, Fenig E, Zeigler M, Yaniv I. (2007) Successful treatment of Wolman disease by unrelated umbilical cord blood transplantation. *Eur J Pediatr*.166(7):663-6.

198. Gramatges MM, Dvorak CC, Regula DP, Enns GM, Weinberg K, Agarwal R. (2009) Pathological evidence of Wolman's disease following hematopoietic stem cell transplantation despite correction of lysosomal acid lipase activity. *Bone Marrow Transplant*.44(7):449-50.

199. Yanir A, Allatif MA, Weintraub M, Stepensky P. (2013) Unfavorable outcome of hematopoietic stem cell transplantation in two siblings with Wolman disease due to graft failure and hepatic complications. *Mol Genet Metab*.109(2):224-6.

200. Ferry GD, Whisennand HH, Finegold MJ, Alpert E, Glombicki A. (1991) Liver transplantation for cholesteryl ester storage disease. *J Pediatr Gastroenterol Nutr*.12(3):376-8.

201. Cagle PT, Ferry GD, Beaudet AL, Hawkins EP. (1986) Pulmonary hypertension in an 18-year-old girl with cholesteryl ester storage disease (CESD). *Am J Med Genet*.24(4):711-22.

202. Michels VV, Driscoll DJ, Ferry GD, Duff DF, Beaudet AL. (1979) Pulmonary vascular obstruction associated with cholesteryl ester storage disease. *J Pediatr*.94(4):621-3.

203. Arterburn JN, Lee WM, Wood RP, Shaw BW, Markin RS. (1991) Orthotopic liver transplantation for cholesteryl ester storage disease. *J Clin Gastroenterol*.13(4):482-5.

204. Leone L, Ippoliti PF, Antonicelli R, Balli F, Gridelli B. (1995) Treatment and liver transplantation for cholesterol ester storage disease. *J Pediatr*.127(3):509-10.

205. Ambler GK, Hoare M, Brais R, Shaw A, Butler A, Flynn P, et al. (2013) Orthotopic liver transplantation in an adult with cholesterol ester storage disease. *JIMD Rep*.8:41-6.

206. Du H, Witte DP, Grabowski GA. (1996) Tissue and cellular specific expression of murine lysosomal acid lipase mRNA and protein. *J Lipid Res*.37(5):937-49.

207. Du H, Duanmu M, Rosa LR. (1998) Mouse lysosomal acid lipase: characterization of the gene and analysis of promoter activity. *Gene*.208(2):285-95.

208. Du H, Heur M, Duanmu M, Grabowski GA, Hui DY, Witte DP, et al. (2001) Lysosomal acid lipase-deficient mice: depletion of white and brown fat, severe hepatosplenomegaly, and shortened life span. *J Lipid Res*.42(4):489-500.

209. Hoeg JM, Demosky SJ, Jr., Pescovitz OH, Brewer HB, Jr. (1984) Cholesteryl ester storage disease and Wolman disease: phenotypic variants of lysosomal acid cholesteryl ester hydrolase deficiency. *Am J Hum Genet*.36(6):1190-203.

210. Duta-Mare M, Sachdev V, Leopold C, Kolb D, Vujic N, Korbelius M, et al. (2018) Lysosomal acid lipase regulates fatty acid channeling in brown adipose tissue to maintain thermogenesis. *Biochim Biophys Acta*.1863(4):467-78.

211. Schlager S, Vujic N, Korbelius M, Duta-Mare M, Dorow J, Leopold C, et al. (2017) Lysosomal lipid hydrolysis provides substrates for lipid mediator synthesis in murine macrophages. *Oncotarget*.8(25):40037-51.

212. Du H, Duanmu M, Witte D, Grabowski GA. (1998) Targeted disruption of the mouse lysosomal acid lipase gene: long-term survival with massive cholesteryl ester and triglyceride storage. *Hum Mol Genet*.7(9):1347-54.

213. Leopold C, Duta-Mare M, Sachdev V, Goeritzer M, Maresch LK, Kolb D, et al. (2019) Hepatocyte-specific lysosomal acid lipase deficiency protects mice from diet-induced

obesity but promotes hepatic inflammation. *Biochim Biophys Acta Mol Cell Biol Lipids*.1864(4):500-11.

214. Ferrannini E. (1988) The theoretical bases of indirect calorimetry: a review. *Metabolism*.37(3):287-301.

215. Stoeckman AK, Towle HC. (2002) The role of SREBP-1c in nutritional regulation of lipogenic enzyme gene expression. *J Biol Chem*.277(30):27029-35.

216. Dieterle F, Ross A, Schlotterbeck G, Senn H. (2006) Probabilistic quotient normalization as robust method to account for dilution of complex biological mixtures. Application in 1H NMR metabonomics. *Anal Chem*.78(13):4281-90.

217. Maher AD, Crockford D, Toft H, Malmodin D, Faber JH, McCarthy MI, et al. (2008) Optimization of human plasma 1H NMR spectroscopic data processing for high-throughput metabolic phenotyping studies and detection of insulin resistance related to type 2 diabetes. *Anal Chem*.80(19):7354-62.

218. Sattler W, Puhl H, Hayn M, Kostner GM, Esterbauer H. (1991) Determination of fatty acids in the main lipoprotein classes by capillary gas chromatography: BF3/methanol transesterification of lyophilized samples instead of Folch extraction gives higher yields. *Anal Biochem*.198(1):184-90.

219. Titford M. (2005) The long history of hematoxylin. *Biotech Histochem*.80(2):73-8.

220. Mallory FB. (1900) A Contribution to Staining Methods : I. A Differential Stain for Connective-Tissue Fibrillae and Reticulum. Ii. Chloride of Iron Haematoxylin for Nuclei and Fibrin. Iii. Phosphotungstic Acid Haematoxylin for Neuroglia Fibres. *J Exp Med*.5(1):15-20.

221. Kos CH. (2004) Cre/loxP system for generating tissue-specific knockout mouse models. *Nutr Rev*.62(6 Pt 1):243-6.

222. Postic C, Shiota M, Niswender KD, Jetton TL, Chen Y, Moates JM, et al. (1999) Dual roles for glucokinase in glucose homeostasis as determined by liver and pancreatic beta cell-specific gene knock-outs using Cre recombinase. *J Biol Chem*.274(1):305-15.

223. Ioannou GN, Haigh WG, Thorning D, Savard C. (2013) Hepatic cholesterol crystals and crown-like structures distinguish NASH from simple steatosis. *J Lipid Res*.54(5):1326-34.

224. Shirley M. (2015) Sebelipase alfa: first global approval. *Drugs*.75(16):1935-40.

225. Valayannopoulos V, Mengel E, Brassier A, Grabowski G. (2017) Lysosomal acid lipase deficiency: Expanding differential diagnosis. *Mol Genet Metab*.120(1-2):62-66.

226. Van Klinken JB, van den Berg SA, Havekes LM, Willems Van Dijk K. (2012) Estimation of activity related energy expenditure and resting metabolic rate in freely moving mice from indirect calorimetry data. *PLoS One*.7(5):e36162.

227. Mutel E, Abdul-Wahed A, Ramamonjisoa N, Stefanutti A, Houberdon I, Cavassila S, et al. (2011) Targeted deletion of liver glucose-6 phosphatase mimics glycogen storage disease type 1a including development of multiple adenomas. *J Hepatol*.54(3):529-37.

228. Burgess SC, Hausler N, Merritt M, Jeffrey FM, Storey C, Milde A, et al. (2004) Impaired tricarboxylic acid cycle activity in mouse livers lacking cytosolic phosphoenolpyruvate carboxykinase. *J Biol Chem*.279(47):48941-9.

229. Gao Z, Yin J, Zhang J, Ward RE, Martin RJ, Lefevre M, et al. (2009) Butyrate improves insulin sensitivity and increases energy expenditure in mice. *Diabetes*.58(7):1509-17.

230. Asterholm IW, Halberg N, Scherer PE. (2007) Mouse Models of Lipodystrophy Key reagents for the understanding of the metabolic syndrome. *Drug Discov Today Dis Models*.4(1):17-24.

231. Knights AJ, Funnell AP, Pearson RC, Crossley M, Bell-Anderson KS. (2014) Adipokines and insulin action: A sensitive issue. *Adipocyte*.3(2):88-96.

232. Arita Y, Kihara S, Ouchi N, Takahashi M, Maeda K, Miyagawa J, et al. (1999) Paradoxical decrease of an adipose-specific protein, adiponectin, in obesity. *Biochem Biophys Res Commun*.257(1):79-83.

233. Barr VA, Malide D, Zarnowski MJ, Taylor SI, Cushman SW. (1997) Insulin stimulates both leptin secretion and production by rat white adipose tissue. *Endocrinology*.138(10):4463-72.

234. Sinha MK, Opentanova I, Ohannesian JP, Kolaczynski JW, Heiman ML, Hale J, et al. (1996) Evidence of free and bound leptin in human circulation. Studies in lean and obese subjects and during short-term fasting. *J Clin Invest*.98(6):1277-82.

235. Maffei M, Halaas J, Ravussin E, Pratley RE, Lee GH, Zhang Y, et al. (1995) Leptin levels in human and rodent: measurement of plasma leptin and ob RNA in obese and weight-reduced subjects. *Nat Med*.1(11):1155-61.

236. Shimomura I, Hammer RE, Ikemoto S, Brown MS, Goldstein JL. (1999) Leptin reverses insulin resistance and diabetes mellitus in mice with congenital lipodystrophy. *Nature*.401(6748):73-6.

237. Combs TP, Berg AH, Obici S, Scherer PE, Rossetti L. (2001) Endogenous glucose production is inhibited by the adipose-derived protein Acrp30. *J Clin Invest*.108(12):1875-81.

238. Miller RA, Chu Q, Le Lay J, Scherer PE, Ahima RS, Kaestner KH, et al. (2011) Adiponectin suppresses gluconeogenic gene expression in mouse hepatocytes independent of LKB1-AMPK signaling. *J Clin Invest*.121(6):2518-28.

239. Xu A, Wang Y, Keshaw H, Xu LY, Lam KS, Cooper GJ. (2003) The fat-derived hormone adiponectin alleviates alcoholic and nonalcoholic fatty liver diseases in mice. *J Clin Invest*.112(1):91-100.

240. Baratta F, Pastori D, Del Ben M, Polimeni L, Labbadia G, Di Santo S, et al. (2015) Reduced Lysosomal Acid Lipase Activity in Adult Patients With Non-alcoholic Fatty Liver Disease. *EBioMedicine*.2(7):750-4.

241. Burton BK, Deegan PB, Enns GM, Guardamagna O, Horslen S, Hovingh GK, et al. (2015) Clinical Features of Lysosomal Acid Lipase Deficiency. *J Pediatr Gastroenterol Nutr*.61(6):619-25.

242. Smith SJ, Cases S, Jensen DR, Chen HC, Sande E, Tow B, et al. (2000) Obesity resistance and multiple mechanisms of triglyceride synthesis in mice lacking Dgat. *Nat Genet*.25(1):87-90.

243. Zhao Y, Su B, Jacobs RL, Kennedy B, Francis GA, Waddington E, et al. (2009) Lack of phosphatidylethanolamine N-methyltransferase alters plasma VLDL phospholipids and attenuates atherosclerosis in mice. *Arterioscler Thromb Vasc Biol*.29(9):1349-55.

244. Ivashkin V, Zharkova M. (2017) Cholesteryl Ester Crystals in Lysosomal Acid Lipase Deficiency. *N Engl J Med*.376(9):e14.

245. Yan C, Lian X, Li Y, Dai Y, White A, Qin Y, et al. (2006) Macrophage-specific expression of human lysosomal acid lipase corrects inflammation and pathogenic phenotypes in lal-/- mice. *Am J Pathol*.169(3):916-26.

246. Seki E, De Minicis S, Gwak GY, Kluwe J, Inokuchi S, Bursill CA, et al. (2009) CCR1 and CCR5 promote hepatic fibrosis in mice. *J Clin Invest*.119(7):1858-70.

247. Heinrichs D, Berres ML, Nellen A, Fischer P, Scholten D, Trautwein C, et al. (2013) The chemokine CCL3 promotes experimental liver fibrosis in mice. *PLoS One*.8(6):e66106.

248. Berres ML, Koenen RR, Rueland A, Zaldivar MM, Heinrichs D, Sahin H, et al. (2010) Antagonism of the chemokine Ccl5 ameliorates experimental liver fibrosis in mice. *J Clin Invest*.120(11):4129-40.

249. Du H, Zhao T, Ding X, Yan C. (2015) Hepatocyte-Specific Expression of Human Lysosome Acid Lipase Corrects Liver Inflammation and Tumor Metastasis in lal(-/-) Mice. *Am J Pathol*.185(9):2379-89.

Appendix

Permissions granted by the publishers to use their figures in this doctoral thesis

Figure number	Licensed content publisher and granted license number
Figure 5	McGraw Hill, 4543020866760
Figure 6-9	Elsevier, permission not required for author of publication
Figure 13-17	Elsevier, permission not required for author of publication
Figure 19	Elsevier, permission not required for author of publication
Figure 21	Elsevier, permission not required for author of publication
Figure 23-30	Elsevier, permission not required for author of publication

Note: Detailed PDF copies of the license documents will be furbished upon request.

List of Tables

List of Figures